CAAP FINAL REPORT

CAAP Final Report

Date of Report: June 28, 2023

Prepared for: United States Department of Transportation

Pipeline and Hazardous Materials Safety Administration

Office of Pipeline Safety

Contract Number: 693JK31950007CAAP

Project Title: "Unmanned Aerial Systems for Pipeline Inspection, Monitoring, and Landscape Analysis"

Prepared by: Dr. Michael P. Strager

Team Project Manager
Professor Division of Resource Economics and Management
School of Natural Resources, Davis College
West Virginia University
Morgantown, WV 26506-6108
mstrager@wvu.edu
304-293-6463

Executive Summary

The Appalachian region of the United States has experienced significant growth in the production of natural gas. Developing the infrastructure required to transport this resource to market creates significant disturbances across the landscape, as both well pads and transportation pipelines must be created in this mountainous terrain. Midstream infrastructure, which includes pipeline rights-of-way and associated infrastructure, can cause significant environmental degradation, especially in the form of sedimentation. The introduction of this non-point source pollutant can be detrimental to freshwater ecosystems found throughout this region. This ecological risk has necessitated the enactment of regulations related to midstream infrastructure development. Weekly, inspectors travel afoot along new pipeline rights-of-way, monitoring the reestablishment of surface vegetation and identifying failing areas for future management. The topographically challenging terrain of West Virginia makes these inspections difficult and dangerous to the hiking inspectors. We evaluated the accuracy at which unmanned aerial vehicles replicated inspector classifications to evaluate their use as a complementary tool in the pipeline inspection process. We investigated the use of various sensors to determine the most cost-effective methodology for performing pipeline monitoring and analysis in Appalachia. We found RGB and multispectral sensor collections combined with a support vector machine classification approach to be effective at predicting vegetation cover. Using inspector defined validation plots, our research found comparable high accuracy between the two collection sensors. This technique displays the capability of augmenting the current inspection process, though it is likely that the model can be improved further. The high accuracy thus obtained suggests valuable implementation of this widely available technology in aiding these challenging inspections. The UAV-based remote sensing approach can aid in the inspection of erosion and sediment control features as well as support overall pipeline safety, inspection, and management.

Main Objective

Determine the most cost-effective combination of Unmanned Aerial System (UAS) sensors to monitor and evaluate pipeline conditions.

Public Abstract

Unmanned Aerial Systems (UASs) have data resolution and scale advantages that fit between in-person field sampling and fixed wing aircraft and imagery acquisition. The use of UASs for natural resource management is a growing area that has been shown to have key advantages over traditional sampling approaches. Our work focused on better understanding the options for applying appropriate drone technologies under different natural resource management objectives. We investigated this main question with applications of UAS technology in the areas of pipeline safety and management. Our results found that an UAS-based remote sensing approach can aid in the inspection of erosion and sediment control features as well as support overall pipeline safety, inspection, and management. Increased land access and accuracy assessment can provide a more robust evaluation of this emergent technique.

Though current analysis shows UAS based inspections to be more costly than traditional approaches, the evaluation of additional identified factors may create a more complete picture of the relationship between these two techniques, and aid in reducing this cost differential. After determining effective performance and cost optimization, a purpose-built drone could be

deployed over a pipeline stretch using a previously created flight plan on a regular basis. From this, models of a reasonably high accuracy are derived, which could in turn be used to identify larger issues requiring immediate responses. This tasking could cover post-rain inspections, where there is a time sensitive nature to detecting large failures within the corridor or at the pipeline itself. Trained and certified professionals will still be needed in inspections, as they can seek-out conditions which the drone may miss; however, their time spent traversing difficult terrain would be reduced. On such terrain, both worker safety and cost savings may be realized. Thus, the inclusion of UASs in pipeline inspection procedures appears to be a promising enterprise.

Student Mentoring

Anthony Mesa earned a WVU MS in Energy Environments in 2022

Matt Boothe earned a WVU MS in Energy Environments in 2021

Sam Bearinger earned a WVU MS in Forestry in 2021

Joseph Kimmett earned a WVU MS in Energy Environments in 2020

Lucas Kinder earned a WVU MS in Energy Environments in 2022

Isaac Kinder is currently pursuing a WVU MS in Energy Environments with expected graduation in May of 2024

Matt Walker is currently pursuing a WVU PhD in Resource Management with expected graduation in December of 2025

Student Internship

Matt Boothe secured an internship with Pikewood Energy in 2019 and has continued employment with them since finishing his WVU MS degree.

Educational activities

The RESM 405 three credit class “Drones in Resource Management” taught each Fall semester by Dr. Kinder has integrated students since 2020. The students from the program that have participated in teaching lab exercises on the use of drones includes Tony Mesa, Lucas Kinder, and Isaac Kinder.

Career employed

Anthony Mesa is currently employed as a research analyst with the Energy Land Management Program at West Virginia University.

Matt Boothe is currently employed as an energy analyst at Pikewood Energy.

Sam Bearinger is currently employed as a state forester UAV operator/pilot with the Pennsylvania Department of Conservation and Natural Resources.

Joseph Kimmett is currently a project manager with Eagle Creek Renewable Energy.

Lucas Kinder is currently a research coordinator with the Natural Resource Analysis Center at West Virginia University.

Dissemination of project outcomes

Strager, M. P. Spatial Modeling of Palustrine Forested Wetland Occurrence Using ArcGIS Pro. Environmental Systems Research Institute, Mid Atlantic Users Group Meeting. Virtual meeting. Apr 22, 2021.

Mesa, T. M. P. Strager, P. Kinder, S. Grushecky. Evaluation of Vegetation Success on Reclaimed Natural Gas Pipelines. 24th Annual Virtual Graduate Student Research and Creative Scholarship Conference, Davis College of Agriculture, Natural Resources and Design. Davis College, WVU, Apr 16, 2021.

Mesa, T., M. P. Strager, S. Grushecky. Using UAVs for Surface Runoff Analysis. National Extension Energy Summit (NEES) + National Sustainability Summit (NSS), State College, PA, Oct 5, 2021.

Strager, M. P., P. Kinder, S. Gruchecky, D. Hruska. Unmanned Aerial Systems for Pipeline Inspection, Monitoring, and Landscape Analysis. Pipeline Research Council International, 2021 Virtual Research Exchange. Mar 2-4, 2021.

Strager, M. P. Mapping and Analysis of Landscape Conditions to Better Understand Receiving Water Quality and Biological Impacts in Appalachia. Institute of Water Science and Security Spring Workshop Series: Advances in West Virginia Water Research, Morgantown, WV. Jun 2, 2021.

Mesa, T. M. P. Strager, P. Kinder, S. Grushecky. Evaluation of Vegetation Success on Reclaimed Natural Gas Pipelines. 13th Southern Forestry and Natural Resource Management GIS Conference. Athens, GA. Dec 6-7, 2021.

Boothe, M., M. Strager, S. Grushecky, and P. Kinder. Unmanned aerial systems for pipeline inspection, monitoring, and landscape analysis. Virtual Meeting of Pittsburgh Right of Way Group, Waynesburg, PA. June 9th, 2020.

Citations of the publications

Mesa, T., M. P. Strager, S. G. Grushecky, P. Kinder. 2023. Using Unmanned Aerial Vehicles to

Evaluate Revegetation Success on Natural Gas Pipelines. Environmental Management. https://doi.org/10.1007/s00267-023-01842-9.

Strager, M. P., A. M. Klein Hentz, P. Kinder, S. Grushecky. 2020. Using unmanned aerial vehicles to model surface runoff during well pad development. Journal of the American Society of Mining and Reclamation. ISSN Number 2328-8744. Vol 9, No. 1.pp. 51-69.

Mesa, A., S. Grushecky, M. P. Strager, and P. Kinder. 2022. Evaluation of vegetation success on reclaimed natural gas pipelines. In Merry, K., P. Bettinger, C. Cieszewski, M. Crosby, A.R.G. Garzon, J. Siry, B. Song, Z. Ucar, and J. Uzu (eds.), Proceedings of the 13th Southern Forestry and Natural Resource Management GIS Conference. Warnell School of Forestry and Natural Resources, University of Georgia, Athens, GA. (Best Student Paper Award)

Strager, M. P., P. Kinder, S. Grushecky. 2021. Utilizing unmanned aerial vehicles to predict surface runoff. Reclamation Matters. American Society of Reclamation Sciences. Pp. 14-22.

Grushecky, S., F. Zinkham, M. P. Strager, T. Carr. 2022. Energy Production and Well Site Disturbance from Conventional and Unconventional Natural Gas Development in West Virginia. Energy, Ecology and Environment. Vol 7. Issue 4. 358-368pp. https://doi.org/10.1007/s40974-022-00246-5.

Grushecky, S., K. J. Harris, M. P. Strager, J. Wang, A. N. Mesa. 2022. Land cover change associated with unconventional oil and gas development in the Appalachian Region. Environmental Management. Vol. 70. 869-880pp. https://doi.org/10.1007/s00267-022-01702-y.

Merriam, E. R., M. P. Strager, J. T. Petty. 2022. Source water vulnerability to elevated total dissolved solids within a mixed-use Appalachian River basin. PLOS One Water. https://doi.org/10.1371/journal.pwat.0000035 A.

MacKenzie, A., W. E. Veselka, P. Kinder, M. P. Strager, S. T. Grushecky, J. A. Hubbart, and J. T. Anderson. 2023. Restoring a first order stream and adjacent riparian wetlands in West Virginia: Integrating lessons from wetland science and practice. Wetland Science and Practice 41(2):61-69.

List of Acronyms

AAPS Alignment Assessment Point Set

AAPS Alignment Assessment Point Set

CWA Clean Water Act

DEM Digital Elevation Model

EQT EQT Corporation is the largest producer of natural gas in the United States

EXIF Exchangeable ImageFile Forma

GIS Geographic Information System

GNSS Global Navigation Satellite System

GPS Global Positioning Systems
GSOD Global Summary of the Day
GWPCP General Water Pollution Control Permit
IMU Inertial Measurement Unit
LiDAR Light Imaging Detection and Radar
MEMS Micro electro mechanical Mirror
MSL Mean Sea Level
NDVI Normalized Difference Vegetation Index
NG Natural Gas
NIR Near Infra Red
NOAA National Oceanic and Atmospheric Administration
OPUS Online Positioning User Service
RGB Red Blue Green visible lightspectrum
RTK Real Time Kinematic
RTL Red Talk LiDAR
SAGA System for Automated Geoscientific Analyses
SBET Smoothed Best Estimate of Trajectory
SE Standard Error
SME Subject Matter Expert
SVM Support Vector Machines
TSS Total Suspended Solids
UAS Unmanned Aerial System
UAV Unmanned Aerial Vehicle
UGCS Universal Ground Control Software
UgCS Universal Ground Control Station
US FAA United States Federal Aviation Administration
USEPA United States Environmental Protection Agency
USGS United States Geologic Survey
VLOS Visual Line of Sight

Table of Contents

Introduction

When considering the application of modern techniques into traditional practices, modernity must undergo an evaluation of its capabilities at replicating the task at hand. Gains in efficiency and safety must have their accuracy and precision costs weighed. Unmanned aerial vehicles (UAVs or drones), remotely piloted aircraft capable of varied data collection and often equipped with visual sensors (Alley-Young, 2020), have been found to be increasingly capable in such measures. Many industries have witnessed their inclusion to effect new functionality or augment and enhance existing techniques. Industrial facilities with dangerous or inaccessible structures in need of safety inspections have been able to include UAVs in their operations to minimize risk without sacrificing evaluation coverage (Nikolic et al., 2013). Civil engineers needing to inspect large structures for minor faults have found the value in UAV inclusion (Hallermann and Morgenthal, 2014). Agricultural operations utilize UAVs equipped with multispectral sensors to optimize fertilizer application and harvest (Kim et al., 2019). With the realized value found in so many diverse sectors of industry, the performance potential in novel utilization is worthy of calculating.

Natural gas (NG) production in the United States (US) has surpassed that of all other countries (Doman and Kahan, 2018). Of the natural gas development regions in the US, the Appalachian basin has been developed into the largest NG producer, producing 33% of the total national output (U.S. Department of Energy, 2020; U.S. Energy Information Administration, 2021). NG is rich in this region due to two shale plays extending beneath it. They are known as the Marcellus and Utica shales, which extend across 298,000 km^2 and 240,000 km^2 respectively (Kargbo et al., 2010; Popova, 2017a; Popova, 2017b). Modern unconventional drilling and hydraulic fracturing (fracking) techniques have led to the large growth seen in this region, which is projected to double its NG productivity by 2050 (U.S. Department of Energy, 2020).

Typical NG production in the Appalachian basin begins with the establishment of a well pad, whereupon unconventional wells are established. These wells draw from a large area of the NG bearing shale with vertical well bore descending up to 2.4 km in depth with a lateral leg that can extend over 6 km (Marcellus Drilling News, 2021). NG flowing to the surface from this process is directed into a near surface gathering pipeline (midstream), through which it travels to the fuel's final users. The midstream is lined with compressor stations to maintain the pipeline's pressure (Messersmith et al., 2015). Each midstream compressor station is situated upon its own pad structure. In all, the installation of the pad and midstream infrastructure require large quantities of land alterations, potentially causing large ecological disturbance events across the landscape, with midstream segments creating the greatest footprint of landscape impact (Langlois et al., 2017).

In the early stages of development, standing timber and surface vegetation are removed, and the land surface is graded across the extent of the NG infrastructure. Drilling locations cause an average of 5.6 hectares of disturbance (Grushecky et al. 2022), additional midstream and allied infrastructure can increase disturbance up to 250% (Langlois et al. 2017). This infrastructure development has been found to significantly impact surface water flow (Warner et al., 2013) and total suspended solids (TSS) quantities in associated watersheds (Olmstead et al., 2013). Further, increased sediment in freshwater ecosystems has caused significant ecologic impacts. Sediment introduction has been found to decrease the populations of lower trophic level aquatic species (Richards and Bacon, 1994), and lead to severe reduction in primary producers' photosynthetic activity and overall health (Cederholm and Lestelle, 1974). At higher trophic levels, larger vertebrates show organ damage and recruitment loss in sediment rich waterways

(Kemp et al., 2011).

The potential for such drastic ecological impacts has prompted the regulation of NG from both state and federal agencies across the US. Federally, the US Environmental Protection Agency, Clean Water Act (CWA) Section 404, prohibits companies from discharging sediments and establishes a specific permitting process for NG development. In the Appalachian basin state of West Virginia (WV), the Department of Environmental Protection (DEP) provides development advice as well as regulates NG development within the state. Guidance comes in the form of a best management practice manual (West Virginia Department of Environmental Protection, 2016), which notes the establishment of surface vegetation in sediment and erosion control on NG sites. This is also noted in the General Water Pollution Control Permit (GWPCP) (West Virginia Department of Environmental Protection, 2013).

Frequent site inspections are to be conducted by a permittee, both weekly and after a significant rain event of over 0.25 in (0.635 cm). Inspections are conducted by certified site inspectors, who travel the entire pipeline length on-foot. Typically, permittees divide the pipeline into inspection sections. Under the GWPCP sediment reduction adherence, hiking inspectors look for vegetation failures, surface soil movement, or failure of erosion control structures of a site. Finding any failure requires immediate reporting, and the issue to be addressed promptly. When a permittee believes a site to be stable, the WV DEP provides their own afoot inspectors to evaluate the site. State inspectors evaluate the permanence of erosion control measures, as well as the health and quantity of surface vegetation on all permeable surfaces. When a site passes this inspection, it is declared to have reached final stabilization, and the bond is returned to the permittee.

As outlined in the GWPCP, passing vegetation coverage is defined as a minimum of 70% surface vegetation across the site. Current afoot inspections determine this coverage with a surface sampling ring, often using a Hula hoop, approximately 0.75 m^2 to 1 m^2 in area. During the state's inspection, this hoop is randomly cast multiple times throughout the permit area. Wherever the sampling device lands, the inspector provides an ocular estimation of the vegetation coverage within. The sampling ring is not mentioned in the GWPCP, and there is no further guidance on evaluating this 70% standard. Industry representatives state that the sampling intensity and vegetation can vary from inspector to inspector and from site to site. Frequently, a single random sample from within the site judged to be below 70% will generate a failing report from the state inspector, keeping the permit open, and the weekly inspections ongoing.

To construct well pads and transmission lines, land is graded, removing timber, vegetation, and layers of topsoil. Exposure of barren ground can lead to high sediment loading in nearby watersheds due to erosional factors of surface water. Although sedimentation is a natural geophysical occurrence, freshwater ecosystems like those found in Appalachia are susceptible to substantial ecological impacts caused by an influx of suspended sediments (Berry et al, 2003).

Federal and state agencies highly regulate natural gas infrastructure development regarding sediment discharge. Within the Appalachian region of West Virginia, the United States Clean Water Act Section 404, and West Virginia Department of Environmental Protection (WV DEP) institute a system of permitting and guidance regarding development of natural gas infrastructure. The WV Department of Environmental Protection's General Water Pollution Control Permit requires final stabilization of natural gas development to exhibit a healthy vegetation coverage of at least 70% in disturbed areas with all fill slopes protected by measures to divert runoff (General Water Pollution Control Permit, 2013). Within the Erosion and Sediment Control Best Management Practice Manual, vegetation coverage is emphasized as the most important practice to prevent erosion and sediment (2016). It is also mentioned that right-of-way diversions, called “waterbars”, are the most common sediment control used in pipeline construction.

In West Virginia, during and after natural gas pipeline construction, permits are held by the responsible company. Inspection by the permit holder is required weekly during active disturbances, bi-weekly in restored areas, and after any rain event greater than 0.5 inches (General Water Pollution Control Permit, 2013). When a site is deemed to be stable by the permit holder, a WVDEP inspector will conduct a final inspection of all permit-required features before the permit holder’s bond is released. All inspections are completed on-foot across designated sections of pipeline. With the undulating topography of West Virginia, this can be a difficult and sometimes dangerous task. The use of UAVs and remote sensing systems can supplement pipeline safety, inspection, and management especially in areas that are remote or in topographies that are difficult to traverse (Gómez, C., & Green, D. R., 2017).

UAVs could be used as a supplementary tool in this inspection process. The mountainous terrain of the Appalachian region makes frequent afoot inspections both difficult and an ongoing safety concern for the inspectors. Moreover, remote sensing may provide a more objective approach to vegetation evaluations. Though UAVs have addressed the needs and safety concerns of many industries, to the best of our knowledge, the use of UAVs in inspecting NG pipeline vegetation coverage has not yet been evaluated. Our research assessing the accuracy performance of drones in NG inspections was completed using machine learning classifier models created from two widely available UAV sensor technologies, simple RGB and agriculturally designed multispectral capture. The evaluation of these technologies provides an introductory evaluation of the accuracy gap between current standards and novel techniques.

UAVs found development initially through military necessity eliminating potential injury or death to a human pilot in high-risk situations (Nex, F., & Remondino, F., 2014). In recent years, rapid advancements in UAV technology have diminished barriers to entry pertaining to cost, reliability, and availability while creating an influx of commercialized products with ever expanding civil applications. Researchers and industry have begun to incorporate UAVs, augmenting old methods, and adopting new uses. We have seen the introduction of purpose-built UAVs as well as those that are modular, able to carry a varying suite of remote sensing systems and devices with multiple goals in mind. Miniaturization of remote sensing systems as well as the ability to operate close to the ground allows for collection of high spatial and temporal resolution data (Noor et al., 2018). This combined with GIS software allows for advanced spatial analyses to be conducted at scales not previously feasible.

Many economic, environmental, and energy sectors have introduced UAVs and remote sensing systems into their toolboxes. Agricultural use of this fruitful technology includes mapping of unwanted vegetation (weeds and invasive species), monitoring growth and potential yield, assessing health of crops, and managing irrigation (Tsouros et al., 2019). Early UAV-based remote sensing in agriculture was conducted using a model aircraft equipped with a consumer grade RGB camera (Hunt et al, 2005). This study used RGB imagery to create a Normalized Green-Red Difference Index to evaluate crop biomass of corn, alfalfa, and soybean as well as the nitrogen status of corn. The UAV remote sensing methodology worked well, and the study found that crop biomass was better estimated using RGB imagery. Newer remote sensing systems such as multispectral cameras can collect specific wavelengths of light more suitable for vegetation analysis. A newer study found that high resolution NDVI, or Normalized Difference Vegetation Index, was able to identify overall crop growth as well as subtle anomalies in growth of wheat and rice plants (Guan et al, 2019). The NDVI was created using red and near-infrared bands (specific wavelengths) collected from a UAV-based multispectral camera.

UAVs are used in many facets of engineering and construction. Remote sensing in construction management uses UAV platforms to monitor entire work sites at a moment's notice. These systems can also be used to inspect and map buildings, bridges, highways, windmills, cell towers and many other engineered structures and features (Chen et al, 2014). Surveying companies have adopted the use of LiDAR remote sensing into their workflow. These sensors can collect highly accurate data used to create 3-dimensional models which in some circumstances, can be more useful than traditional total station-based surveys. A study by Schroder et al found that LiDAR surveys were extremely useful in identifying and documenting historical and archaeological sites in Mexico (2021).

Many areas of environmental/natural resource management utilize UAVs and their remote sensing abilities. Federal governments all the way down to local governments as well as scientists and scholars continuously use them for research, resource management, decision support, surveillance, and mapping purposes. These technologies are highly useful in forest management. Use of UAV-based LiDAR and camera sensors has allowed for forest inventory, individual tree detection, and tree/canopy measurements (Wallace et al, 2012; Wu et al, 2019). Global Positioning System (GPS) deprived under-canopy forest surveys for tree location and measurement are possible with UAV and LiDAR technology (Chrisholm et al, 2013). This is an impressive feat as most UAV systems rely heavily on GPS for flight positioning and autonomy. In addition, GPS is almost always needed in remote sensor data processing and post processing workflows. In another study, traditional stream physical habitat assessments were compared to those collected using a UAV equipped with an RGB camera. This study found that there was little differentiation between remotely sensed measurement and field-based measurement accuracies with data collection being far more efficient and cost effective using a UAV (Klein Hentz et al, 2018).

As efficiencies are continually being sought after throughout research and industry, we see constant adoption of new technology and methods. The United States is currently the top producer of oil and natural gas in the world (Maizland, L., & Siripurapu, A., 2022). This expansive network of energy supplementation has some adoption of UAS and remote sensing technologies although there is ample opportunity for application of new methodologies. The use of UAVs for pipeline monitoring and security purposes is a prominent focus in the industry. Large-scale implementation has been slow due to constraints on current technology such as battery life limitations, changing atmospheric conditions, and regulatory restrictions. (Cho et al, 2015; Wanasighe et al, 2020; Asadzadeh et al, 2022). Another barrier for entry in the use of UAV technology also includes Federal Aviation Administration (FAA) remote pilot licensing which requires extensive training in rules regarding our nation's airspace as well as successfully passing a FAA knowledge exam (*Certificated remote pilots*, n.d.). There has been more recent focus on UAV application within the oil and gas industry such as the use of UAV remotely sensed imagery to model surface runoff of total suspended solids concentrations on a well pad (Strager et al, 2020).

The Appalachian region of the United States is responsible for the predominant expansion in natural gas production with the Marcellus and Utica shale formations producing over 32% of the United States' supply of natural gas (*An Appalachian Petrochemical*, 2019). Shale gas production relies on upstream unconventional wells placed atop well pads. Extracted natural gas is then transported to midstream processing facilities through transmission pipelines accompanied by compressor stations placed between long sections of pipeline. After processing, downstream natural gas is distributed to market (Goellner, 2012).

To construct well pads and transmission lines, land is graded, removing timber, vegetation, and layers of topsoil. Exposure of barren ground can lead to high sediment loading in nearby watersheds due to erosional factors of surface water. Although sedimentation is a natural geophysical occurrence, freshwater ecosystems like those found in Appalachia are susceptible to substantial ecological impacts caused by an influx of suspended sediments (Berry et al, 2003).

Federal and state agencies highly regulate natural gas infrastructure development regarding sediment discharge, though it should be noted that these particular regulations are not under the pipeline safety program. Within the Appalachian region of West Virginia, the United States Clean Water Act Section 404, and West Virginia Department of Environmental Protection (WV DEP) institute a system of permitting and guidance regarding development of natural gas infrastructure. The WV Department of Environmental Protection's General Water Pollution Control Permit requires final stabilization of natural gas development to exhibit a healthy vegetation coverage of at least 70% in disturbed areas with all fill slopes protected by measures to divert runoff (*General Water Pollution Control Permit*, 2013). Within the *Erosion and Sediment Control Best Management Practice Manual*, vegetation coverage is emphasized as the most important practice to prevent erosion and sediment (2016). It is also mentioned that right-of-way diversions, called "waterbars", are the most common sediment control used in pipeline construction.

In West Virginia, during and after natural gas pipeline construction, permits are held by the responsible company. Inspection by the permit holder is required weekly during active disturbances, bi-weekly in restored areas, and after any rain event greater than 0.5 inches (*General Water Pollution Control Permit*, 2013). When a site is deemed to be stable by the permit holder, a WVDEP inspector will conduct a final inspection of all permit-required features before the permit holder's bond is released. All inspections are completed on-foot across designated sections of pipeline. With the undulating topography of West Virginia, this can be a difficult and sometimes dangerous task. The use of UAVs and remote sensing systems can supplement pipeline safety, inspection, and management especially in areas that are remote or in topographies that are difficult to traverse (Gómez, C., & Green, D. R., 2017).

This study applies several UAV types carrying various remote sensing systems to a specific section of natural gas pipeline which contains several WV DEP permit-required features. Permission to access this pipeline section was secured from the responsible entity. Occupational Safety and Health Administration regulations were adhered during our research (*Enforcement Policy*, 2010). Multiple analyzes were conducted to identify the utility of each data type regarding pipeline safety, inspection, and management. Remote sensing systems utilized in the study include Light Detection and Ranging (LiDAR), RGB imagery, multispectral imagery, thermal imagery, and hyperspectral imagery. United States Geological Survey (USGS) manned aircraft LiDAR data was also included for comparison to UAV-based LiDAR.

These UAVs and accompanying remote sensors are cutting edge technology with vast opportunities of implementation within the oil and gas industry. As more utility is discovered regarding remote sensing systems, we highly anticipate an influx in the application of these technologies. UAV and remote sensing systems stand to greatly benefit oil and gas safety, inspection, and management. Enrichment of current methodologies through augmentation of UAV and remote sensing technology holds promise in increasing safety, efficiency, and accuracy for the industry. The goal of this study is to spotlight these technologies, identifying their utility as well as their shortcomings, and ultimately, encouraging future research regarding safety, inspection, and management of infrastructure within the oil and gas industry.

Background

Study Area

Our original proposal was to fly 2 one-mile contiguous sections for this project including ground sampling and GPS surveys. After multiple test flights on non-pipeline areas to calibrate equipment, develop workflow procedures, and test analytical approaches, we were granted access for ground sampling and permission to fly an Arsenal Resources (arsenalrsources.com) pipeline segment in Harrison County, WV. We also collected data on two properties owned by EQT (eqt.com) called Polar Vortex and Lako using multiple sensors. These flights were adequate to conduct our proposed research and answer our research questions.

The Arsenal Resources pipeline right-of-way extends southeast from a well pad with an area of 42,491m^2 (10.5 acres) (Figure 1). The elevation of this section of corridor is 417 meters MSL at its highest with the lowest being 345 meters MSL. This area contains several erosion and sediment control features including a nearly full coverage of perennial vegetation and water diverting structures, known as “water bars”, on sloping sections. The surrounding area consists of mostly sloping forest. The top section of pipeline closest to the well pad crosses under a gravel well pad access road; the southeast section runs adjacent to another gravel road which allowed for easy access to the site.

This area was comprised of two sections of a continuous pipeline separated by a natural gas well pad (Figure 1). The combined length of the two branches was approximately 2.3 km (1.45 miles) of managed and monitored pipeline was available for analysis. The southern branch was approved for construction 3 years ago and is bordered by forested lands. The northern branch completed construction and installation in early 2021 and runs through lands used for livestock grazing. There is no physical barrier barring animals from grazing upon the pipeline area. Flow interruption angled water bars are created along all pipeline areas with significant length and slope. Additional erosion control features on the test site include the surface application of hay, coir mats, hydro-seed, silt socks, and silt fences.

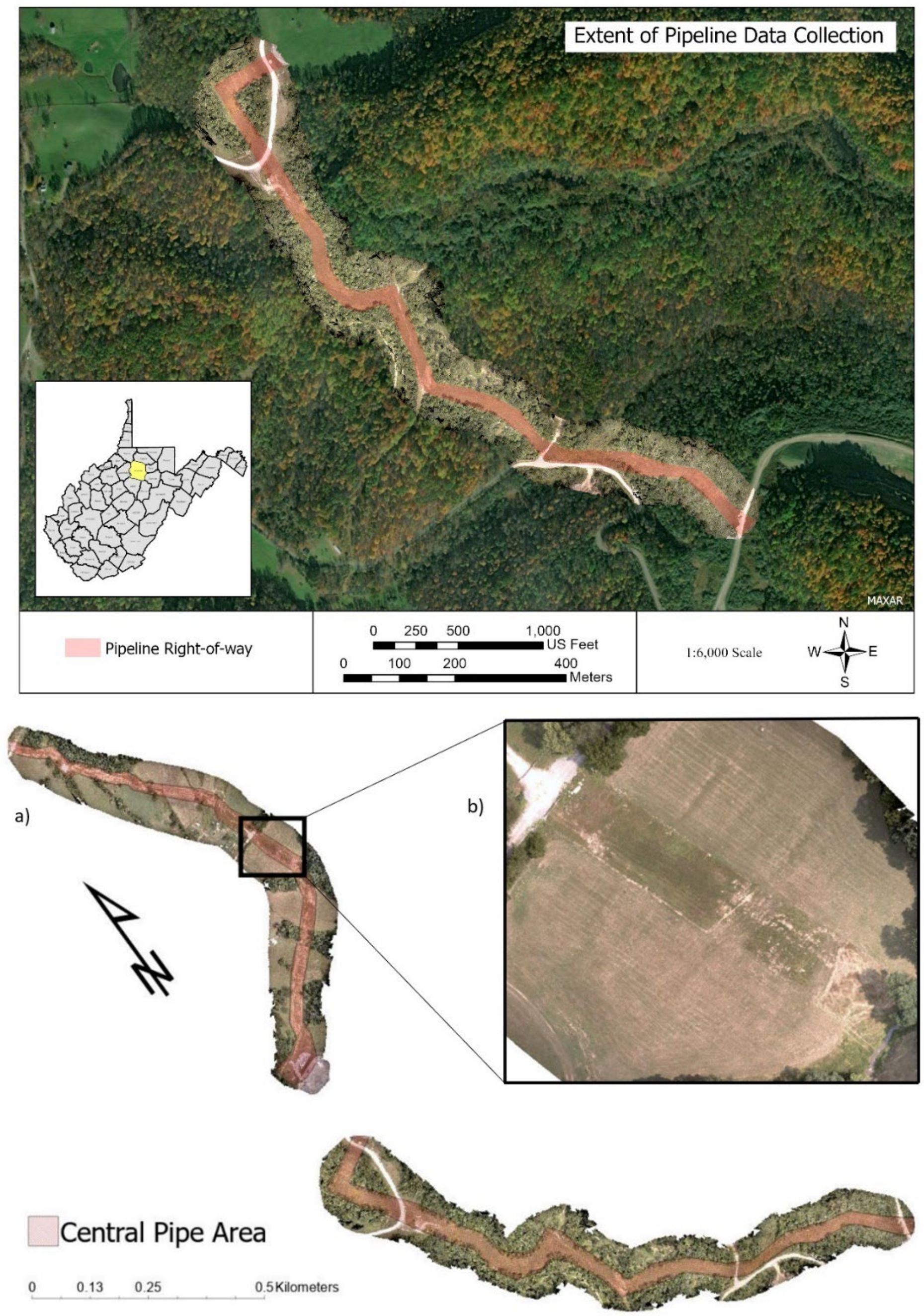

Figure 1. RGB orthomosaic of the study area displayed over satellite imagery
Approximately 2.3 km of natural gas pipeline used as study area for the UAV based evaluation of vegetation success in Northern West Virginia, USA. a) The full extent collected along the pipeline, with the area of vegetation assessment marked with red crosshatch. b) An expanded view of area enclosed in a) to enable a detailed view of the surface at the site. Note the surface variance in vegetation and disturbance in the linear pipeline area as compared to the surrounding agricultural field.

Pipeline Sites and Flight Dates

Arsenal Resources

Pritt South – Two 1.609km (1 mile) sections of pipeline.

3-4-2020 0.8km (0.5 mile), LiDAR

3-9-2020 0.8km (0.5 mile), LiDAR

4-21-2020 Two sensors, 0.8km (0.5 mile) per sensor, LiDAR and Multispectral/RGB

4-27-2020 Two sensors, 0.8km (0.5 mile) per sensor, LiDAR and Multispectral/RGB

5-5-2020 Two sensors, 0.8km (0.5 mile) per sensor, LiDAR and Multispectral/RGB

7-21-2020 Three sensors, 1.609km (1 mile) per sensor, LiDAR, Multispectral/RGB, and Hyperspectral

8-11-2020 Two sensors, 0.8km (0.5 mile) per sensor, LiDAR and Multispectral/RGB

8-15-2020 Two sensors, 0.8km (1 mile) per sensor, LiDAR and Multispectral/RGB

10-30-2020 Two sensors,0.8km (0.5 mile) per sensor, LiDAR and Multispectral/RGB

11-16-2020 Two sensors, 0.8km (1 mile) per sensor, LiDAR and Multispectral/RGB

12-9-2020 Two sensors, 0.8km (1 mile) per sensor, LiDAR and Multispectral/RGB

12-23-2020 Two sensors, 3.21km (2 miles) per sensor, LiDAR and Multispectral/RGB

1-6-2021 Two sensors, 3.21km (2 miles) per sensor, LiDAR and Multispectral/RGB

1-12-2021 Two sensors, 3.21km (2 miles) per sensor, LiDAR and Multispectral/RGB

3-6-2021 Two sensors, 0.8km (1 mile) per sensor, LiDAR and Multispectral/RGB

3-30-2021 Two sensors, 0.8k (1 mile) per sensor, LiDAR and Multispectral/RGB

5-13-2021 Two sensors, 3.21km (2 miles) per sensor, LiDAR and Multispectral/RGB

7-19-2021 Two sensors, 3.21km (2miles) 2 miles per sensor, LiDAR and Multispectral/RGB

8-27-2021 Two sensors, 1.6km (1 mile) per sensor, LiDAR and Multispectral/RGB

11-16-2021 Two sensors, 0.8km (0.5 mile) per sensor, LiDAR and Multispectral/RGB

12-8-21 0.8km (0.5 mile), LiDAR

3-29-2022 Three sensors, 1.6km (1 mile) per sensor, LiDAR, Multispectral/RGB, Thermal

Pipeline Near Grafton WV

4-22-2020 multiple sensors and flights .402km (0.25 mile), LiDAR and Multispectral/RGB

EQT Corporation

Polar Vortex Pipeline

1-13-2021 multiple sensors and flights, 1.609km (1 mile), LiDAR and Multispectral/RGB

Lacko Pipeline

5-25-2021 multiple sensors and flights, 0.8km (0.5 mile), LiDAR and Multispectral/RGB

Technologies Used

LiDAR is an acronym for Light Detection and Ranging (Argall and Sica, 2003). These systems are known as active sensors as a LiDAR unit emits its own light source. In contrast, passive remote sensing systems rely on reflected light from an external source such as the sun. LiDAR systems use a single or multiple lasers to scan an object or area (Argalland Sica, 2003). When laser photons contact an object such as the ground, some of the energy is reflected back to the LiDAR unit where a receiver acknowledges its presence (Royo and Ballesta-Garcia, 2019). The LiDAR system measures the amount of time it takes for the laser pulse to reach an object and return to the receiver. By doing so, it calculates the precise measurement of distance to the object. A single laser pulse may hit several objects consecutively from top to bottom which emit multiple returns (distance measurements) to the LiDAR receiver. The first return is typically from taller objects such as high vegetation while the last return is usually from the ground or a solid object. The inertial measurement unit (IMU) within the LiDAR unit measures yaw, pitch, and roll of the system which is combined with GPS data from an onboard GPS receiver. These two systems in conjunction with the distance measurement from the laser pulse allow for the creation of what is known as a point (Nex and Remondino, 2014).

A LiDAR generated point is a spatial reference of X and Y coordinate location and an associated elevation value. When scanning an object or area with a LiDAR system, this process happens hundreds to millions of times depending on the length of collection time. The data collected during the scanning is saved onboard the system. The data is then exported to computer software where a point cloud is generated. A point cloud consists of hundreds to millions of points with each point having an attribute of X-Y location and elevation (Figure 2). It is essentially a vector derived 3-D model with vast capabilities in computer software. From the point cloud, raster-based surfaces such as a Digital Elevation Model (DEM) can be generated for use in GIS mapping, modeling, and analysis.

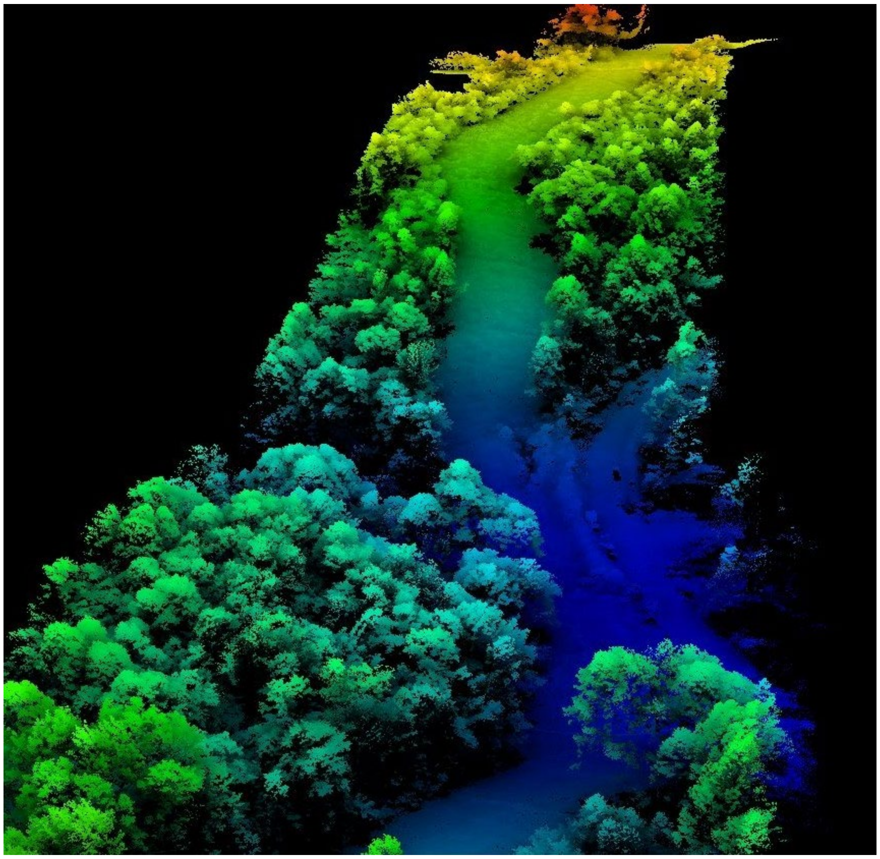

Figure 2. RedTail RTL-400 LiDAR point cloud of the pipeline right-of-way

The UAV-based RedTail RTL-400 LiDAR system used in the study functions using a microelectromechanical mirror (MEMS) and a 1550 nanometer laser to scan 40 degrees at up to 400,000 times per second (*Redtail LiDAR Systems*, 2022). It receives up to 3 returns per pulse with 20% reflectivity captured at up to 120 meters (400 feet) above ground level. Onboard the system is an Applanix APX-18 IMU/GNSS that utilizes a dual antenna system to output an absolute accuracy of 3-5 cm after data processing (*Trimble APX-18 LAND, 2022*). The RedTail RTL-400 LiDAR system outputs point clouds with 100 to over 1,200 points per square meter depending on flight height and object reflectivity. The flight platform used to carry the 2.2 kilogram (4.8 pound) RedTail LiDAR system is a DJI Matrice 600 Pro (Figure 3). Other heavy-lift UAV systems can be equipped with this system as well. The Matrice 600 Pro is a hexacopter style UAV that weighs 10 kilograms and has a max takeoff weight of 15.5 kilograms (*DJI Matrice 600 Pro*, (2022). It has a max speed of 64.37km (40 miles) per hour in a windless environment and can handle wind speeds up to 28.9km (18 miles) per hour at reduced flight speeds. We typically see flight times around 15 minutes per set of batteries when the Matrice 600 Pro is carrying the RedTail RTL-400 LiDAR system.

Figure 3. DJI Matrice 600 Pro equipped with the RedTail RTL-400 LiDAR System

UAV-based RGB Imaging and Photogrammetry

RGB cameras are passive sensors that capture the red, green, and blue wavelengths of light transmitted by the sun. When an RGB photograph is taken, each pixel within the photo captures a red, green, and blue value which are combined within the pixel to produce a color in the visible electromagnetic spectrum of light. Each pixel is combined into a grid that produces a photograph. Photogrammetry is a process of taking photos of an object or area with each photo overlapping front to back and side to side in raster fashion. The photos are processed using computer software that creates homologous points by matching pixels found in several images' overlap (Lingua & Rinaudo, 2000). Tie-points are created based on homologous points found in overlapping images, the orientation of the camera during the capture of each image, and the focal length of the sensor. Computer software then uses tie-points, triangulation, and depth maps to create a point cloud similar to LiDAR outputs. This process is complex but can be compared to how the human eyes are able to judge location and distance based on stereo view. Points within the photogrammetry point cloud are generally given a color attribute based on the RGB values from the initial image capture creating a colorized point cloud (Figure 4).

GPS integrated into a UAV-based camera system allows for spatial reference of photogrammetry outputs using horizontal and vertical coordinate systems. UAV onboard GPS systems used during aerial photo collection have an accuracy of around 2 to 15 meters (Rieke et al, 2011). The onboard GPS accuracy reflects directly on the spatial reference accuracy of the photogrammetry outputs. To increase these accuracies and reduce spatial error in the photogrammetry processing, ground control targets can be incorporated. These targets are positioned within the collection area. At least 3 ground control targets should be used; more than 3 are needed in larger areas. They should be placed at edges of the collection area and should also be evenly distributed around the center of the area. Ground control targets should be colored with high contrast for easy recognition within captured imagery.

Ground control targets or targets are placed throughout the area of interest before UAV-based imagery is collected. The center of each target is subsequently georeferenced using PPK (Post Processed Kinematic) or RTK (Real Time Kinematic) GPS receivers. PPK GPS requires post-processing of the collected data to correct the GPS measurements by referencing the National Oceanic and Atmospheric Administration, Continuously Operating Reference Stations network (*NOAA CORS Network*, 2022). This is easily completed by uploading the PPK GPS collection data to a GPS post-processing service website such as OPUS, the Online Positioning User Service (*OPUS*, 2022). PPK GPS data cannot be corrected using the Online Positioning User Service until 12 hours after collection. In contrast, RTK collection uses either two GPS receivers, a base station positioned on a known reference point and rover communicating through radio, or one GPS receiver connected to a GPS correcting service via an internet connection. This type of GPS collection corrects the GPS data in real-time with no need for post-processing. Once the center of each ground control target is collected with GPS, the corrected locations are input into the photogrammetry software during initial processing. Within the UAV-based imagery, the corrected GPS locations are applied to the center of each corresponding ground control target for every image in which one appears. Photogrammetry processing of imagery using ground control targets will output products such as point clouds, with far higher spatial reference accuracy using survey grade GPS receivers.

Another highly useful photogrammetry output is called an orthomosaic (Figure 1). This is a seamless aggregation of overlapping photographs into one image with an applied spatial reference. The pixel resolution of a single image used to create an orthomosaic is kept throughout the entire product displaying far higher resolution imagery than a single image taken of the same orthomosaic area. Edge distortion in a single image caused by the camera lens and sensor is greatly reduced or removed within an orthomosaic due to the high image overlap used in the photogrammetry processing. These products are extremely useful in GIS mapping, modeling, and analysis due to high pixel resolution, accurate spatial reference, and a new standard of temporal resolution compared to older methods.

Figure 4. RGB Photogrammetry colorized point cloud of the pipeline right-of-way

A DJI Phantom 4 Pro V2 with an integrated, gimbaled 20-megapixel RGB camera (Figure 5) was the UAV chosen to collect RGB imagery of the pipeline right-of-way. This system is a quadcopter with a total weight of 1.38 kilograms (3.03 pounds) (*DJI Phantom 4 Pro V2.0*, 2022). It can reach a maximum speed of 72.42km (45 miles) per hour and can fly in wind speeds of up to 35.4km (22 miles) per hour with slow flight speed. The battery allows for flight time of approximately 30 minutes per discharge cycle. The Phantom 4 Pro V2 has a forward, backward, and downward infrared vision system that aids in obstacle avoidance and autonomous landings. We have found that the newer Phantom series UAVs efficiently collect quality imagery for photogrammetry processing.

Figure 5. DJI Phantom 4 Pro V2

UAV-based Multispectral Imaging and NDVI Photogrammetry

Multispectral cameras are passive sensors which capture targeted bands or wavelengths of light within and out of the visible electromagnetic spectrum-based on their configuration. There are two main configurations of multispectral cameras. The first uses a single sensor and lens that captures and filters specific wavelength ranges. The other configuration uses multiple sensors and lenses with each capturing a specific range of wavelengths. Most multispectral sensors are designed to collect light wavelengths from approximately 300 nm (ultraviolet) up to 14,000 nm (long-wave infrared). The design of a multispectral camera and the wavelengths of light it can capture is generally dictated by its application. Multispectral cameras, such as those implemented in space exploration, can be configured to capture wavelengths from ultraviolet all the way to infrared. Another use of multispectral imaging is to conduct analyzes in an agricultural setting or other applications regarding vegetation. These types of sensors are generally designed to capture the red, green, blue, and near infrared spectrums of light.

Specific bands of light such as red and near infrared are captured for vegetation analysis due to the photosynthetic properties of most flora. Most vegetation appears green as it is reflecting green light and absorbing most of the other visible electromagnetic spectrum. What we are unable to see with our eyes is the reflection of near infrared light. Multispectral sensors optimized to analyze vegetation allow for the creation of raster-based indices such as NDVI which stands for Normalized Difference Vegetation Index. This index is created using the red and near infrared bands of light in which the reflectance values are applied to a normalizing equation (NIR-Red) / (NIR + Red) to output a value between -1 and 1. Healthy vegetation reflects more near infrared light and absorbs more red light. Unhealthy vegetation and other objects such as soil exhibit the inverse, absorbing more near infrared light and reflecting higher percentages of red light. Healthy vegetation will output values closer to 1 using NDVI while degraded vegetation will give values closer to -1. This index has become a standardized measurement of vegetation health and abundance.

Using UAV-based multispectral imaging, we can capture the red and near infrared bands in images within a study area which can be input into photogrammetry software in a similar manner as the RGB photos mentioned earlier. Rather than the output from the photogrammetry software being an RGB orthomosaic and point cloud, the software computes an NDVI value for each pixel and point in the output, combining the red and near infrared imagery into an NDVI referenced orthomosaic and point cloud. This process allows for NDVI analysis to be conducted on an area of interest in a relatively short period of time.

To collect multispectral imagery of the pipeline right-of-way, we used a Sentera 6X multispectral sensor (Figure 6). This sensor weights just over half a pound at 290 grams and has a gimbaled array of 6 imaging sensors those being a blue (475 nm), green (550 nm), red (670 nm), red edge (715 nm), and near infrared (840 nm) single band sensor as well as a 3 band, 20-megapixel RGB camera sensor (*6X Sensor*, 2022). The system also uses a sun irradiance sensor attached to the UAV to correct for lighting changes within the collected imagery. A DJI Matrice 200 V2 was used to carry the Sentera 6X multispectral camera (Figure 6). This UAV platform weighs 4.69 kilograms (10.78 pounds) with a max flight time of 38 minutes without a payload (*Matrice 200 series V2*, 2022). We typically get 30 to 35 minutes of flight time with the Sentera 6X payload attached. The Matrice 200 V2 is capable of flight speeds up to 80.95km (50.3) miles per hour and can operate in wind speeds of up to 43.45km (27 miles) per hour (*Matrice 200 series V2*, 2022). The gimbal mounting attachment is versatile, able to power and communicate with multiple sensor types. Another intriguing feature of the UAV is the Ingress Protection rating of 43 meaning it can withstand ingress of small objects and is water resistant (dirt and rain resistant). It too includes a forward, upward, and a downward infrared visioning system for obstacle avoidance and autonomous landing. Some UAV systems struggle to operate in low ambient temperatures due to reduction of lithium-ion battery output when the cells become cold. This is not an issue with the Matrice 200 V2 as the batteries are internally heated to allow for operation in temperatures down to –20 C (4 degrees F).

Figure 6. DJI Matrice 200 V2 equipped with Sentera 6X Multispectral sensor

UAV-based Hyperspectral Imaging

Hyperspectral cameras are passive sensors configured to capture many, small bands of the electromagnetic spectrum. In contrast, the RGB and Multispectral sensors mentioned earlier capture fewer, large bands of the electromagnetic spectrum. Depending on the design, hyperspectral sensors can capture anywhere from 20 to several hundred narrow bands of light. Hyperspectral images store information from each band in what can be thought of as a 3-dimensional stack of images known as a cube. The X and Y dimensions of the cube consists of the extent of each image or pixel array, the spatial dimension. The Z dimension, known as the spectral dimension, represents layers of images, each containing an adjacent electromagnetic band captured during the hyperspectral collection. Each pixel within an image layer or spectral dimension of the cube contains a reflectance value for its corresponding band. Obtaining the pixel values for the same spatial dimension coordinate in every image layer creates a spectral reflectance curve of all bands captured by the hyperspectral sensor (Padoan et al, 2008). In other words, a single image can be created in which every pixel contains a spectral reflectance value for every band that was collected; if 200 bands were collected by a hyperspectral sensor, the final image would have 200 reflectance values within each pixel. This technology introduces the ability to conduct a multitude of spectral analyses including production of spectral index rasters such as NDVI, mentioned earlier.

Hyperspectral imagery of the study area was captured using the Bayspec OCI-F Hyperspectral Imager (Figure 7) carried by a Matrice 600 Pro, the same UAV used to collect LiDAR. The Bayspec OCI-F collects 120 spectral bands from 400nm to 1000nm (visible to near infrared) in 5nm increments (OCI™-F Hyperspectral Imager, 2020). It is described as a miniaturized push-broom style hyperspectral sensor ideal for all airborne applications. The system functions under a UAV via a large gimbal to keep the sensor facing nadir; a small remotely operated computer triggers imagery collection and stores the data.

Figure 7. Bayspec OCI-F Hyperspectral Imager

UAV-based Thermal Imaging and Photogrammetry

Thermal cameras are another type of passive sensor that utilize a special lens and sensor array to capture infrared radiation. The intensity or quantity of infrared energy emitted by an object is captured by each pixel in the sensor array (Akula et al, 2011). Computations within the sensor are conducted to convert the per pixel infrared energy intensity into a Fahrenheit or Celsius value. A grayscale or color gradient symbology is applied to each pixel based on the associated temperature value of the pixel creating a visible image where image color or brightness corresponds to a temperature value. Most modern thermal imaging sensors function as such which is referred to as radiometric. This describes the image output as having a temperature value for every pixel. Radiometric outputs can be calibrated if needed to compensate for error due to data collection conditions. Non-radiometric thermal sensors are only able to output a temperature value measured at the center of the sensor or viewport and do not store a per-pixel temperature value. Radiometric thermal imaging has vast application throughout research and industry.

UAV-based thermal imagery capture was performed flying the DJI Matrice 200 V2 (Figure 8), the same UAV used to collect the multispectral imagery. For this collection, it was equipped with the DJI Zenmuse XT2. This gimbaled thermal sensor weighs 0.62 kilograms (1.39 pounds) and is produced by FLIR (*Zenmuse XT2 – DJI*, 2022). It has a 13mm lens on the thermal sensor able to collect 7,500nm to 13,000nm (long-wave) infrared radiation. The detectable temperature range is from -40° to 550° C (-40° to 1022° F). A 12-megapixel RGB camera accompanies the thermal sensor for visual aid and optional RGB imagery capture. The RGB sensor can also outline objects within the thermal imagery in real-time to enhance the visual edge of objects within the thermal imagery. This sensor is highly useful for visual temperature inference and mapping.

Figure 8. DJI Matrice 200 V2 equipped with DJI Zenmuse XT2

Airplane-based USGS LiDAR

The United States Geological Survey LiDAR derived DEM used in this study was collected via a manned aircraft equipped with a LiDAR sensor. USGS has flown LiDAR over almost the entire United States. Manned airplane LiDAR sensors work on the same basic principles as UAV-based LiDAR sensors with the same datatype outputs. An airplane is flown in a grid pattern, as is a UAV, to scan a study area with a LiDAR sensor's laser, obtaining point locations with elevation values to produce a point cloud. The USGS LiDAR data has a vertical accuracy of 10cm and a point density of 2 to 8 points per square meter (3D Elevation Program, n.d.). High accuracy DEMs are generated using point cloud-based interpolation methods such as Triangulated Irregular Networks (TINs) (Worstell et al, 2014). The 1m resolution DEM tile covering the pipeline right-of-way study area was found through a USGS website containing a map interface displaying all U.S. areas with available data. These DEM tiles as well as other spatial products are easily obtained from the USGS National Map – Data Delivery website (*The National Map - Data Delivery,* n.d.). All these products are applicable to a GIS setting and no payment for data acquisition is required.

Sensor Tests

For testing the sensors, thermal was evaluated for surface water detection, and RGB was evaluated for terrain mapping (structure for motion) and surface derivatives including the pipelines at a landscape context scale. The multispectral and NDVI derivatives are discussed further in this study and the LiDAR data was used to model surface water flow and erosion potential.

The hyperspectral camera did not produce useable data products. The GPS integration with data, manufacturer data processing software and workflow did not perform as advertised. The specific units were relatively inexpensive hyperspectral units from BaySpec which was essentially a bench spectrometer gimbalized to fly on a drone. The manufacturer could not provide technical support to make this data collection and processing feasible. Even with the project extension, a solution was not found from the vendor to allow us to include the hyperspectral test for this study. We look forward to future advances and a more mature product roll out of hyperspectral and drone integration by BaySpec for us to investigate this further.

Methods for Vegetation Classification

Test Plots and Classification

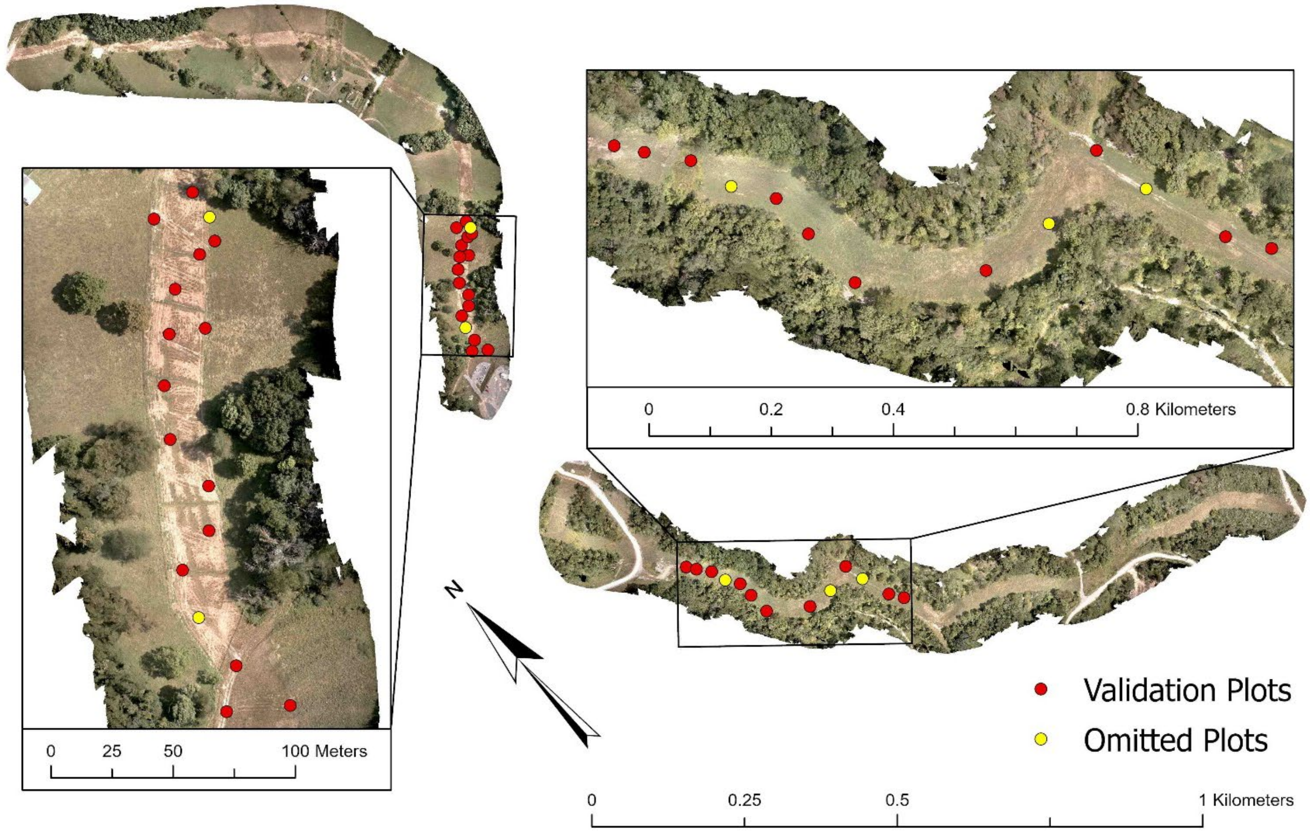

Figure 9.Location of the ground validation plots established in the study area. Inserts show each of the allowed access areas of the pipeline. Red indicates plots used for validation and yellow indicates omitted plots.

The study area's permit holder allowed the establishment of 30 small unobtrusive testing plots for the purpose of conducting a vegetation analysis. Across the study area, 30 randomly placed plots were established and located using a Garmin Dakota 10. The Garmin Dakota 10 is a high sensitive GPS with HotFix satellite prediction and Wide Area Augmentation System (WAAS) accuracy for better than 1m 95% of the time (Kumar and Dutt, 2020). Each plot was created using high-visibility survey marking spray to create the 4 corners surrounding an area of approximately 1.44 m^2 (1.2 m × 1.2 m) (Figure 9). This size was selected to allow the internal area of each plot to provide an area of approximately 1 m^2 of pixels unaltered by the survey marking spray. This area was selected after interviewing several pipeline inspectors, as a sample size of 1 m^2 was stated as the size used for current evaluations as captured from a randomly cast surface sampling hoop. To create continuity between foot and drone imagery, the top of each test plot was indicated by a solid line connecting the two respective corners, and a two-digit number was created just outside and beneath the bottom right corner. Numbers ranged from 00 – 29. Upon completion of marking the plot, an image was captured using a hand-held 12-megapixel camera from a height of approximately 1.8 m. These ground perspective high-resolution images were collected for the future integration of subject matter expert (SME) classification into this study.

Figure 10. Example of training plot established to denote areas on pipeline that failed vegetative cover threshold. Plot is approximately 1m square and used a 2-digit identifier outside the bottom right corner

After establishing a sample plot, the field technician recorded the approximate center using the handheld GPS. The plot was then evaluated to be passing or failing based on the percent of the plot that was vegetated. Greater than 70% of the plot being vegetated indicated a passing site and less than 70% was failing. An example of a failing site is shown in Figure 10. To avoid over-selection from a single area, the field technician was tasked with creating no more than two test plots of the same category within 25 m of each other. This distance was calculated in the field from measurements provided by the handheld GPS unit. Plots were established in this way across the study area.

Multispectral Collection

Once sample plots were established, a DJI Matrice 200v2 quad-propeller drone with a direct interfacing Sentera 6x Multispectral sensor conjoined with an apex oriented solar sensor was used for remote data collection. The deployed combination of drone and sensor used in this study were selected for their flexibility and capability in UAV based multispectral research. The 6x Multispectral sensor simultaneously collects from 5 individual wavelengths: blue (475 nm), green (550 nm), red (670 nm), red edge (715 nm), and near infrared (NIR, 840 nm). Additionally, the 6x sensor is equipped with a 20MP RGB camera. The Sentera 6x sensor performs a simultaneous capture from all 6 sensors on a preset trigger period. For our collection, we set the trigger to occur every 2 seconds. Flight planning and execution was achieved with the UgCS Client. Through this software we could load in elevation maps, break each branch into transects, and generate a total flight path at a fixed distance above the terrain. The height above terrain used was 91.44 m (300 ft), and the sensor was oriented at nadir throughout the flight. Both flights occurred on the same day between 1130 and 1330 EST to minimize light variance and shadows. Immediately prior to collection, the multispectral sensor captured a series of calibration images of a Sentera Reflectance Panel for future radiometric correction. When the flights were completed, research moved into the analysis portion of the plan of study (Figure 11).

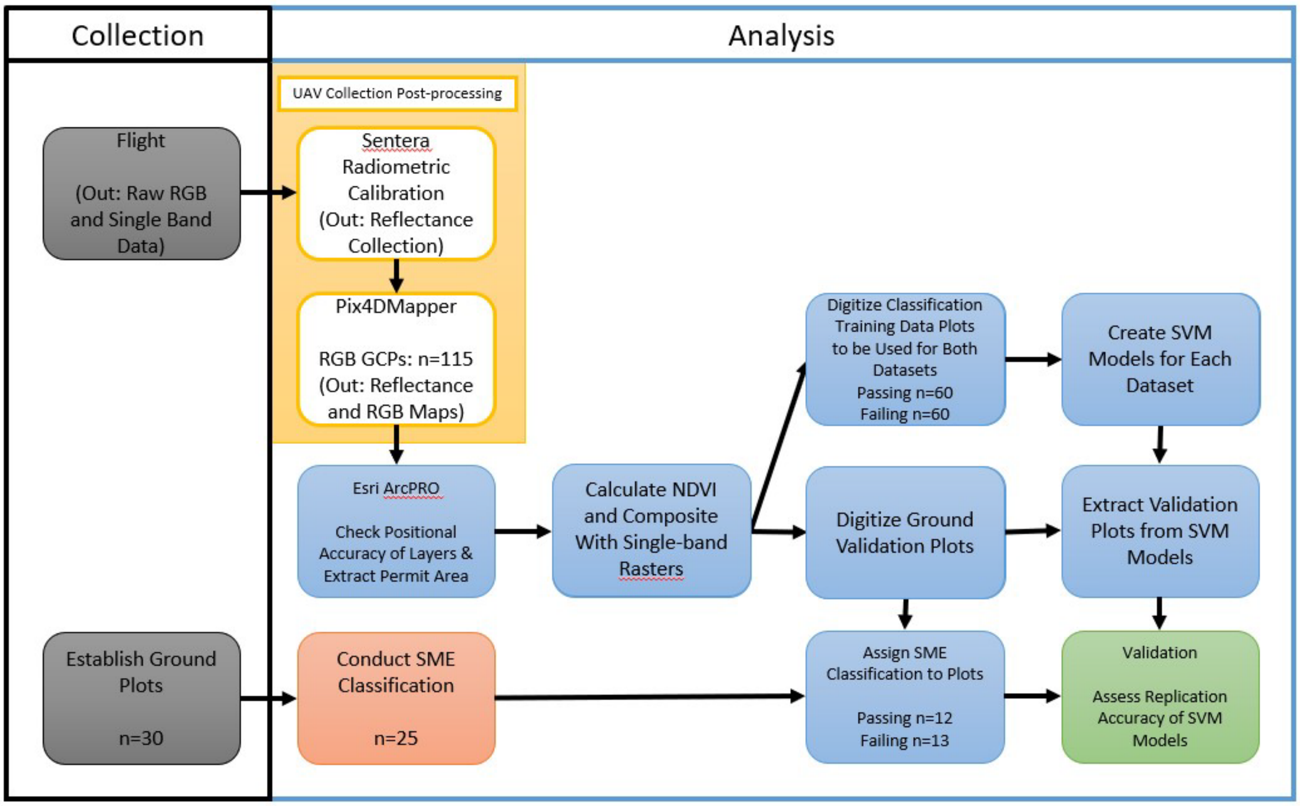

Figure 11. Workflow used to capture remote sensor data and ground sample points. Post-processing of the UAV data was conducted in two separate programs, with final analysis occurring in Esri ArcGIS Pro v2.9.2.

Plot Classification

Desiring the integration of current inspection quality standards into our study, the research team coordinated with SMEs to collect a classification judgement from each plot. For this area of study, an SME was defined as an individual who had received training and certification in the pipeline inspection process and conducted such inspections in the

Appalachian region for a period of at least 5 years. As most approached SMEs were still associated with this industry, anonymity was promised for their assistance.

The previously collected pictures of each plot were shared, and judgments were made as to the official classification of either passing or failing for the plot. Many plots had images taken at different angles with all pictures capturing the same plot being grouped by file. These groups of images were shared on a 17.3 inch 1920 x 1080 monitor in a random order for the classification step. At the request of the inspector, images of any single plot could be switched between, enlarged, and scrolled over to assist in this assessment step. Final classification was determined from the grouped judgment of each plot individually. If the classification was uniform, the plot was classified as either passing or failing as appropriate. If there was a discrepancy in SME classification, we marked the plot as being of an indeterminate class.

Reflectance Map Creation

The Sentera 6x Multispectral sensor performs limited on-the-fly sensor adjustments based on changes in detected solar intensity; however, radiometric calibration is only achieved through a post-processing technique provided to the end user by Sentera. This software reviews all collected single band images and detects the calibration images captured pre-flight to determine reflection adjustments to be made. Additionally, the software identifies the sensor settings and solar readings recorded in the metadata of each image. From these pieces of information, the radiometric correction software adjusts the values of every pixel in the dataset to the reflectance values correct to the atmospheric conditions at collection. The corrected single band images were then loaded into Pix4Dmapper Version 4.6.4 to create total reflectance maps for the site.

Pix4Dmapper aligns the images according to the GPS data recorded in the EXIF portion of each image and begins to identify tie-points between neighboring images. These tie-points guide the final orientation and transformation of each image. The data from the separate bands is also aligned, creating a near absolute georeferencing between the separate simultaneously captured data. The output of this process is a separate single band rasters in the form of an orthomosaic map of the reflectance values, as calculated across the site. This process was repeated with the RGB dataset collected by the 20 MP sensor. 115 ground control points were identified in a composite display of the red, green, and blue reflectance bands, and these points were used to tie the RGB dataset to the reflectance maps. A natural color orthomosaic was then produced and exported for the study area. The spatial resolution of the multispectral raster and the RGB raster were 0.042 m and 0.063 m respectively.

GIS Analysis for Classification

The red, green, blue, and NIR reflectance maps, and the RGB orthomosaic for the study area were then loaded into Esri's ArcGIS Pro (Esri, 2021) for preparation, extraction, classification, and analysis. A new set of ground control points, hereafter called the alignment assessment point set (AAPS), were established between the two datasets to quantify any distortion, ensuring the data were reasonably aligned for analysis. Using the RGB orthomosaic of the site, polygon features were created to digitize the permit areas at a 1:1,000 viewing scale. All pixels from every dataset within this polygon boundary were extracted for analysis. The single band layers were composited using the Composite Bands tool, and the Band Indices tool was used to calculate a normalized difference vegetation index (NDVI) layer. NDVI acts as a simplified indication of vegetation health by detecting photosynthetic activity (Tucker, 1979). NDVI is calculated for each pixel from collected reflection values of the red and near-infrared

(NIR) bands of light as:

$$NDVI = \frac{NIR - Red}{NIR + Red}$$

As solar light reaches a plant, red light is absorbed by the chlorophyll, while the unusable NIR light is reflected or scattered by the mesophyll layer (Campbell and Wynne, 2011). NDVI values range from -1 to 1, with higher scores associated with healthier vegetation and lower scores being associated with artificial objects. Agriculturally minded multispectral sensors, like the Sentera 6x, are often designed for derivative NDVI calculation, and as such, this technique was included. The produced NDVI layer was composited with the clipped single band rasters for simplified inclusion in classification.

Ground sample plots were then digitized using the RGB raster. All 30 plots previously established were successfully identified. The associated plot numbers and determined SME classification were entered for each plot. 1 and 0 was used to indicate passing and failing classification respectively. Plots with an indeterminate classification were left with a null value.

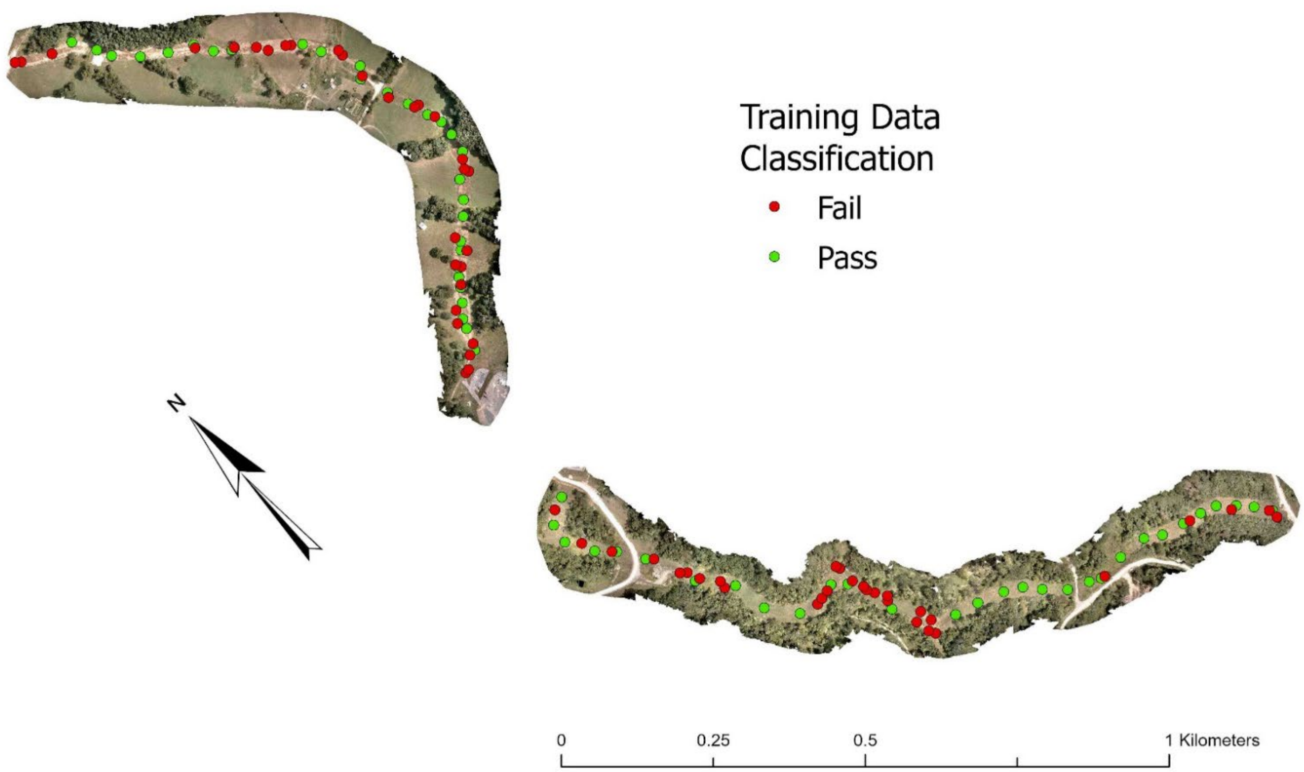

Figure 12. Manually digitized training data samples for SVM classification. Samples were created at a scale of 1:100. There were 120 samples created, 60 for each class, with 30 per class established in each branch of the pipeline.

A GIS technician manually digitized the classification training data across the study site at a 1:100 display scale following a simple random sampling plan. This process was completed using the ArcGIS Pro Training Samples Manager on the RGB dataset. Classes for this training data set were either pass or fail, with the associated values of 1 and 0 respectively. Training samples did not include any digitized ground sample plots and were established across the entire study area. There were 30 features established each for passing and failing classes in each branch, totaling 120 training features for the study area (Figure 12).

There are two separate categories of items which were digitized in this study. The first type are ground sample plots. Prior to UAS collection, these plots were established in the field by a team member using survey paint. An image of each ground sample plot was then captured by the team member. After the UAS collection was completed, the images captured by the field team member were then shown to the SMEs, so that a classification would be assigned to each of these ground sample plots. These classified plots would then be used for validation of the model, having them referred to as validation plots for this step of the process. During this SME step, ground sample plots which had an inconsistent classification, meaning that there was disagreement between SMEs whether the plot would pass or fail their vegetation evaluation, were identified. As these inconsistently classified plots would be unsuitable to use as validation data, as this study is evaluating how closely this technique replicates inspector classifications, these plots were omitted.

Once the orthomosaic of the site was formed, these ground sample plots were all located in the imagery. A shapefile was formed inside the bounds of each of these plots, care being given to not capture any of the survey paint that marked the exterior of the plot. It was necessary to digitize these plots in order to avoid any of their usage in the soon to be discussed training data, as well as prepare them for their use in validating the model.

The second category of digitization in this study are data used to train the classification model. This model was created following a supervised classification approach, which is to say the model is formed from training samples selected prior to running the selected algorithm across the study area. The creation of these samples followed standard GIS practices of this type of classification and did not contain any portion of the validation plots. Training data was only categorized as passing or failing, with none having a null value. This allowed the model to produce a binary classification of passing and failing at a pixel to pixel level.

Support Vector Machines (SVM) was the chosen classification algorithm, due to its noted accuracy at smaller spatial resolutions compared to other common algorithms (Sheykhmousa et al., 2020). In ArcGIS Pro, the Train Support Vector Machine Classifier tool was used with both datasets, producing a definition file for each. The maximum number of samples per class was left at the default value of 500 to avoid the over-fit nature of kernel-based classifications (Liu et al., 2017) while avoiding a loss of accuracy from under sampling (Sabat-Tomala et al., 2020). The Classify Raster tool then processed the datasets with their respective SVM definition files, creating sitewide supervised classification of either passing or failing vegetation assessed at the pixel level (Figures 13 and 14).

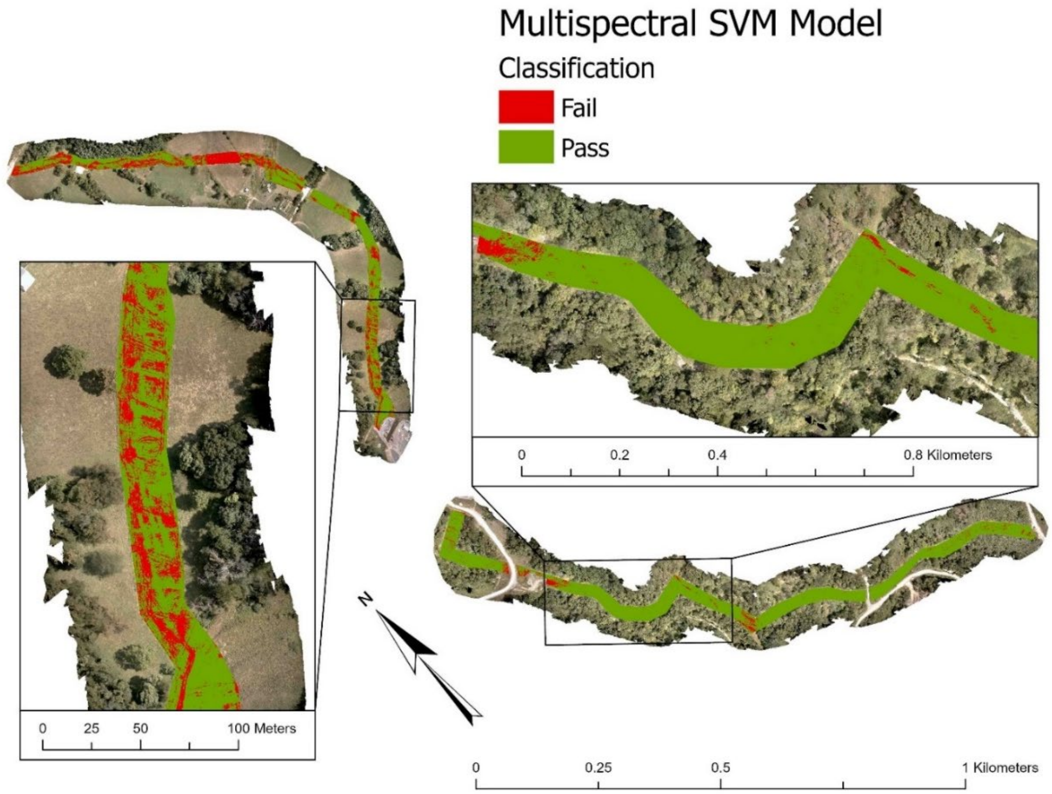

Figure 13. SVM classification model of the multispectral dataset using blue, green, red, and NIR bands with NDVI included. Green and red pixel color indicate passing or failing respectively as determined by the model. Inserts are included for a more detailed look at the extent available for validation plots. Spatial resolution of this model is 0.042 m.

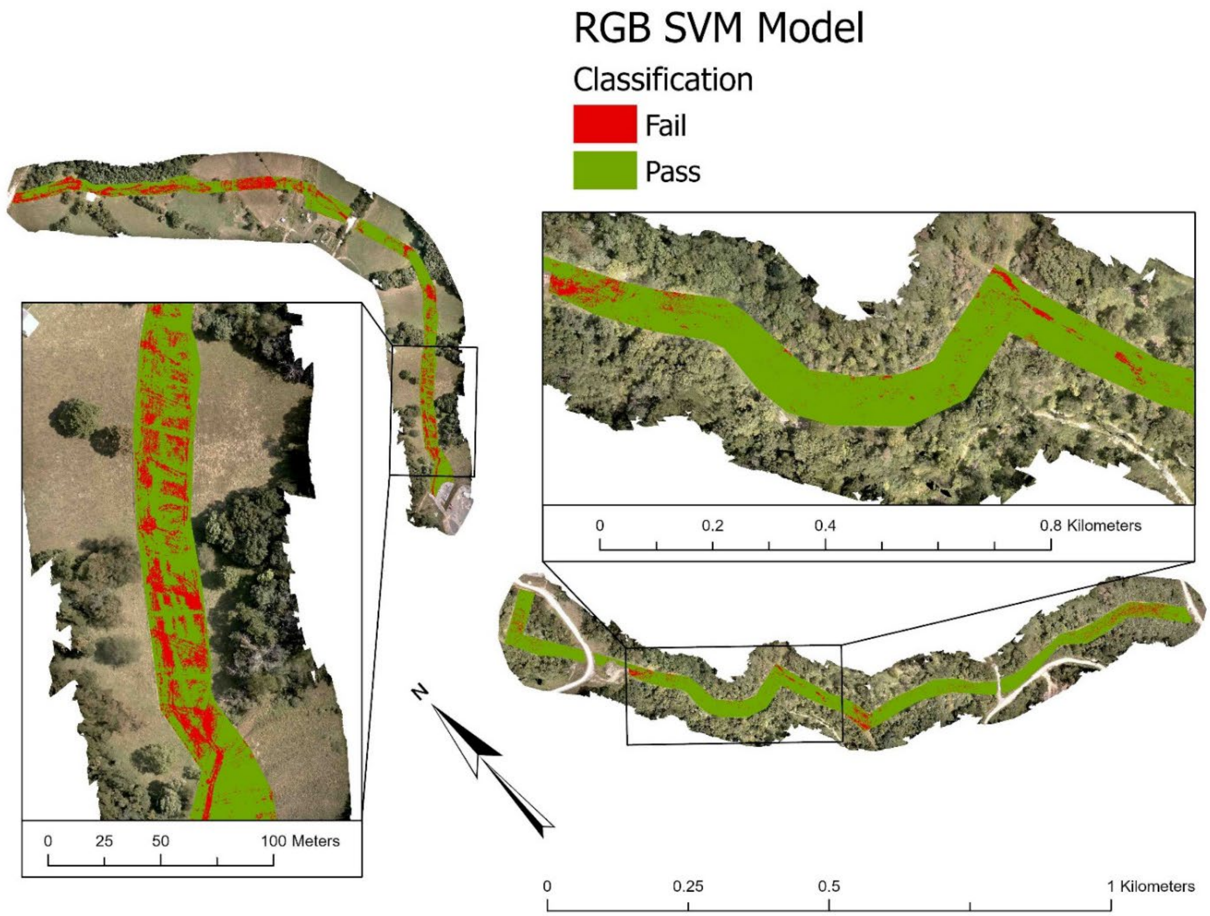

Figure 14. SVM classification model of the RGB dataset. Green and red pixel color indicate passing or failing respectively as determined by the model. Inserts are included for a more detailed look at the extent available for validation plots. Spatial resolution of this model is 0.063 m.

Replication Accuracy

From the SVM models, the cells of the validation plots were extracted. Passing and failing cells were noted as 1 and 0 respectively. The mean value of the cells were calculated with the Zonal Statistics as Table tool in GIS to present the proportion of passing vegetation within each plot. Following the WVDEP definition of passing vegetation (West Virginia Department of Environmental Protection, 2013), mean values above 0.70 were determined to have been modeled as passing, with values below this number indicating a failing plot. A confusion matrix was then structured for each model, comparing the modeled and SME judgments for these plots, and providing a validation assessment for each model's performance. For each model the user's accuracy, producer's accuracy, overall accuracy, and kappa were calculated.

Methods for Sediment Modeling

The pipeline right-of-way which represented the segment used for the field evaluation with the UAV was initially hiked on foot before any UAV-based remotely sensed data was collected. The foot inspection was to familiarize ourselves with the features within this specific pipeline corridor. We were looking for obvious change at the site that would be related to the disturbance area for the pipeline. Examples included changes in vegetation density, health, and contiguity with other vegetation growth in the corridor were considered. This process helped with UAV flight planning as changes in ground elevations and tree canopy heights were noted. Multiple water and sediment control features, required by the *General Water Pollution Control Permit,* were identified (2013). Several water diverting structures "waterbars" were located exhibiting poor structural integrity. A few areas within the pipeline corridor were found with poor or no perennial vegetation coverage. Also, a small landslide "slip" was identified within the pipeline right-of-way.

UAV-based LiDAR

The LiDAR data was collected over the pipeline right-of-way at an altitude of 60 meters (196.85 feet) above ground level with the UAV flying 7 meters per second (15.66 miles per hour). A 15% to 20% side of scan overlap was used to ensure full scanning coverage of the pipeline corridor. The autonomous flight path was created and executed using Universal Ground Control Software known as UgCS (SPH Engineering, n.d.). A function within UgCS called terrain following allows the UAV to fly at a constant elevation above the ground surface. This is highly useful in LiDAR collection as changes in flight elevation above ground level will change the swath width of the laser scanning. Using the software requires a computer or laptop to plan the autonomous flight specifications which are then uploaded to a tablet connected to the UAV's controller. The uploaded autonomous flight specifications were executed within the tablet where current flight attributes such as UAV speed and altitude were monitored. The autonomous flight took approximately 12 minutes to complete, and the UAV was landed manually for a precise touchdown.

A raw LiDAR data processing workflow was followed to assure a consistent and documentable approach to allow duplication (Figure 15). Once the UAV was landed, a data transferring cable was connected from the RedTail RTL-400 LiDAR unit to the RedTail Ground Control Station to transfer a copy of the raw LiDAR data. The raw data stores on both systems after transfer for redundancy. A standalone iGage iG3s GNSS receiver was set up to collect a separate series of PPK GPS epochs before, during, and after the LiDAR collection flight (iGage iG3s, n.d.). This GPS data was corrected using OPUS and was input into a later processing workflow to increase the spatial accuracy of the LiDAR product. The raw LiDAR data was processed using commercial and proprietary software. A Smoothed Best Estimate of Trajectory (SBET) was created using Applanix POSPac MMS 8 software that processes the standalone iGage iG3s receiver GPS data and the flight trajectory and GPS data collected by the Applanix IMU/GNSS onboard the LiDAR unit (*POSPac MMS 8*, 2022). The raw LiDAR data and SBET were input into the proprietary RedTail Point Cloud Generator software provided with purchase of the RedTail RTL-400 LiDAR unit. This software output a highly accurate point cloud in the specified North American Datum 1983, Universal Transverse Mercator Zone 17 North (NAD83 UTM Zone 17N) coordinate system within a few minutes; elevation values of the point cloud were output in ellipsoidal heights.

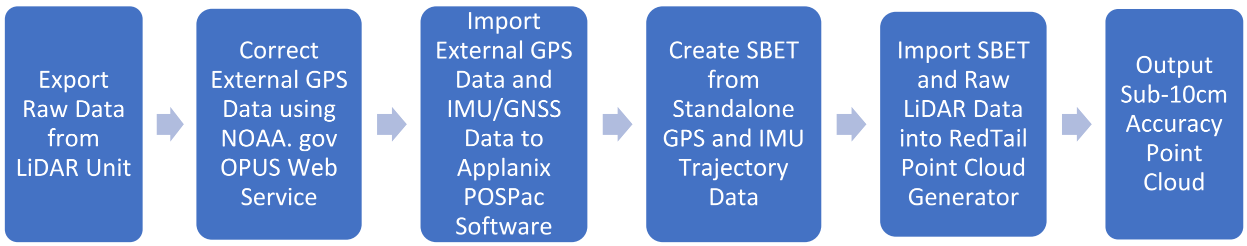

Figure 15. Raw LiDAR data processing

Post-processing of the LiDAR point cloud was completed using *LiDAR360 (Version 5.3)* software (2022) (Figure 16). The unclassified point cloud was first cleaned of outlying (error) points caused by noise within the LiDAR system during collection. Unclassified points are those that have not been given a class attribute such as ground, low vegetation, building, etc. The next step was the removal of points outside of the pipeline right-of-way. We were only interested in the pipeline right-of-way so removing unassociated points helped to reduce post-processing times. Ground points were classified, removing points that reflected anything other than the ground surface. The final step in LiDAR360 processing was generating a 20cm cell resolution DEM for further analysis.

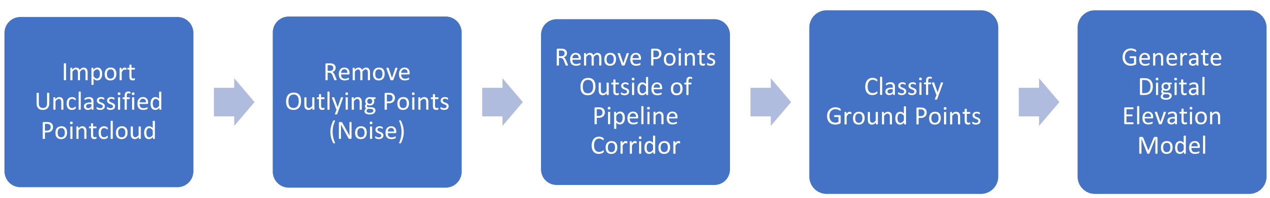

Figure 16. LiDAR360 point cloud post-processing

ArcGIS Pro (Version 3.0.2) was used to produce and analyze terrain derivatives from the LiDAR procured 20cm cell resolution DEM (2022) (Figure 17). The Define Projection tool was used to inform the software of what coordinate system the DEM was created in. A 20cm Hillshade was produced from DEM for viewing purposes. This tool adds grayscale relief to the elevation model using a specified sun azimuth value, adding shadows to the topography of the model. Separate from the creation of the Hillshade, the DEM was filled of sinks, areas that would affect results of a flow accumulation analysis, using the Fill tool. The filled DEM was then input into the Flow Direction tool which outputs a 20cm raster with 8 different flow direction possibilities based on the 8-cardinal direction of slopes within the DEM. Lastly, the Flow Direction surface was used within the Flow Accumulation tool to output a 20cm Flow Accumulation raster grid representing cell-based flow and accumulation paths that water would take throughout the topography captured within the DEM.

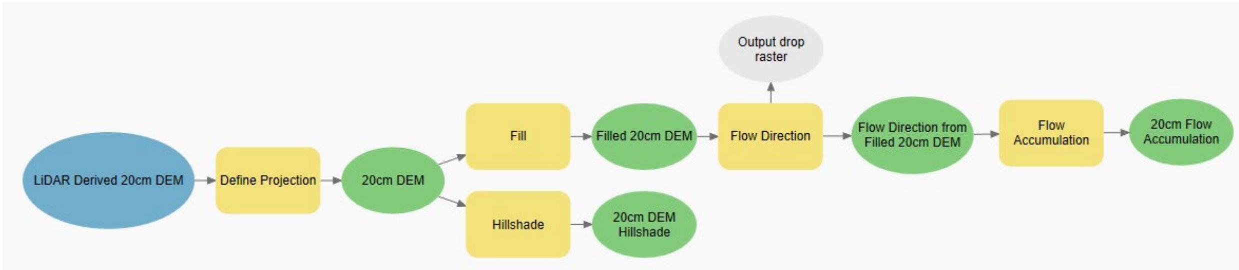

Figure 17. UAV-based LiDAR 20cm Flow Accumulation analysis workflow

The 20cm DEM was used to analyze the elevation profile of waterbar #18. This waterbar was chosen as the flow accumulation analysis highlighted accumulation of synthetic waterflow passing over it rather than being properly diverted by the waterbar, away from the pipeline corridor. (Figure 18). To obtain elevation profile results, the 20cm DEM was used in the Focal Statistics tool to output an averaged 20cm DEM. Within the tool a circular window with a 5-cell radius was chosen. The Focal Statistics tool then computes an averaged value for all cells in the DEM by applying the mean of neighboring cells to the center cell within a 5-cell radius moving window. The original DEM and the Focal Statistics averaged DEM were input into Raster Calculator where the averaged DEM was subtracted from the original DEM to produce a 20cm Slope Position surface. This raster-based surface contains cell values corresponding to local topographic positions of elevations where higher values define higher elevations, or peaks, and lower values define lower elevations, or troughs. A vector Shapefile was drawn across part of waterbar #18 to get the Slope Position values associated with the vector. The vector and Slope position surface were input into the Stack Profile tool to output a Microsoft Excel table containing Slope Position values along the vector. A line graph showing a Slope Position profile of waterbar #18 was then generated within Microsoft Excel. Slope Position was used rather than a DEM as it discounts the effect of slopes within the surface while analyzing the profile of local elevations.

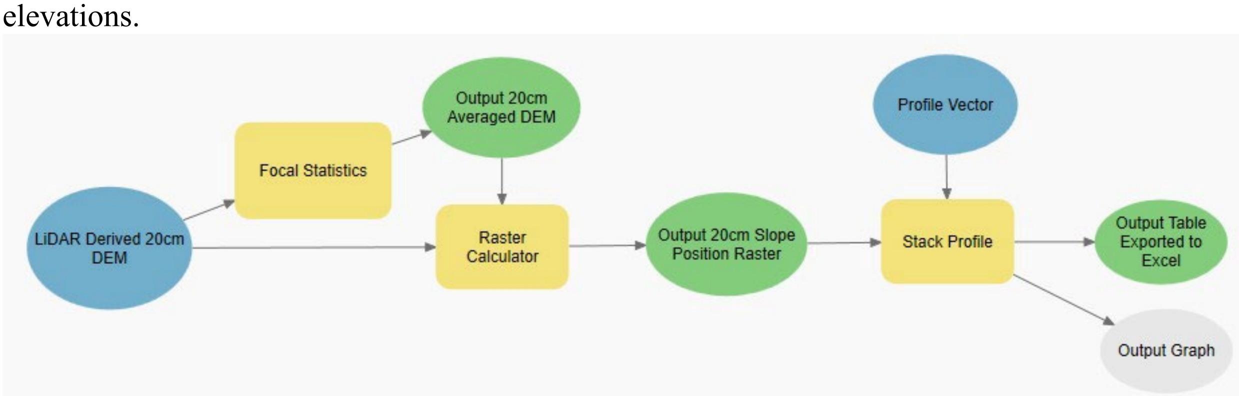

Figure 18. UAV-based LiDAR Slope Position Profile workflow

The System for Automated Geoscientific Analyses (SAGA) was used to produce other terrain derivatives from the LiDAR-based 20cm DEM (Conrad et al., 2022). Within SAGA, the Basic Terrain Analysis tool was executed using the DEM as the input. Wetness Index and Slope Length and Steepness Factor (LS-Factor) raster surfaces were created as part of the Basic Terrain Analysis tool. These data were exported for use in ArcGIS Pro.

UAV-based RGB Imaging and Photogrammetry

UAV-based RGB imagery collection of the pipeline right-of-way was executed using UgCS where the autonomous flight was programmed to keep the UAV at 60 meters (196.85 feet) above ground level flying at 12 meters per second (26.84 miles per hour). Image overlaps of 80% forward and 80% side were specified within the flight planning software. Ground control targets were laid on the ground throughout the pipeline right-of-way before the collection of imagery. The GPS location for the center of each target was captured using a Spectra SP80 RTK GNSS receiver getting live corrections through an internet connection (*SP80 GNSS receiver*, 2022). The flight took approximately 15 minutes to complete collecting 490 images.

Photos captured during the flight were imported into *Pix4Dmapper* for photogrammetry processing (2022) (Figure 19). The photos were aligned within the software based on the location and orientation of their collection. After the photo alignment, the GPS coordinates of the ground control targets were imported into the software. The center coordinate of each target was marked within all photos that captured a target. Photo processing was executed once all target coordinates were marked. An RGB orthomosaic (Figure 1) and a 1.5cm DEM were output in NAD83 UTM Zone 17N coordinate system. The RGB photo processing took approximately 2 hours to produce the photogrammetry products. Processing times can vary depending on the quantity and resolution of photos as well as what computer hardware is being used.

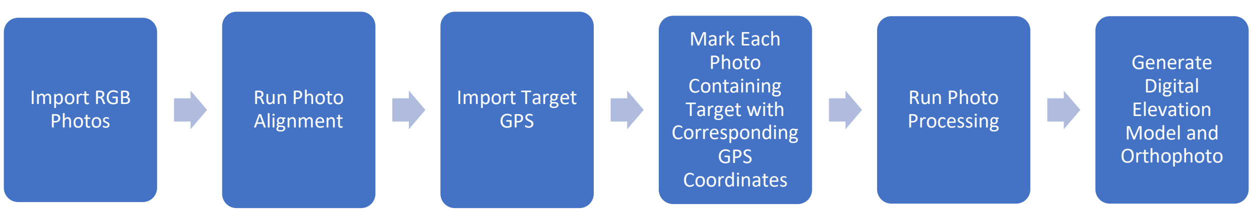

Figure 19. Pix4Dmapper RGB Photogrammetry processing

The 1.5cm DEM was imported into ArcGIS Pro where a polygon Shapefile of the pipeline right-of-way boundary was created (Figure 20). The boundary polygon and 1.5cm DEM were input into the Extract by Mask tool outputting a 1.5cm DEM of just the area within the polygon boundary. The pipeline right-of-way was the area of interest so data outside of it was removed to reduce processing times. Next, the masked 1.5cm DEM was input into the Resample tool. A resampled cell resolution of 20cm was chosen to match the cell resolution of the outputs from the LiDAR data analysis. Further processing conducted to obtain the RGB photogrammetry derived 20cm Flow Accumulation analysis followed the same steps used to create the LiDAR derived 20cm Flow Accumulation discussed earlier.

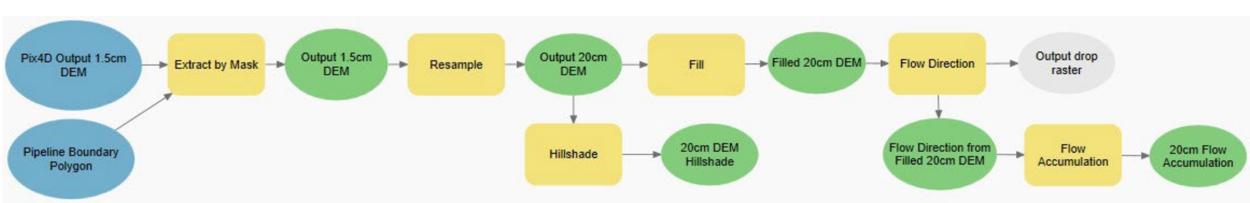

Figure 20. UAV-based RGB Photogrammetry Flow Accumulation analysis workflow

The RGB photogrammetry-based Flow Accumulation analysis showed a model of synthetic flow paths moving over waterbar #18 similar to what was seen in the LiDAR-based Flow Accumulation analysis. A Slope Position Profile for waterbar #18 was created using the RGB photogrammetry-based 20cm DEM (Figure 21). This process followed the same workflow described earlier in the creation of the LiDAR-based Slope Position Profile. The 20cm DEM output by the RGB photogrammetry was also analyzed within SAGA where Basic Terrain Analysis was conducted to create Wetness Index and LS-Factor raster surfaces exported for use in ArcGIS Pro.

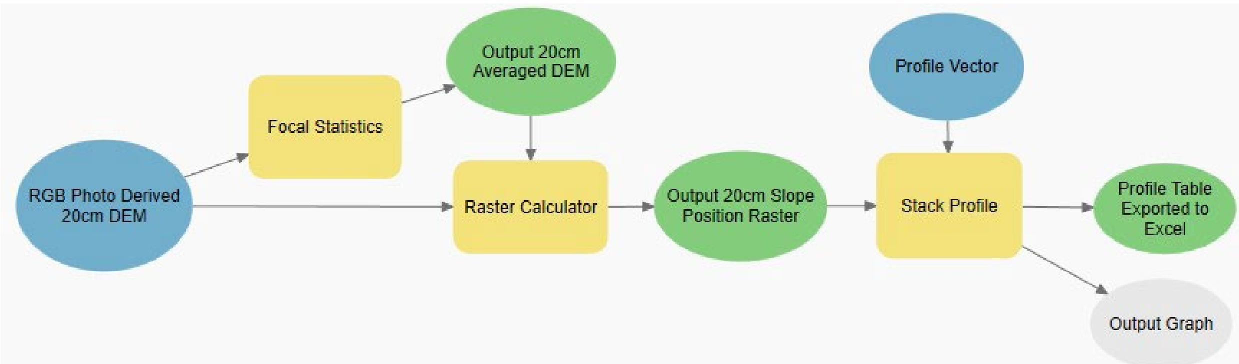

Figure 21. UAV-based RGB Photogrammetry Slope Position Profile workflow

UAV-based Multispectral Imaging and NDVI Photogrammetry

To assess the ability of using UAV multispectral imaging to identify areas of the pipeline right-of-way that lacked quality vegetation, we first outlined plots of good vegetation coverage, and poor vegetation coverage with marking paint based on visual inspection (Figure 23). The center coordinates of each plot were collected using the Spectra SP80 RTK GNSS receiver to get a high accuracy estimation the plot locations. Ground control targets used in the imagery processing workflow were also distributed around the pipeline right-of-way to increase the spatial accuracy of the processed outputs. Their center coordinates were also collected using the Spectra SP80 RTK GNSS receiver. Multispectral imagery was then collected over the pipeline right-of-way. UgCS flight planning software was used to create the flight path. The UAV autonomous flight was programmed to fly 60 meters (196.85 feet) above ground level at a slower, 8 meters per second (17.90 miles per hour). The flight legs of the programmed route were specified to collect imagery with an approximate 80% forward and 80% side overlap.

The red and near infrared images captured by 2 of the 6 sensors onboard the Sentera 6X Multispectral Sensor were imported into Pix4D for processing (Figure 22). The images were then aligned as part of the Pix4D workflow. The ground control target coordinates were imported and marked in each image that captured a ground control target. Before final processing of the red and near infrared imagery, an NDVI output correcting for sun irradiance levels was chosen within Pix4D settings. Final processing output a high resolution NDVI reflectance mosaic in the NAD83 UTM Zone 17N coordinate system. The RGB images collected by the RGB sensor on the Sentera 6X were processed in a separate instance of Pix4D following the same workflow discussed earlier in the RGB photo processing section. This output an RGB orthomosaic of the same area displayed by the NDVI reflectance mosaic.

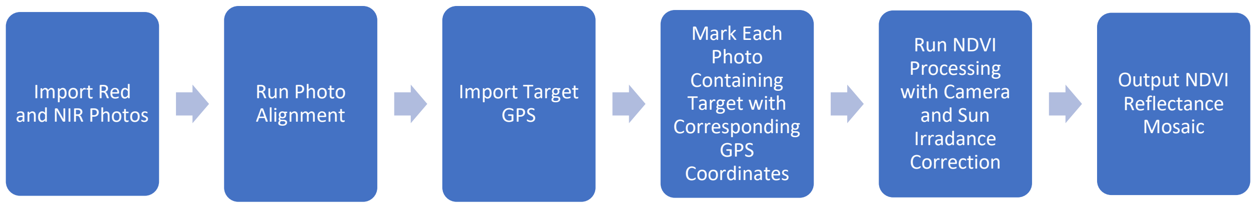

Figure 22. Pix4Dmapper NDVI processing

The NDVI reflectance mosaic and RGB orthomosaic were imported into ArcGIS Pro. The center GPS coordinates of each plot outlined in marking paint were also imported into ArcGIS Pro to identify the location as well as the poor vs. good vegetation visual identification of each plot (Figure 23). Polygon shapefiles were created within each plot's marking paint outline using the RGB orthomosaic. The NDVI reflectance mosaic cell values were averaged within each plot's polygon. The highest averaged NDVI value associated with poor vegetation plots was identified as 0.310. Since NDVI values can correspond to different levels of vegetation health and coverage depending on vegetation type, atmospheric conditions, processing corrections, etc., an NDVI value 0.310 was used as the upper NDVI threshold of poor vegetation. The NDVI reflectance mosaic's symbology was changed to display NDVI values less than or equal to 0.310 in red. Values greater than or equal to 0.311 were displayed as green. The transparency of red and green were increased, and the newly symbolized NDVI reflectance mosaic was displayed over the RGB orthomosaic.

Figure 23. Vegetation coverage identification and GPS location

UAV-based Hyperspectral Imaging

Hyperspectral imagery for a small area of the pipeline right-of-way was collected after creating an autonomous flight path with UgCS flight planning software. The UAV was flown 30 meters (98.43 feet) above ground level at 2 meters per second (4.47 miles per hour). At least

50% forward and side overlap was used to aid in processing. The hyperspectral sensor collects over 100 gigabytes of raw data in a few minutes, so a small area of the pipeline right-of-way was chosen for initial imagery collection. This was decided as to limit issues involved with data management and processing times. The raw hyperspectral imagery was imported into the proprietary software provided with the sensor for processing (Figure 24). Within the software, hyperspectral cubes were created and combined into hyperspectral image strips. The next step of processing was to georeference the image strips. Unfortunately, we were unable to properly georeference the image strips using the supplied proprietary software and failed to do so with other software suites as well. The hyperspectral image strips would not stitch into a usable hyperspectral orthomosaic using available photogrammetry software due to a lack of georeference.

Figure 24. Failed Hyperspectral imagery processing

UAV-based Thermal Imaging and Photogrammetry

Thermal imagery was captured over the pipeline right-of-way following almost the same photogrammetry collection and processing workflow used on the RGB and Multispectral imagery. The weather condition on the collection day was overcast cloud cover with temperatures below freezing. Collecting thermal imagery in these conditions was favorable as flowing surface water would be a higher temperature than its surrounding. Ground control targets were placed throughout the collection area and their GPS locations were collected using the Spectra SP80 RTK GNSS receiver. The UAV was programmed to autonomously collect thermal images at 36 meters above ground level (118.11 feet) flying at 6 meters per second (13.42 miles per hour). Image overlaps of 80% forward and side overlap were specified within UgCS which was used to plan and execute the UAV flight.

Once the UAV-based thermal imagery collection was completed, the imagery was exported from the remote sensor for processing (Figure 25). It was subsequently imported into Pix4D software where the imagery was aligned. The GPS coordinates for the location of each ground control target were then imported into the software and were applied to every image they appeared in. Processing was then run within the software that radiometrically corrected the thermal imagery and produced a Thermal Reflectance Orthomosaic as an output. This product was then imported into ArcGIS Pro for visual analysis of surface water within the pipeline right-of-way.

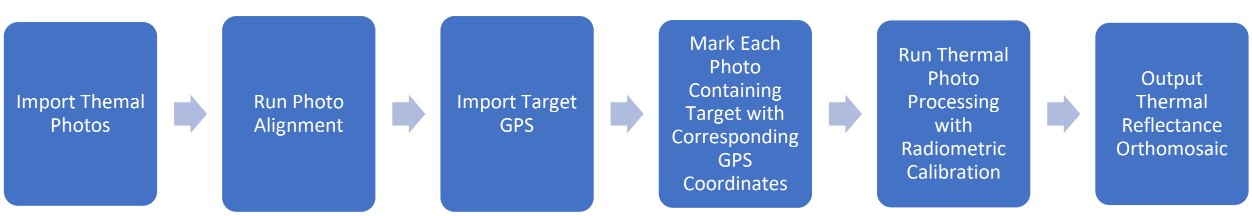

Figure 25. Pix4Dmapper Thermal imagery processing.

Airplane-based USGS LiDAR

A LiDAR-derived 1 meter cell resolution DEM for the pipeline right-of-way area was downloaded from a USGS website. The DEM was then imported into ArcGIS Pro where analyses similar to those used on the UAV-based LiDAR DEM and the UAV-based RGB imagery-derived DEM were conducted (Figure 26). The projection information of the DEM was first defined. A pipeline right-of-way boundary polygon was used in the Extract by Mask tool to mask the USGS 1 meter DEM to show just the pipeline right-of-way. This output was used to create a Hillshade for viewing and was filled using the Fill tool. Flow Direction analysis was then run on the filled DEM using the Flow Direction tool. Lastly, the Flow Direction surface created in the previous step was input into the Flow Accumulation tool outputting a raster surface defining modeled synthetic accumulation of waterflow over the surface.

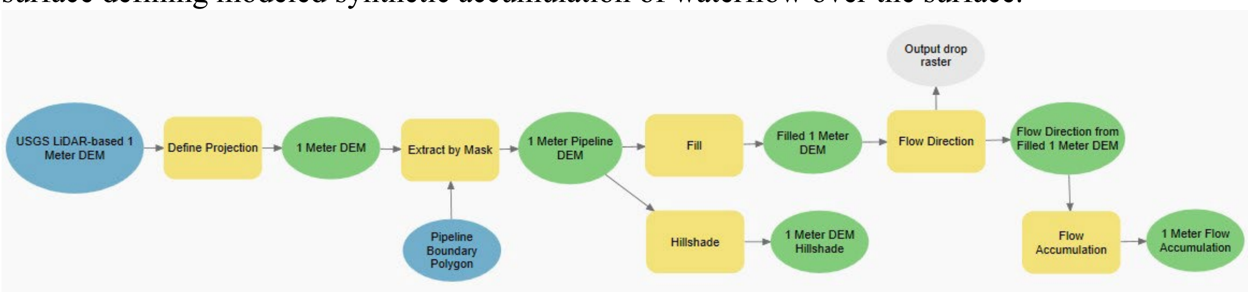

Figure 26. USGS LiDAR-derived 1 meter DEM Flow Accumulation analysis workflow

Cost Effectiveness Analysis and Best Management Practices

The largest portions of inspection expenditures can be categorized under two groups, equipment costs and labor costs. Equipment costs cover both the physical pieces of equipment and the software necessary to collect, process, and analyze the data. Entries in this category can either be one-time costs, such as drone and sensor, or may have annual costs, like software licenses and equipment insurance. Manpower costs vary by tasking, as they are typically calculated hourly, and commonly include an adjustment for overhead to cover the additional costs of having an employee (Weltman, 2019). As inspection costs are realized across variable periods, from hourly to product lifespan, a realized cost standardization was selected of U.S. dollars to kilometer inspected ($/km). This standardization of costs allowed the full realization of all costs associated to an inspection process given a set tasking, as calculated by distance.

UAV financial assessment began during the accuracy assessment portion of this study. As the drone inspection conducted collection and analysis, equipment and software necessary for each step were noted. Additionally, time records were maintained for each step to address the manpower cost portion of analysis. From the larger equipment and software list, entries unique and critical to the UAV method, such as multispectral sensors and GIS analysis software, were selected and used for a final financial analysis. Similarly, the complete time records were reduced to include only those steps which directly contributed to final GIS product used in the accuracy assessment. Current price estimates for equipment, licenses, and services were then gathered from manufacturers or retailers, as appropriate. Manpower pay rates for GIS collection and processing were determined from expert input and set at $20/hr and $40/hr respectively.

Costs for traditional inspections were collected from SME input via phone survey. As with the classification step above, any SME who participated was promised anonymity in the recording of their input. The phone interview used for collection focused on gathering estimates of current tasking as experienced in the Appalachian region. Figures sought were per tasking lists of current necessary equipment, average time to conduct an inspection, approximate time needed to create a report, and expected site length. From these reported figures, an average inspection speed of 1.61 kilometers per hour (1 mph) was established, which is reasonable when considering the impact of terrain on known average walking speeds (Murtagh et al., 2021). Additionally, inquiries into the approximate pay rate for a pipeline inspector on a per hour basis set an expectation of $20/hr for this financial analysis.

Creating the realized cost standardization of $/km required the defining of a collection scenario to which the factors of both methods could be applied. The accuracy assessment study area was selected, as its usage would allow the direct application of the UAV inspection recorded time data. Annual cost amortization to total kilometers inspected at this site required the scenario to include total inspections conducted at this site. For the scenario to be as accurate as possible, the inspection schedule of the GWPCP was applied (West Virginia Department of Environmental Protection, 2013), which outlines weekly and weather inspections, which occur after 0.25 inches of precipitation. For the immediate region of the study site, the average number of precipitation events meeting this criterion annually was determined from the last 3 years climate data, as recorded in the Global Surface Summary of the Day (GSOD) dataset (User Engagement and Services Branch, 2022). Combining the weekly and average weather determined inspections for a year, and multiplying by the study area length, gave the total space to be inspected. Finally, expected lifespan of single expenditure items were determined from the following equation:

$$Y = (H/F) / \mathrm{A}$$

Where Y is the number of years to be expected from an item, H is the expected life of an item in flight hours, F is the flight time per kilometer as recorded during collection, and A is the number of inspections per year. As the multispectral sensor is designed for integration into the UAV's mount, the determined lifespan (Y) was applied to this item as well in cost calculations. With all of these portions calculated, $/km estimates were produced for each method.

An element of flexibility was then entered into the cost calculations each of the inspection methods to broaden the perspective of the impact of changing the input factors on the resultant costs. Terrain of varying difficulty is likely to be encountered by an inspector in Appalachia performing traditional pipeline inspections. As such, cost analyses were conducted for variable inspector speeds, ranging from 0.25 mph to 2 mph in 0.25 mph steps. Similarly, flexibility analysis assumed that improvements are likely to be seen with several portions of the drone inspection process. The first aspect adjusted for was an optimized collection. In this flexibility scenario, the frequent inspections of the site would reasonably lead to a more streamlined set up and flight of the UAV at the study site, shortening total time per inspection. Moreover, the usage of optimized data transfer and storage technologies can reduce the transfer time necessary, leading to a reduced time necessary of the UAV pilot. Further, a general processing optimization was included, to offer a flexible view of the impact which might be seen with improved GIS hardware and software. As there are many difficult to quantify computational variables which can result in improved processing, the analysis as conducted was used as a baseline, and processing times were reduced up to 70% in 10% increments.

Results for Vegetation Classification

Validation Plot Statistics

Across the 30 AAPS, there was a mean residual distance of 0.075 m (SE = 0.009 m) between the two datasets, suggesting a relatively high alignment between the two products. Digitization of the painted ground plots created a sample set with a mean area of 0.90 m^2 (n=30, SE = 0.02 m^2). SME classification of these plots resulted in passing and failing plots numbering 12 and 13, respectively. Passing plots had a mean extracted area of 0.85 m^2 (SE = 0.04 m^2) and the failing class had a mean of 0.96 m^2 (SE = 0.03 m^2). SME review found 5 sample plots to be indeterminate, and they were excluded from the validation accuracy assessment. Digitized training data for SVM creation had a mean area of 3.66 m^2 (n = 120, SE = 0.33 m^2). Passing and failing training plots had an average area of 4.09 m^2 (n = 60, SE = 0.53 m^2) and 2.41 m^2 (n = 60, SE = 0.31 m^2) respectively.

Model Classification Accuracy

The validation plots for the multispectral SVM model had an overall accuracy of 92.00% (Table 1). Accurately classified passing validation plots had an average modeled vegetation coverage of 91.87% (n = 12, SE = 3.05%). Accurate failing plots had an average modeled vegetation coverage of 14.45% (n = 11, SE = 4.60%). The two incorrectly classified plots were both identified as failing by the SME. The vegetation coverage for these two misclassified plots was consistently high, with a mean of 97.77% coverage (SE = 0.73%). For the whole model, the user accuracies were 85.71% and 100% for passing and failing respectively. Conversely, the producer's accuracies were 100% and 84.62% for passing and failing. Overall, the model produced a kappa of 0.8408.

		True			
		Fail	Pass	Totals	User Accuracy
Predicted	Fail	11	0	11	1.0000
	Pass	2	12	14	0.8571
	Totals	13	12		
	Producer Accuracy	0.8462	1.0000	**Overall Accuracy->**	0.9200
				Kappa ->	0.8408

Table 1. A confusion matrix between the True classification of the plots, as determined by the SME classification process, and the Predicted classification derived from the SVM models created from the multispectral and RGB datasets. Both models produced the same classification accuracy, including the classification errors of the same two plots.

All accuracy values of the RGB model exactly matched the validation values of the multispectral model, such as an overall accuracy of 92.00% was achieved by the RGB model (Table 1). Differences were seen in specific coverage in each model. Validation plots accurately classified as passing had an average modeled vegetation coverage of 95.40% (n = 12, SE = 2.60%), and accurately classified failing plots had an average modeled vegetation coverage of 16.73% (n = 11, SE = 5.76%). This model misclassified the same two validation plots as the multispectral model, which were both identified as failing by the SME. In the RGB SVM model, the vegetation coverage for these two misclassified plots was once again high, with a mean of 99.60% coverage (SE = 0.42%). The user accuracies were the same at 85.71% and 100% for passing and failing respectively. Similarly, the producer's accuracies were the same at 100% and 84.62% for passing and failing. Overall, the model produced the same kappa of 0.8408.

Cost Effective and Best Management Practice Results

In the region containing the study area, there were 182 total rain events greater than 0.25 inches for 2019, 2020, and 2021, setting the number of average weather inspections to 61. From this a total of 113 total inspections were projected for this study area. Each inspection was flown in two branches, meaning the total number of inspection flights at this site would be 226 annually. Expert input placed UAV lifespan to be 1,000 flight hours before costly maintenance leads to a likely replacement of the drone system. With each flight in the study area covering approximately 1 km in a period of 20 minutes of flight, the drone would be expected to last 13.25 years until replacement was required.

Using the original flight data and processing times from this analysis, drone inspections had a cost of $194.34/km (Table 2), which was significantly larger than the $46.12/km calculated for the traditional inspections (Table 3). The minimal equipment of the traditional inspections resulted in a small proportion of the final expense at 6% (Figure 27) while the manpower requirements accounted for the majority of the expenses. Despite the increased cost and number of pieces of equipment required for the UAV inspections, equipment only accounted for 7% of the total per kilometer cost. The licenses required for the GIS analysis accounted for 14% of the total at $27.99/km. The remainder of the UAV inspection cost, and the largest portion of the total, was the manpower costs at $153.33/km.

Drone Inspection							
Equipment Costs							
	Item/License	Cost ($)	Qty	Replacement Period (yrs)	$/yr	$/Km	% Of Method Total
	DJI M200 v2	$ 6,000.00	1	13.25	$ 452.83	$ 1.71	1%
	Drone Insurance	$ 728.06	1	1	$ 728.06	$ 2.75	1%
	M200 Battery	$ 480.00	2	1.7	$ 564.71	$ 2.14	1%
	Sentera 6x Multispectral Sensor	$ 13,550.00	1	13.25	$ 1,022.64	$ 3.87	2%
	iPad	$ 599.00	1	1	$ 599.00	$ 2.27	1%
	Apple iCare	$ 149.00	1	2	$ 74.50	$ 0.28	0%
	Pix4d Mapper	$ 3,600.00	1	1	$ 3,600.00	$ 13.61	7%
	Esri ArcGIS Pro License	$ 3,800.00	1	1	$ 3,800.00	$ 14.37	7%
				Equipment Cost Subtotal ($/Km)		$ 41.00	21%
Manpower Costs							
	Position	Hourly Rate	Hourly Rate + 25%		Hrs/Km	$/Km	
	Pilot	$ 20.00	$ 25.00		1.28	$ 32.08	17%
	GIS Analyst	$ 40.00	$ 50.00		2.43	$ 121.25	62%
				Manpower Cost Subtotal ($/Km)		$ 153.33	79%
				Drone Inspection Cost Total ($/Km):		$ 194.34	

Table 2. A complete listing of projected costs to conduct a drone inspection in the study's scenario. Equipment costs are corrected first to annual cost, then cost per kilometer. Manpower costs are shown in hours per kilometer to cost per kilometer. Percent of total cost is shown in the right column.

Traditional Inspection							
Equipment Costs							
	Item/License	Cost ($)	Qty	Replacement Period (yrs)	$/yr	$/Km	% Of Method Total
	iPad	$ 599.00	1	1	$ 599.00	$ 2.27	5%
	Apple iCare	$ 149.00	1	2	$ 74.50	$ 0.28	1%
				Equipment Cost Subtotal ($/Km)		$ 2.55	6%
Manpower Costs							
	Position	Rate ($/hr)	Rate + 25% ($/Hr)		Hrs/Km	$/Km	
	Pipeline Inspector*	$ 20.00	$ 25.00		1.74	$ 43.57	94%
				Traditional Inspection Cost Total ($/Km):		$ 46.12	

Table 3. A complete listing of projected costs to conduct a traditional inspection in the study's scenario. Equipment costs are corrected first to annual cost, then cost per kilometer. Manpower costs are shown in hours per kilometer to cost per kilometer. Percent of total cost is shown in the right column.

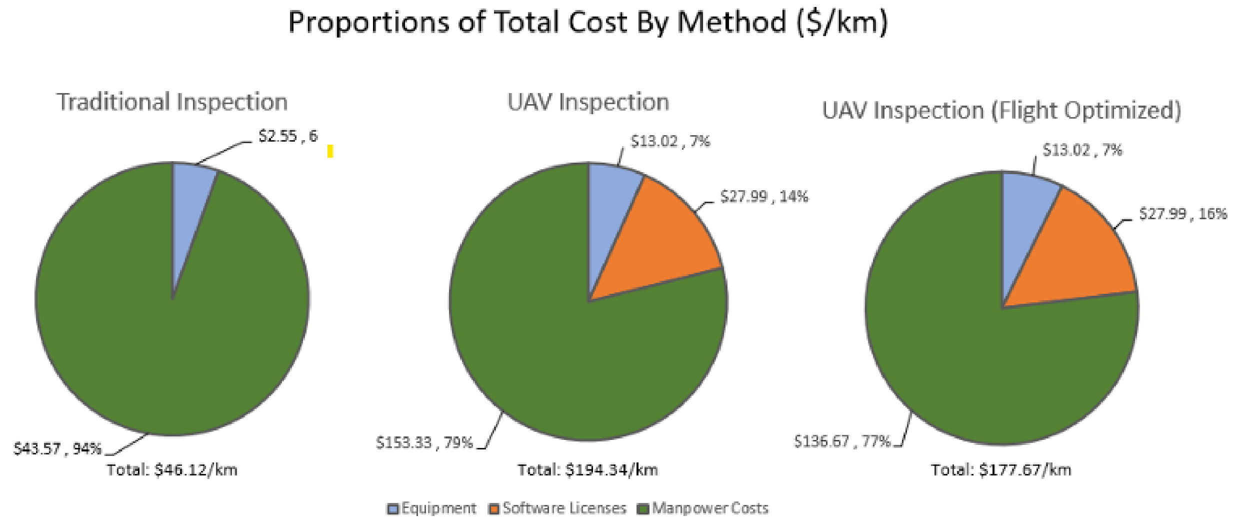

Figure 27. Charts depicting the proportion of each inspection method's cost categories. The three categories depicted are equipment, software licenses, and manpower in blue, orange, and green respectively. Total per kilometer costs are given below each chart.

UAV manpower costs were over 3.5 times greater than the traditional inspection manpower cost of $43.57/km. The largest portion of overall drone inspections cost was the GIS analyst, which accounts for $121.25/km, or 62% of the total. In creating the dataset, the surface model, analysis of the model and report generation, the GIS analysis must spend a total of 2.43 hrs/km (Table 4). Projected reductions in processing times from a hypothetical increase in processing efficiency were generally unable to produce comparable costs to traditional methods, with exceptions being noted at and above 50% time reductions when compared to the slowest hypothesized traditional inspection speed of 0.25 mph (Table 5). At 50% reduction and 0.25 mph, costs were within 5% of each other, favoring the traditional method. The assessment of additional hypothesized drone inspection price reduction through flight optimization found a pilot time reduction of 51.6%, from 1.28 hrs/km to 0.62 hrs/km (Table 6). This reduction lowered the UAV inspection manpower costs 10.9%, to $136.67/km (Figure 10). Including this optimized flight, comparable costs were again only seen at the lowest traditional inspection speed of 0.25 mph, though now only 30% processing optimization was required (Table 7). Further, a greater overhead cost for pipeline inspectors of 40%, in line with some higher estimates from the US SBA, reduced the cost difference seen between the two methods, where costs became comparable at a 0.25 mph traditional inspection speed against a 5% GIS processing increase (Table 8).

Collection (Adjusted to min/Km)		
	Time (Min)	Time (Hr)
Set Up	30	0.50
Calibration	2	0.03
Flight	20	0.33
Moving Pics to Computer	25	0.42
Pilot Total (Hr/Km):		1.28

Processing (Adjusted to min/Km)		
	Time (Min)	Time (Hr)
Align	45	0.75
Set GCP	30	0.50
Products	20	0.33
Processing Subtotal (Hr/Km):		1.58
Modeling		
	Time (Min)	Time (Hr)
Load	15	0.25
Mosaic	2	0.03
Calculate NDVI	1	0.02
Clip	1	0.02
Check Training Features	20	0.33
Train SVM	1	0.02
Reclassify	1	0.02
Total	41	0.68
Modeling Subtotal (Hr/Km):		0.34
Analysis and Report Creation		
	Time (Min)	Time (Hr)
Analysis (Review)	30	0.50
Report	30	0.50
Total	60	1.00
Analysis and Report Subtotal (Hr/Km):		0.50

GIS Analyst total (Hr/Km):	2.43

Table 4. Times of different collection and processing steps needed for drone collection. Times were first recorded in minutes and converted to hours. Corrections were then made hours needed to produce one kilometer of results. Drone pilot tasks are in the upper section, totaling in blue. Orange contains the GIS analyst subtotals, with the GIS analyst total in green.

		$/Km Proportional Cost Comparison								
		Drone Processing Efficiency Increase								
		0%	5%	10%	20%	30%	40%	50%	60%	70%
Inspector Speed (km/hr) 25% Overhead	0.40	0.72	0.74	0.75	0.80	0.84	0.89	0.95	1.02	1.10
	0.80	0.40	0.41	0.42	0.44	0.47	0.50	0.53	0.57	0.61
	1.20	0.29	0.30	0.31	0.32	0.34	0.36	0.39	0.41	0.44
	1.60	0.24	0.24	0.25	0.26	0.28	0.30	0.32	0.34	0.36
	2.01	0.21	0.21	0.22	0.23	0.24	0.26	0.27	0.29	0.31
	2.41	0.18	0.19	0.19	0.20	0.22	0.23	0.24	0.26	0.28
	2.81	0.17	0.17	0.18	0.19	0.20	0.21	0.22	0.24	0.26
	3.21	0.16	0.16	0.17	0.17	0.18	0.20	0.21	0.22	0.24

Table 5. Proportionate comparison of the cost per kilometer, calculated as traditional / drone cost for the original flight times and inspector overhead costs. Proportionate comparisons are shown across variances in inspector walking speed and GIS processing time reductions achieved through more efficient computing. Traditional inspections are applying a 25% overhead. Results closer to 1 denote costs closer in similarity. Cells containing values with less than 10% difference, or which favor drone inspections are highlighted in green.

Optimized Collection (Adjusted to min/Km)		
	Time (Min)	Time (Hr)
Set Up	15	0.25
Calibration	2	0.03
Flight	10	0.17
Moving Pics to Computer	10	0.17
Pilot Total (Optimized, Hr/Km):		0.62

Table 6. Time budget for drone collection using more optimized flight settings and better data transfer technology. Figures are calculated from advertised capabilities of the used drone system.

		$/Km Proportional Cost Comparison								
		Drone Processing Efficiency Increase with Flight Optimization								
		0%	5%	10%	20%	30%	40%	50%	60%	70%
Inspector Speed (km/hr) 25% Overhead	0.40	0.78	0.81	0.83	0.88	0.94	1.00	1.08	1.16	1.26
	0.80	0.43	0.45	0.46	0.49	0.52	0.55	0.60	0.64	0.70
	1.20	0.32	0.33	0.34	0.36	0.38	0.41	0.44	0.47	0.51
	1.60	0.26	0.27	0.27	0.29	0.31	0.33	0.36	0.38	0.42
	2.01	0.22	0.23	0.24	0.25	0.27	0.29	0.31	0.33	0.36
	2.41	0.20	0.21	0.21	0.23	0.24	0.26	0.28	0.30	0.32
	2.81	0.18	0.19	0.20	0.21	0.22	0.24	0.25	0.27	0.30
	3.21	0.17	0.18	0.18	0.19	0.21	0.22	0.24	0.26	0.28

Table 7. Proportionate comparison of the cost per kilometer, calculated as traditional / drone cost for the optimized drone flight times and original traditional inspection overhead. Proportionate comparisons are shown across variances in inspector walking speed and GIS processing time reductions achieved through more efficient computing. Traditional inspections are applying a 25% overhead. Drone flight times have been optimized in this scenario Results closer to 1 denote costs closer in similarity. Cells containing values with less than 10% difference, or which favor drone inspections are highlighted in green.

Results from Sediment Work

UAV-based LiDAR

The UAV-based LiDAR Flow Accumulation and Slope Position Profile analyses on waterbars within the pipeline right-of-way were able to detect possible structural failures of waterbar #18. Low sections of local elevations within the Slope Positions Profile analysis, shown by the blue arrows in Figure 28, modeled the accumulation of synthetic waterflow passing over waterbar #18 rather than it being properly diverted away from the pipeline right-of-way (Figure 28). These analyses may find use in augmenting current waterbar structure and function inspection by prioritizing the inspection of waterbars identified as possibly failing before a human-based visual inspection occurs.

The Hillshade produced from the LiDAR 20cm DEM allows for identification of features and elevation changes within the pipeline right-of-way. It is also useful for visual change detection of the landscape when analyzing Hillshade surfaces produced at different times. Within the Hillshade that was created, a small landslide known in the industry as a “slip” was identified within waterbar #9 (Figure 29).

The Topographic Wetness Index surface created in SAGA using the LiDAR 20cm DEM models the predicted wetness of the pipeline right-of-way (Figure 30). The LS-Factor surface also produced in SAGA models predicted soil erosion locations **(**Figure 31) These surfaces are useful in pipeline safety, inspection, and management allowing for modeled prediction of hydrological processes based on remotely captured topography, contributing to optimum design and placement of water and sediment control features such as waterbars, silt fence, and silt sock.

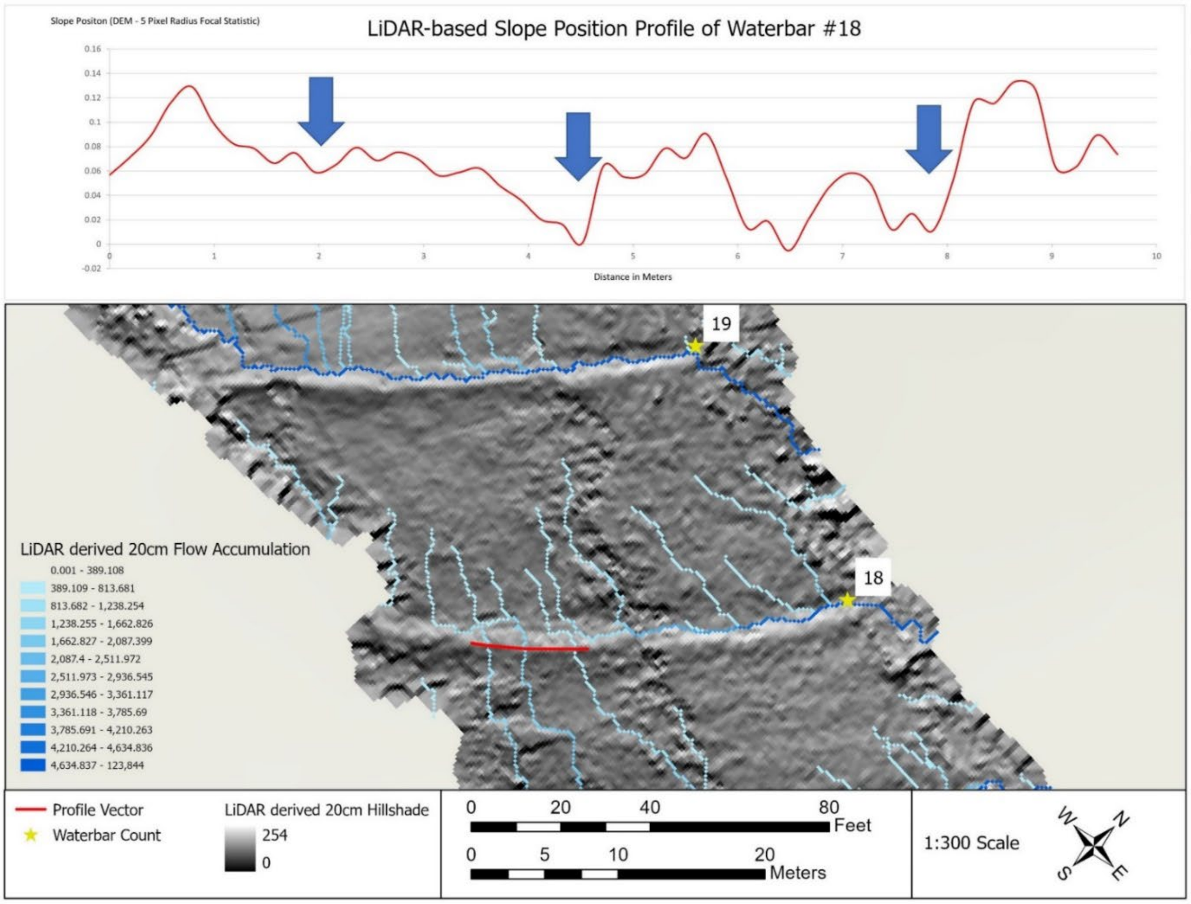

Figure 28. UAV LiDAR-based Flow Accumulation and Slope Position Profile analysis

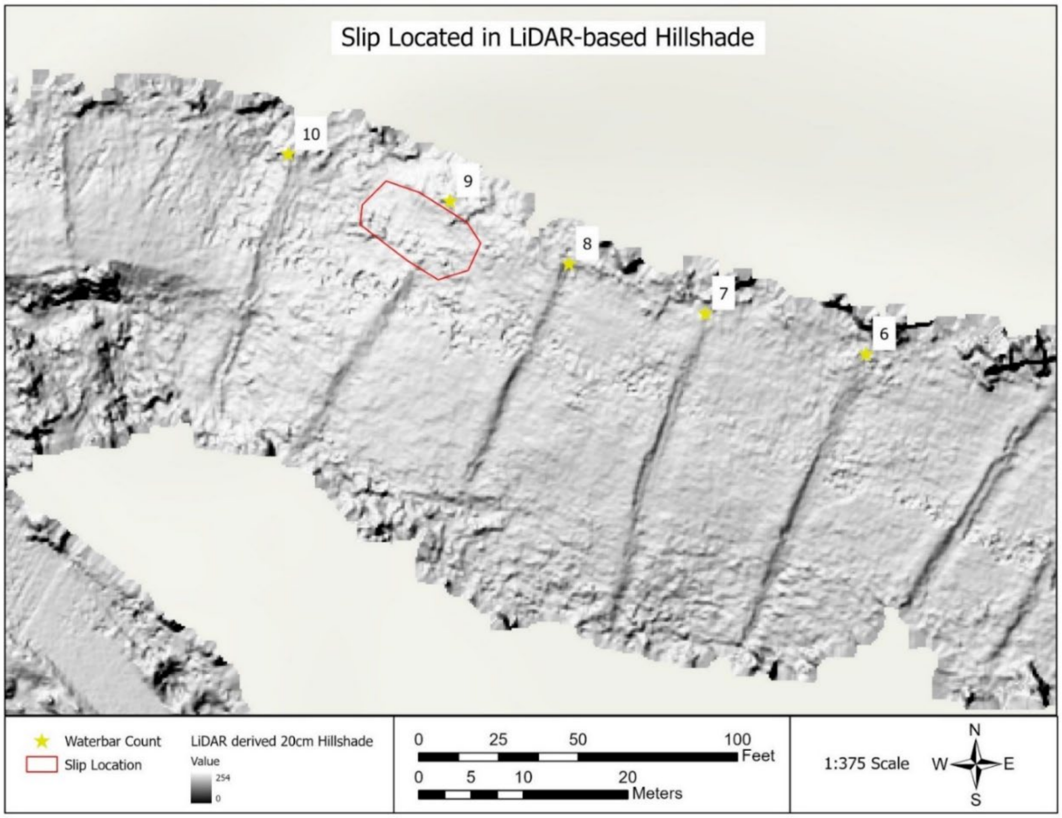

Figure 29. UAV LiDAR-based Hillshade identifying the location of a slip

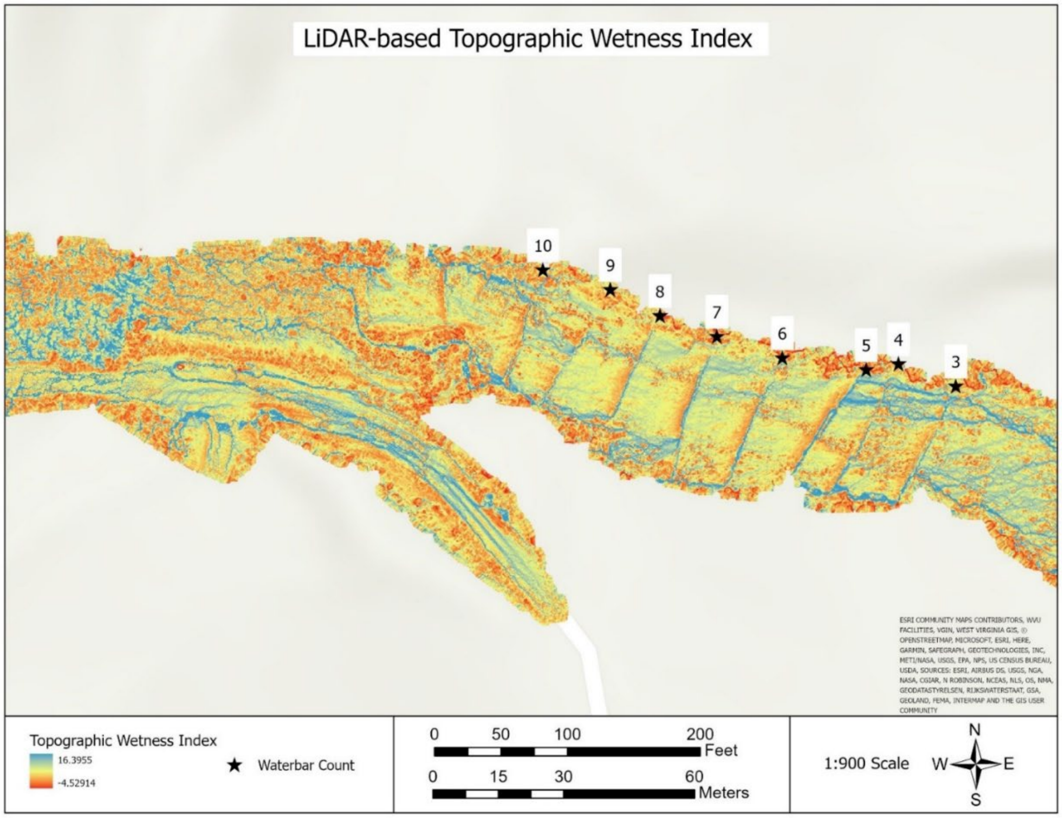

Figure 30. UAV LiDAR-based Topographic Wetness Index

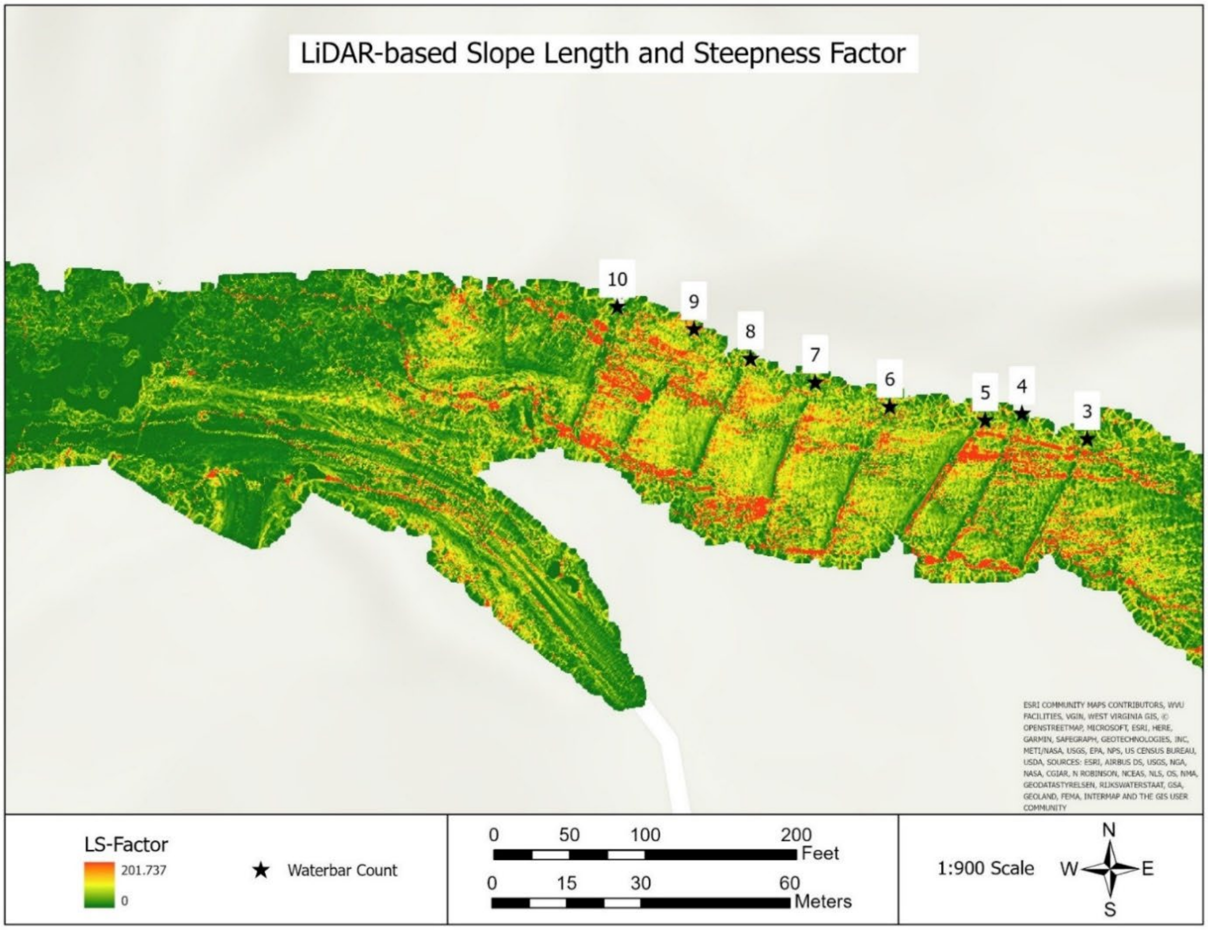

Figure 31. UAV LiDAR-based Slope Length and Steepness Factor

UAV-based RGB Imaging and Photogrammetry

The UAV-based RGB photogrammetry Flow Accumulation and Slope Position Profile analyses were also able to detect possible structural failures of waterbar #18. The blue arrows in the Slope Position Profile point to low local elevations within waterbar #18 where the synthetic flow and accumulation of water from the Flow Accumulation analysis was able to pass over the waterbar rather than be diverted off the pipeline right-of-way (Figure 32). The Hillshade produced from the 20cm DEM was used as the basemap in the Flow Accumulation analysis. The elevation contrast in the Hillshade was also used to identify the slip seen within waterbar #9 (Figure 33).

SAGA output a Topographic Wetness Index using the RGB photogrammetry 20cm DEM (Figure 34). An LS-Factor surface was also created using the same 20cm DEM (Figure 35). These surfaces, like those created using the LiDAR-based 20cm DEM, may supplement water and erosion control inspection and management as well as the safety aspects of current methods.

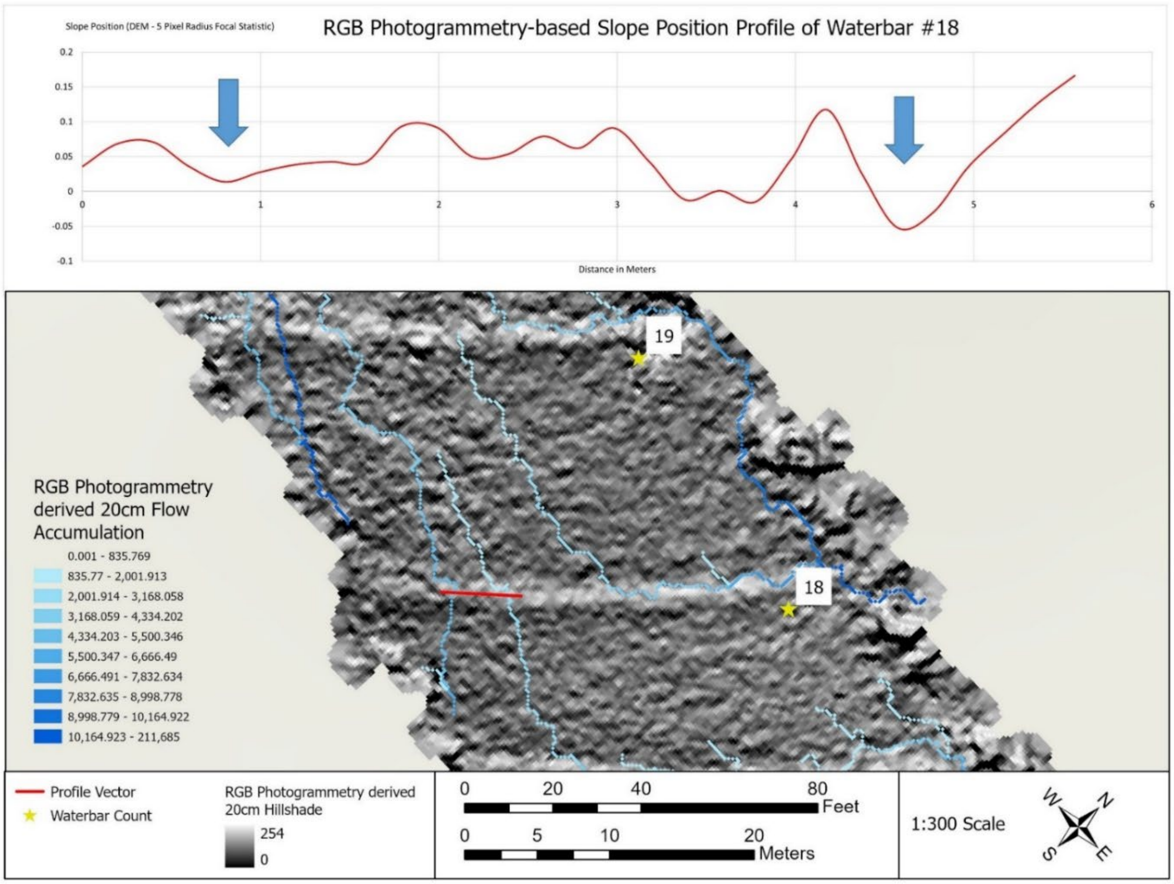

Figure 28. UAV RGB Photogrammetry-based Flow Accumulation and Slope Position Profile analysis

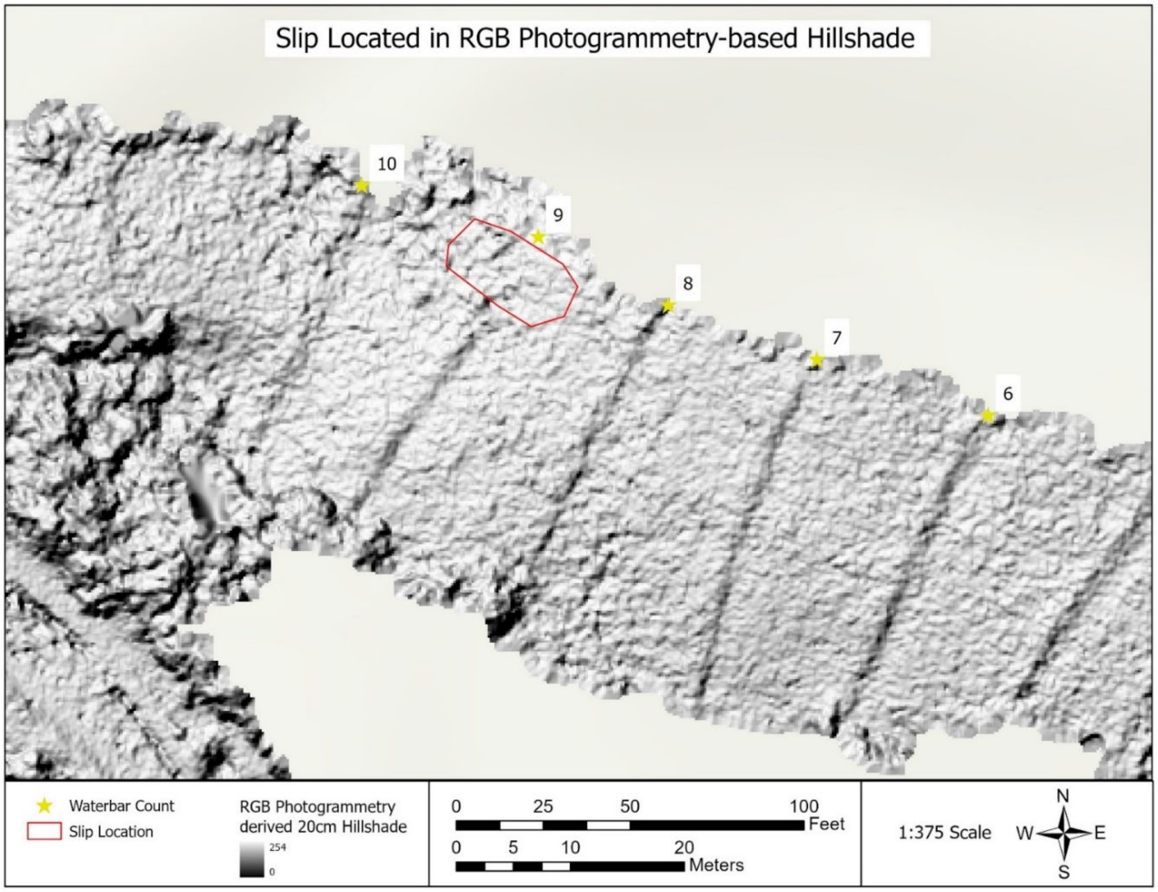

Figure 29. UAV RGB Photogrammetry-based Hillshade identifying the location of a slip

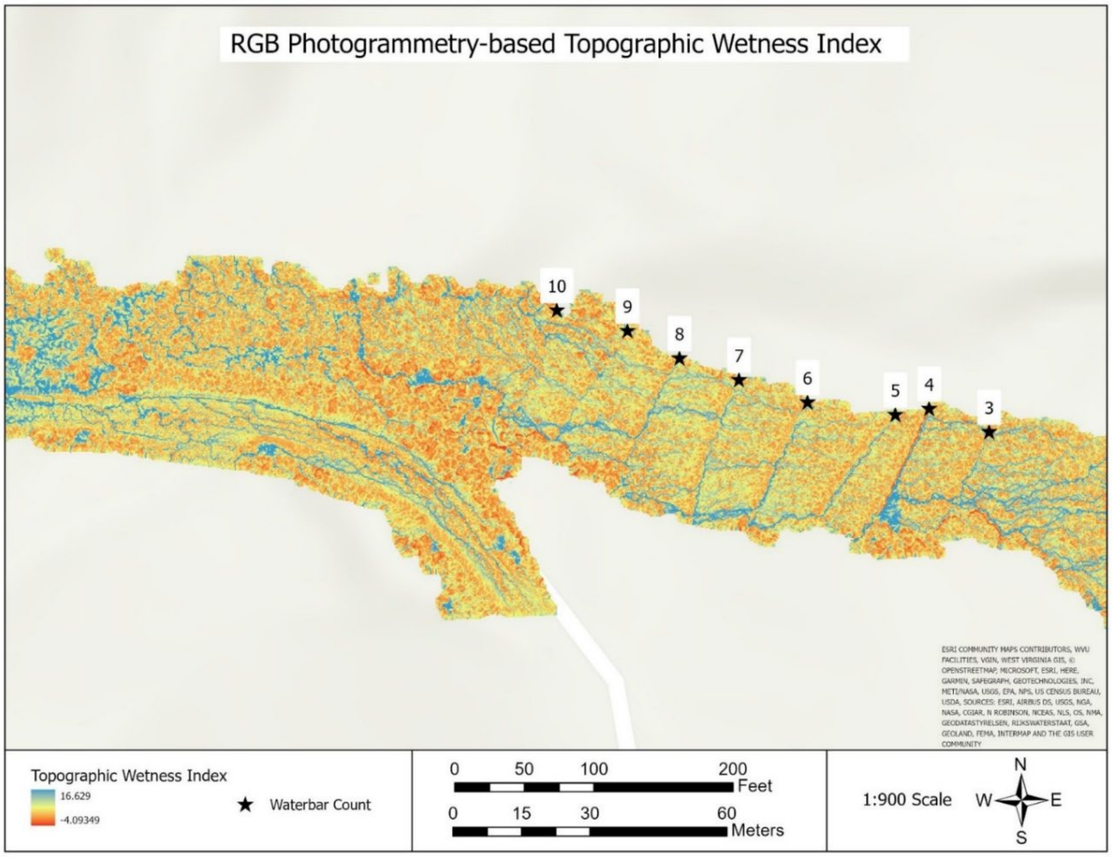

Figure 30. UAV RGB Photogrammetry-based Topographic Wetness Index

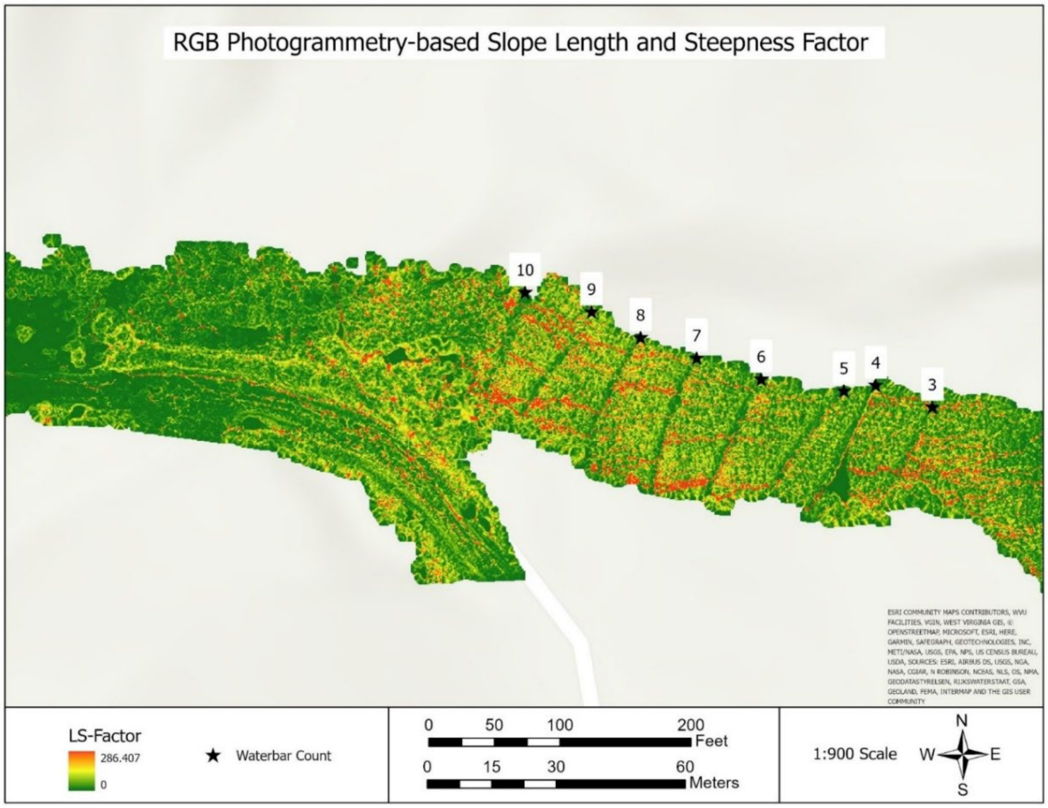

Figure 31. UAV RGB Photogrammetry-based Slope Length and Steepness Factor

UAV-based Multispectral Imaging and NDVI Photogrammetry

The product of the NDVI photogrammetry analysis was a map showing all areas of relative good and poor vegetation within the pipeline right-of-way based on the initial visual identification of vegetation coverage **(**Figure 36**)**. The use of NDVI photogrammetry may increase vegetation coverage walking inspection efficiencies and reduce some of the involved risk.

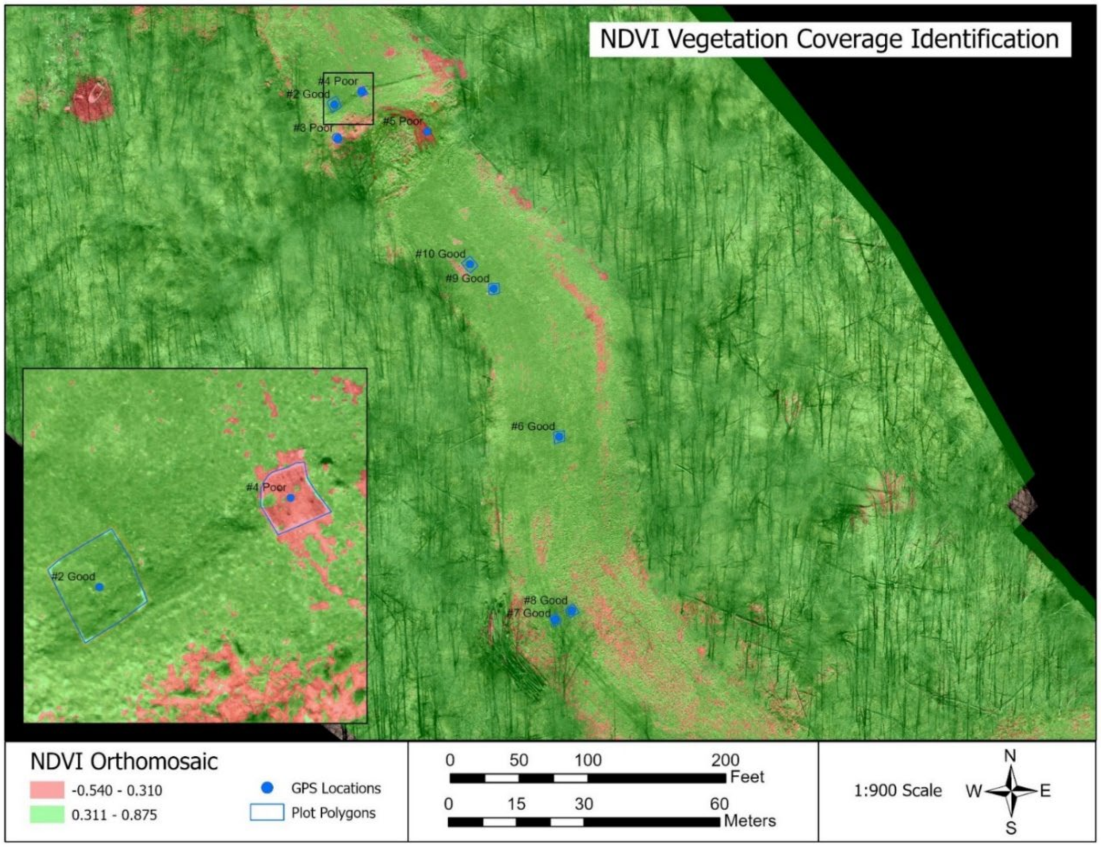

Figure 32. UAV Multispectral NDVI Photogrammetry of pipeline right-of-way vegetation coverage

UAV-based Hyperspectral Imaging

The single hyperspectral image strips were too limited in scope to conduct the desired UAV-based analyses. The Bayspec OCI-F Hyperspectral Imager has since been converted into a tabletop hyperspectral scanner used for lab-based analyses.

UAV-based Thermal Imaging and Photogrammetry

The Thermal photogrammetry analysis resulted in a map showing a cell-based temperature gradient of the pipeline right-of-way in grayscale. Flowing surface water was a higher temperature than its surroundings. This allowed the temperature differences within the grayscale map to highlight the locations of flowing surface water in white. Flowing surface water can be seen being diverted by waterbars. Flowing water can also be seen within the map exiting the ground in the location of the slip, which probably contributed to its cause (Figure 37).

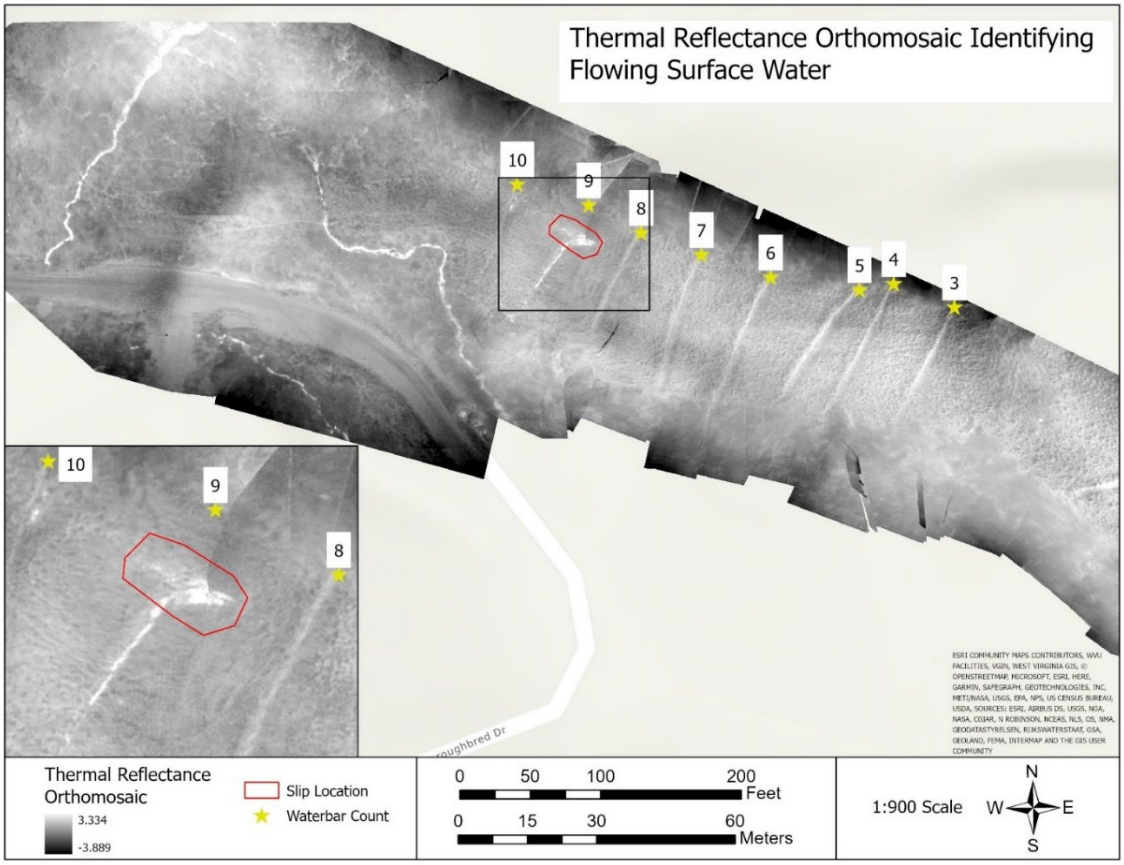

Figure 33. Thermal Reflectance Orthomosaic Identifying Flowing Surface Water

Airplane-based USGS LiDAR

The Flow Accumulation analysis with a Hillshade basemap produced using the 1 meter DEM was not very useful at this scale of pipeline right-of-way analysis due to the large cell resolution (Figure 38). A Slope Position surface and waterbar Slope Position Profile were not created from the 1 meter DEM due to the coarse cell resolution lacking necessary detail. The Hillshade produced from the 1 meter DEM displays the small-scale, large area mapping potential of the data (Figure 39).

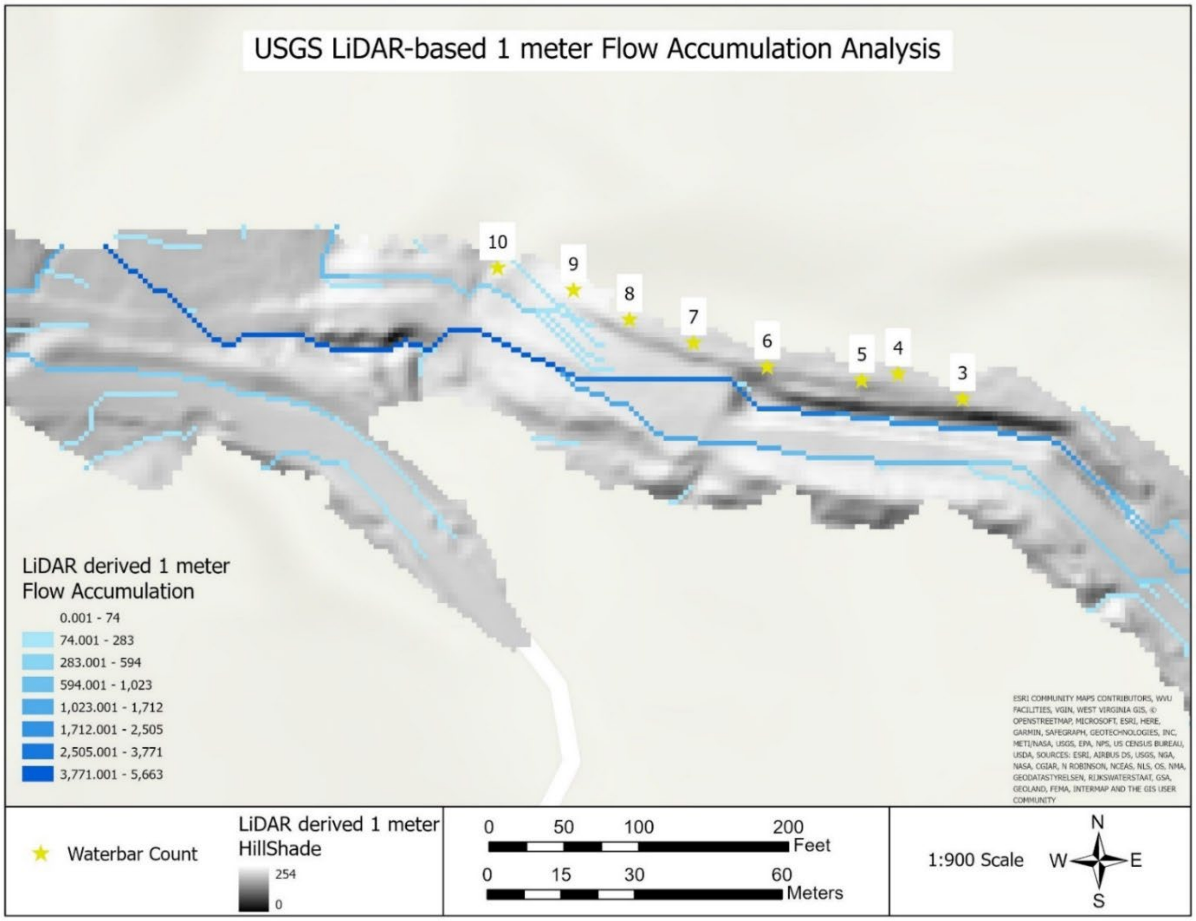

Figure 34. USGS LiDAR-derived 1 meter DEM Flow Accumulation analysis

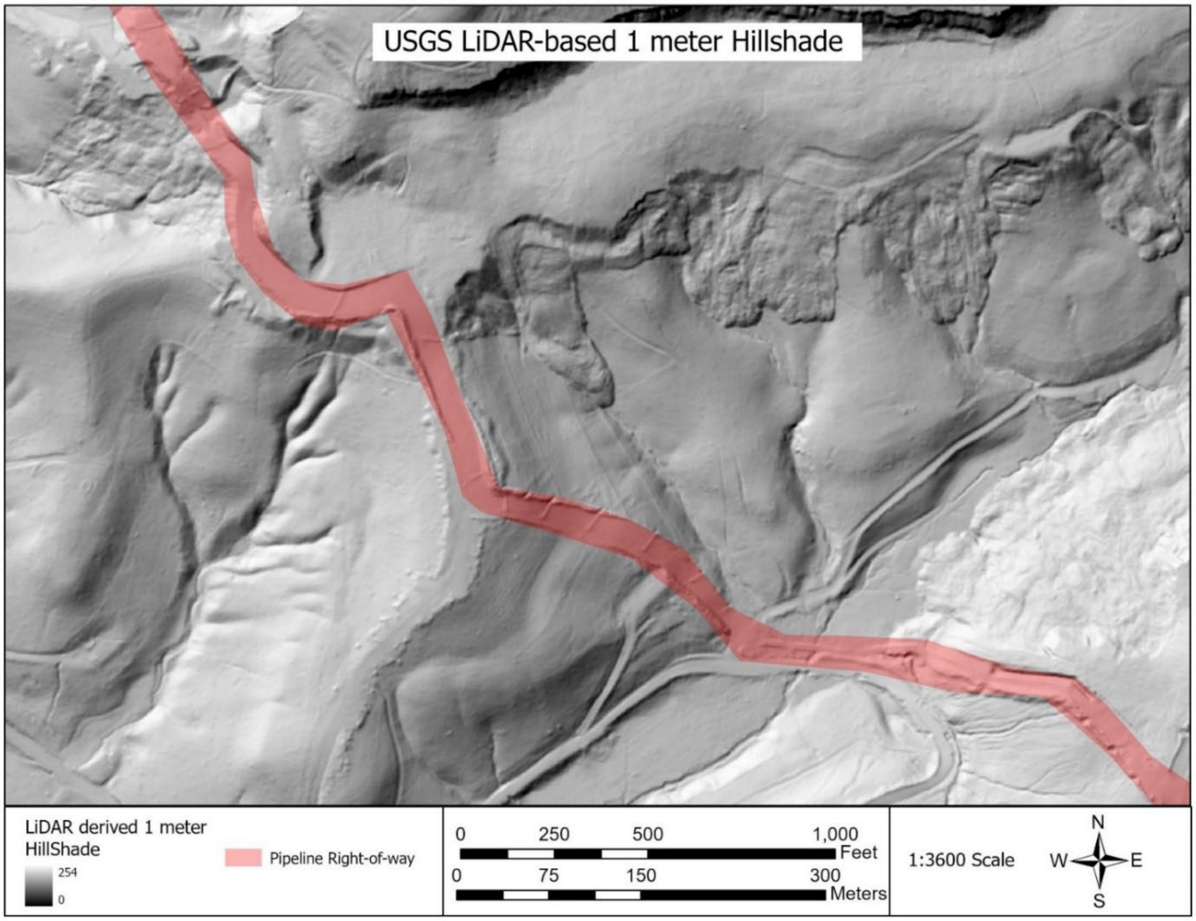

Figure 35. USGS LiDAR-derived 1 meter DEM Hillshade

Discussion of Vegetation Classification

The accuracy assessments of both models suggest the ability of either multispectral or RGB equipped UAVs to provide pipeline vegetation inspections at high accuracy. Both datasets sharing the same accuracy is uncommon, as previous studies typically find one sensor to outperform the other (Carabassa et al., 2020; Grybas and Congalton, 2021; Zheng et al., 2020). Results indicate that the applied technique is capable and SVM does appear to be an appropriate classification approach at this small spatial resolution. Several points of concern remain, which warrant further evaluation of this technique.

Of central concern is the fact that both dataset models misclassified the same two plots, ground samples 24 and 26. These two plots had different vegetation patterns from each other and were each unique from the rest of the validation plots. Plot 24 was noted to be marginal but failing during SME classification (Figure 40). Vegetation across this plot was rather evenly distributed, and no soil was visible inside the plot. The reason noted for this plot to be labeled failing in SME classification was the broad presence of erosion control netting in the areas between visible vegetation. Construction efforts often use this type of material to cover bare earth, as it protects the surface layer of the soil from direct rain exposure, resists the displacement of applied seeds, offers some stability to the soil beneath, and is typically biodegradable, thus requiring minimal future maintenance. As noted by an SME, it is common to see this material on pipeline construction operations upon steep and otherwise difficult to revegetate surfaces. As this material is a permeable impermanent cover, inspectors sometimes treat it as bare earth in their assessments, leading this plot to be considered failing.

Figure 36. A detailed image taken immediately after ground plot establishment of validation plot 24, one of two plots misclassified by both models. SME classification determined this plot to be failing due to the presence of straw-laden erosion control matting between the present vegetation.

The material used at this site was made of a twine type netting interwoven with straw. Being vegetation derived materials, they were likely a significant contributor to the failure seen in both models. While there are spectral differences between living vegetation and dried vegetative material, those nuances were not adequately captured in the SVM's training dataset. Moreover, pipeline inspectors note that the presence of dry vegetation itself is not enough to fail a plot, and a more complete view of vegetation health must be taken for a proper assessment. Future studies concerned with inaccurately identifying erosion control should consider the creation of a third class of ground cover comprised of dry vegetation. While not yet assessed from our data, the hope is that areas of dry vegetative material would be flagged for further inspection without indicating them as outright failing or passing. Further, SVM may need to be evaluated against other machine learning models should a third class be created, as SVM is essentially binary in its classification design (Sheykhmousa et al., 2020).

Unlike plot 24, plot 26 did present bare soil in significant enough quantities as to be deemed failing. Vegetation structure was larger and more clumped than plot 24, but the likely cause of misclassification is high soil moisture. Plot 26 was located downhill of a water seep which forms a marsh-like area on the pipeline. Water is noted for high spectral absorbency in the visible and NIR ranges of light, in turn reducing the soil reflections from this plot. Detecting high soil moisture is possible in remote sensing with the collection of thermal data and calculation of NDVI from a site (Zeng et al., 2004), and would aid in avoiding this issue in the future. Sensors with simultaneous capture of thermal and multispectral data are not commonly available, with options like the Sentera 6x Thermal arriving on the market only recently. Future studies with access to such sensor technologies should consider conducting a soil moisture calculation for inclusion in surface modeling.

Discussion of Sediment Work

UAV-based LiDAR and RGB photogrammetry products are highly useful for spatial analyses and aid in surveying, construction, monitoring, and change detection of a pipeline. These data are helpful in preventing, identifying, and remediating negative environmental factors related to pipeline construction and operation (Breinl, 2016). DEMs and Digital Surface Models (DSMs) as well as terrain derivatives generated from them grant vast applications within pipeline settings. The Hillshade created from both the LiDAR and the RGB photogrammetry DEMs served as the basemaps for the Flow Accumulation and Slope Position Profile analyses. Hillshade surfaces are very useful as a basemap for pipeline mapping during the design, construction, and management stages. Airplane-based LiDAR has been identified to supplement oil and gas safety and management practices regarding infrastructure design, construction, operation, and mapping (Tao & Hu, 2002). UAV-based LiDAR, as well as RGB photogrammetry which outputs similar products, have higher spatial and temporal resolutions than Airplane-based LiDAR at lower costs to purchase and operate. These remote sensing systems should supplement oil and gas safety and management practices gathering more data in less time at a lower cost than other methods currently being practiced.

UAV-based LiDAR systems are less expensive and far faster at deployment for data collection compared to more traditional manned aircraft-based LiDAR systems. The UAV-based LiDAR is generally of higher point density than manned aircraft-based LiDAR data as scanning occurs at lower elevations above ground while flying at lower speeds. Manned aircraft flown

LiDAR systems can collect data over larger areas at higher elevations and airspeeds; they are not as limited in flight times due to the use of internal combustion engines or turbines where electric motor driven UAVs are limited to battery storage capacity.

UAV-based LiDAR systems are more expensive than UAV-based RGB sensing systems, but LiDAR data is more spatially accurate and is faster to process. RGB imagery takes longer to collect, especially when using ground targets. The imagery can take hours to process and requires advanced computer hardware to shorten processing times. Though both remote sensing systems output similar products, there is a tradeoff between monetary costs, spatial accuracy, data collection effort, and data processing times. Note that the RGB photogrammetry Flow Accumulation analysis (Figure 28) is different from what is seen in the LiDAR Flow Accumulation analysis (Figure 32). This is most likely due to ground vegetation attributing to errors in the ground elevations of the RGB photogrammetry-based DEM. The RGB photogrammetry is also prone to include some taller vegetation in the DEMs produced. LiDAR is less prone to these errors as it can penetrate sparse vegetation obtaining a more accurate representation of ground elevations. Future research should foster an increase in the use of UAV-based LiDAR and RGB photogrammetry products for pipeline safety, inspection, and management. This may lead to breakthroughs such as large-scale prediction and detection of small landslides using UAV-based LiDAR or RGB photogrammetry within a pipeline right-of-way. Fusion of these data, producing colorized point clouds, may also hold value within this setting as LiDAR is better at modeling the ground while incorporated RGB color is helpful in identifying features of interest.

UAV-based Multispectral NDVI photogrammetry processing is like RGB photogrammetry processing with an extra step to create the NDVI reflectance mosaic. As with RGB imagery processing, NDVI processing is a time intensive process requiring expensive computer hardware to shorten processing times. Multispectral imagery systems and the UAVs used to carry them are generally more expensive than UAV-based RGB imagery systems. One advantage to using the Sentera 6X multispectral sensor is the integrated RGB sensor removing the need for a separate UAV-based RGB imagery system. An NDVI reflectance orthomosaic and an RGB orthomosaic can be created from a single data collection flight.

The NDVI reflectance map created in this study could be useful in identifying areas with poor vegetation coverage before a walking inspection occurs, increasing the efficiency of the inspection process. It may also help to identify areas with poor vegetation coverage that may have been missed after a walking inspection. These NDVI products may also introduce precision fertilizer applications to ground vegetation within a pipeline right-of-way as well. Poor vegetation coverage is an indicator of erosion susceptible areas which may also be prone to landslides. Further research should introduce new and improved UAV-based multispectral sensor application within oil and gas pipeline infrastructure.

The UAV-based hyperspectral data analyses unfortunately could not be conducted due to problems involved with this specific system's data processing workflow. UAV-based hyperspectral remote sensing systems are expensive compared to traditional RGB imaging systems. Hopefully, the software and data processing workflow issues surrounding the hyperspectral system used in this study will be alleviated so that others can conduct hyperspectral research. We are very interested in identification of invasive species using UAV-based hyperspectral remote sensing systems. Hyperspectral data in general should be able to assist in pipeline safety, inspection, and management after future software refinements.

UAV-based thermal remotely sensed data was able to locate flowing surface water on the pipeline right-of-way in below freezing weather as well as a small landslide "slip" with water seeping from it. Further research should dictate if the same is possible in warmer weather. UAV-based thermal imagery, whether it be live streamed imagery, video recording, or thermal reflectance orthomosaics from collected and processed imagery, can precisely measure temperature differences of pipeline infrastructure features in a remote manner, removing risks involved with person-based inspections. UAV-based thermal remote sensors are already deployed in other sectors of industry for security and inspection purposes. There are limitations to thermal imagery. Thermal sensors can get expensive quickly depending on the specifications of the sensor. Radiometric correction of thermal imagery is usually needed to account for errors attributed to reflectance and atmospheric conditions during data collection. Future research using UAV-based thermal remote sensors may produce new methodologies and augment current pipeline safety, inspection, and management practices.

The USGS 1 meter DEM is highly useful for small scale analyses and mapping of large areas and are relevant to pipeline planning and design. It was also used in large landslide prediction which is applicable in pipeline infrastructure planning and risk management (Maxwell et al, 2021). Within this study, the USGS 1 meter DEM and its derivatives had too large of a cell resolution to conduct analyses at the same scale as those executed using the UAV-based LiDAR and RGB photogrammetry DEMs and their derivatives. Although, if fine detail is not required for base mapping of a pipeline for safety, inspection, and management purposes, a Hillshade derived from the USGS 1 meter DEM is a great solution.

This study identified that UAV-based LiDAR is the preferred remote sensing system to use for inspecting, monitoring, and managing structural features including those specific to sediment control within a pipeline right-of-way. Ideally, UAV-based LiDAR could be flown twice a month. Also, LiDAR flights after any rain event 0.5 inches or more allows for water and erosion related change detection. All LiDAR flights should be conducted after standing ground water has dissipated due to water absorbing some laser wavelengths used in LiDAR systems. The LiDAR collections could happen at any time of the day as these remote sensing systems are not dependent on ambient light conditions. Flights at night are possible with proper FAA required equipment such as anti-collision strobe lights visible from at least 4.82 statute km (3 miles) (Operations Over People General Overview, 2021). LiDAR can be flown in any season as long as vegetation coverage of the targeted features being scanned is not too dense. Avoid scanning snow covered areas as snow will absorb some LiDAR wavelengths.

Once the LiDAR data is collected and processed, DEMs should be generated at an appropriate resolution. These can be used to create flow accumulation analyses to model water flow over the pipeline right-of-way which can aid in proper placement of sediment control features as well as identify those features which are not properly functioning to remediate sediment. Other digital surfaces such as the Topographic Wetness Index and LS-Factor can be produced from the LiDAR-derived DEMs to aid in proper placement of sediment control features within a pipeline right-of-way.

We also identified that UAV-based multispectral remote sensing systems are the most useful for identifying vegetation coverage within a pipeline corridor. This data collection could happen in conjunction with LiDAR data collection twice a month and after any rain event of 0.5 inches or more. These data should be collected during solar noon to limit shadows within the area of interest. Also, multispectral data collection should occur when targeted vegetation coverage appears green and is not dormant. In Appalachia, winter months should be avoided as multispectral indices will have a difficult time differentiating dormant vegetation from lack of vegetation. Once multispectral data is collected, NDVI orthomosaics and other multispectral index orthomosaics can be produced through photogrammetry software. These allow for vegetation coverage analysis identifying total vegetation coverage and specific areas lacking proper vegetation within a pipeline corridor.

Land access limitations also reduced the assessment strength of this study. With 30 validation plots established, 25 of which were suitable for analysis, a limited range of site conditions was sampled. Further, landscape variability is untested, as only 15% of the study area was available for validation plots. Varied soils are found in the study area and its immediate surroundings, with 21 different soil units being identified by the Natural Resource Conservation Service (NRCS) Web Soil Survey (Natural Resource Conservation Service, 2019). As found in previous research, varied soils produce unique spectral returns (Meerdink et al., 2019; Baldridge et al., 2009). However, the impact of soil-type variability is difficult to determine in this instance due to the significant disturbance and mixing of soils which occurs during construction. Vegetation species variability can also confound spectral returns (Kokaly et al., 2017). Ultimately, additional samples would provide a better depiction of the accuracy and limitations of this technique.

Another significant improvement in analysis of this type could occur with the integration of GIS data reflecting permit areas and management actions. All assigned boundaries of areas included and excluded for analysis and modeling are based on heads-up digitization. As such, there is the possibility that areas not intended to be included in inspections were used for either training or validation. Further, areas with their own management actions, like areas with erosion matting or wetland presence, can be evaluated separately. Being granted access to this data may enable the subdivision of models into management units, where more accurate models can be created for known surface conditions.

Data from traditional and UAV inspection processes are very different, and the recording and analysis benefits of the UAV approach is difficult to quantify against a traditional approach. Drone collection creates a complete surface model of the site, containing fixed coordinates and time metrics. Traditional inspections, while capable of addressing the finer detail at some locations, lack a complete capture product, and instead provide limited data on the entire site. UAV-based inspections make wide computational assessments of the entire site possible. This enables whole site issues to be identified and assessed. Likewise, surface changes at any location can be evaluated over time, enabling improved assessment of management actions. Should the addition of these type of products increase the industry valuation of UAV inspections, the cost & benefit relationship of performing a UAV inspection should be assessed.

Conclusions

The Marcellus and Utica shale plays in the Appalachian basin have seen significant growth in unconventional NG production. Installation of the required midstream infrastructure disturbs long tracts of difficult to traverse land which can cause significant ecological impact if not managed. Regulations have been created to guide site inspections, which are heretofore completed afoot. Inspectors traversing these stretches hike across difficult terrain, creating both health and safety concerns. A key aspect to these inspections is the assessment of vegetation re-establishment across the permit area. UAVs have been implemented across various industries due to their speed, size, and collection capabilities. Our study begins the evaluation process and lays foundational expectations of UAV capabilities as compared to traditional approaches in the energy industry.

Our study evaluated a wide range of available sensors for use. As noted previously, we identified that UAV-based LiDAR is the preferred remote sensing system to use for inspecting, monitoring, and managing structural features including those specific to sediment control within a pipeline right-of-way. In addition, the multispectral sensor allowed the inclusion of an NDVI dataset, but this did not appear to improve performance when evaluating SME classified plots. The SVM models derived from each sensor produced implementable results, with both models producing erroneous classification on the same 2 plots. These 2 plots contained unique ground conditions not yet modeled for, suggesting the need for future inclusion of an additional class, or use of a thermal sensor. Increased land access and accuracy assessment can provide a more robust evaluation of this emergent technique.

While our modeling results were not able to replicate those of local inspectors on the ground, implementing our approach and techniques can effectively complement and add to those efforts. Models of a reasonably high accuracy can be derived, which could in turn be used to identify larger issues requiring immediate responses. This tasking could cover some weekly and post-rain inspections, where there is a time sensitive nature to detecting large failures. Trained and certified professionals will still be needed in inspections, as they can seek-out conditions which the drone may miss; however, their time spent traversing difficult terrain would be reduced. On such terrain, both worker safety and cost savings may be realized. Thus, the inclusion of UAVs in pipeline inspection procedures appears to be a promising enterprise.

The financial analysis of our study's scenario suggests that the tested UAV pipeline inspection approach will be fiscally difficult to implement in all but the most complex terrain. From the factors included, the analysis suggests that the traditional inspection approach, using a simple equipment set and lower inspector pay rate, is likely to produce lower costs than the UAV approach per kilometer. The greatest individual cost in the UAV inspection method was the projected cost of the GIS analyst. As a manpower factor, this will be difficult to avoid, though it is reasonable to expect that future operations may be able to reduce the time spent performing GIS analysis per kilometer. As UAV efficiency increases, inspection costs become more comparable to traditional inspections (Figure 41).

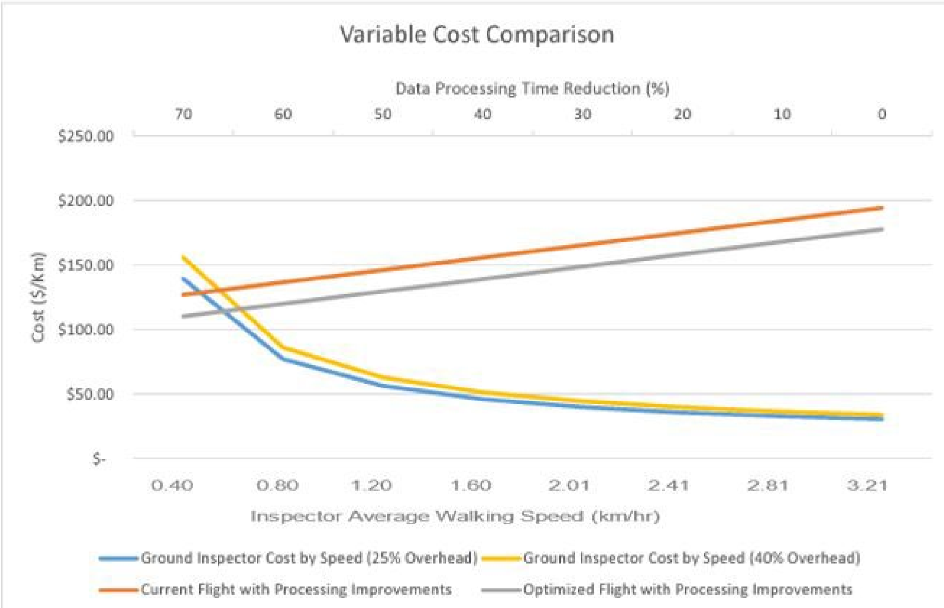

Figure 37. Cost trends per kilometer are shown including the variables of inspector speed and processing time reduction. Inspector speed is shown on the lower axis and increases from left to right. Data processing time reduction by percentage is shown on the upper axis and increases from right to left. Ground inspector plots show both a 25% overhead and 40% overhead in blue and yellow respectively. Similarly, drone cost with and without flight optimization are shown in grey and orange respectively. Note that the costs cross near 0.25 mph and 70% time reduction. This shows the point where cost per kilometer are lower using the drone inspection method.

The scenario used for analysis is likely an overly generalized representation of the final form a UAV pipeline inspection might take. Future research focused on method optimization will likely produce an inspection scheme which better capitalizes heretofore unquantified drone benefits. One such unaccounted benefit is the reduction in inspection time per kilometer between the drone and traditional inspection approaches. Even the unoptimized flight process reduced per kilometer time by 30%. This time reduction per site may enable the inspection of more sites in a single day. As the current scenario was formed using the study area and expected annual inspections thereupon, overall mission wide multisite productivity increases from a single inspector over a single day remain an unrealized element. Exploration of these time reductions can be accomplished in future studies with the creation of a larger dataset of traditional and UAV inspections across multiple sites. Reasonable expectations would suggest that should UAV inspections consistently produce a reduced on-site time compared to traditional inspections, implementation of the technology would enable the same number of employees to inspect a larger quantity of sites for the same amount of work hours.

UAV inspections in this study did not undergo a time reduction optimization for collection and data transmission. The drone used, a DJI M-200 v2 quadcopter, is a general use drone capable of accepting a wide range of sensors, making it an optimal choice for research and evaluation of various technologies. Quadcopter drones, however, can be outperformed by purpose-built drones with higher speed fixed wing flight, integrated multispectral collection, or longer flight times. As the flight optimization used in this analysis is based off of the published capabilities of the DJI M-200 v2, it is reasonable to suspect that another currently available drone may outperform these figures. Of the same thread, the GIS processing used in this study was following common research practices on general purpose computing machines. The hypothetical optimization figure used in this study generally reduces processing times to address gross potential improvements from the technological optimization of hardware and software used. Due to the nature of specialized computing suites, it would be unsurprising to find a purpose-built suite capable of further reducing the time needed of a GIS analyst in the UAV inspection process. Optimization may also find some steps used in our analysis, like the manual assigning of ground control points during dataset construction, may not be needed to produce pipeline inspection reports of the desired quality and format.

The tested financial analysis scenario may also contain unaccounted factors creating cost errors in favor of UAV inspections. The use of civilian and commercial drones in the US are governed under a regulation set known as the Part 107 – Small Unmanned Aircraft Systems regulations (Federal Aviation Administration, 2016). In these rules, §107.31 mandates that UAVs remain within the line of site of the flight team throughout any operations. Should a drone's flight path be visually obstructed, flight crews can deploy a drone observer afield with a reliable means of communicating with the flight team. It is possible to seek a waiver from the Federal Aviation Administration to excuse this requirement, but lacking a waiver, UAV inspections may require increased manpower costs on some sites. Additionally, technology limitations may also diminish the total distance covered by a drone. Drone missions loaded through a mission planning software, such as the UgCS client used in this study, pre-load a series of waypoints which the drone will follow, even if it loses connection with a ground controller station. Though the flight is thusly set, many drone operating systems will instruct a midmission return to take-off location if they cannot re-establish communication with the controller after a hard-set period of time. Different manufacturers use various periods of time, so post-signal lost collection will be heavily dependent on the equipment selected for the mission. Signal loss may also vary from day to day at the same site, as many as many environmental factors from humidity to foliage to sunspot activity will all impact signal attenuation. Finally, unlike traditional inspectors, drones are generally incapable of conducting a pipeline inspection in precipitation or extreme cold. The downtime created by a location's annual climate will hinder UAV usage to a currently unquantified degree. These unquantified factors can all lead to increased costs not included in this financial analysis. These factors can likely be addressed in future studies through a more thorough equipment evaluation, included assessment of the current FAA waiver process, and efforts to assess the impacts of annual climate.

Traditional inspections contain variables and unknowns that will need to be addressed in future studies. One of the greatest sources of error is likely found in the self-reporting of traditional inspection efficiency. An economics performance assessment study found that self-reporting of performance may not accurately represent objective performance (Pransky et al., 2006). Moreover, the method with which a self-reporting survey is conducted is of high importance to the data's accuracy (Peters et al., 2000; Stewart et al., 2000). Further, the given financial analysis does not include a precise capture of overhead costs for the traditional pipeline inspector and may be grossly inaccurate. Though the base rate of overhead noted by the US SBA is 25%, with a common maximum of 40% (Weltman, 2019), these datapoints do not specifically represent hazardous work, such as that which is conducted on pipelines. On many fully installed and operational sites, pipeline inspectors are expected to wear flame resistant gear, high visibility markers, hardhats, and steel toed boots. This gear suggests a hazardous exposure to employees, which may cause employer costs, such as insurance, to be far more expensive than a standard overhead amount would address. Future studies should gather more accurate data of traditional performance and overhead cost factors to better represent the true cost of the common inspection approach.

Finally, the data created from each of these inspection processes is very different, thus the recording and analysis benefits of the UAV approach is difficult to quantify against a traditional approach. Drone collection creates a complete surface model of the site, containing fixed coordinates and time metrics. Traditional inspections, while capable of addressing the finer detail at some locations, lack a complete capture product, and instead provide limited data which the inspector determined to be pressing. While much of these data appear to be extractable from a GIS dataset, as shown in the accuracy assessment portion of this study, UAV inspections make wide computational assessments of the entire site possible. Potential products include the ability to identify and assess whole site issues, such as an underperforming seed mix, and surface change at any location can be evaluated over time, which enables improved assessment of management actions. Should the addition of these type of products increase the industry valuation of UAV inspections, the increased costs of performing a UAV inspection would be offset by the value of the products delivered.

With an explosion of innovative use cases within academia, government, and industry, we find that UAV-based remote sensing systems and their array of valuable data outputs display an immense opportunity to increase safety, efficiency, and accuracy within the oil and gas industry. In addition, limitations of these remote sensing systems and their outputs in an oil and gas setting are defined. Further technological advancements, improvements in U.S. FAA UAV and airspace policy, and continued research has shown to increase widespread implementation of these systems. Augmentation of foot inspections with the application of UAVs and remote sensing systems stands to increase safety and efficiency of current methods especially when FAA visual line-of-sight laws are waived. This research inquired the utility of a suite of current UAV remote sensing technologies identifying possible applications of their data outputs. There is no doubt these technologies will change rapidly, becoming ever more advanced and practical with diminishing costs. However, we find in their current state that UAV and remote sensing systems hold significant promise regarding the support of pipeline safety, inspection, and management with the results of this study demonstrating the advantages and disadvantages of each system and approach.

References

Alley-Young G (2020) Drone (Unmanned aerial vehicle). Salem Press Encyclopedia. Salem Press, Ipswich

An Appalachian Petrochemical Renaissance within Reach. (2019). Office of Fossil Energy and Carbon Management. Energy.gov. Retrieved September 13, 2022, from https://www.energy.gov/fecm/articles/appalachian-petrochemical-renaissance-within-reach

Akula, A., Ghosh, R., & Sardana, H. K. (2011). Thermal imaging and its application in defence systems. In AIP conference proceedings (Vol. 1391, No. 1, pp. 333-335). American Institute of Physics.

ArcGIS Pro (Version 3.0.2). (2022). Esri Inc. Retrieved October 21, 2022, from https://www.esri.com/en-us/arcgis/products/arcgis-pro/overview

Argall, P. S., R. J. Sica. (2003). LiDAR Atmospheric Soundind Introduction. Encyclopedia of Atmospheric Sciences. pp1169-1176. Academic Press. https://doi.org/10.1016/B0-12-227090-8/00203-7

Asadzadeh, S., de Oliveira, W. J., & de Souza Filho, C. R. (2022). UAV-based remote sensing for the petroleum industry and environmental monitoring: State-of-the-art and perspectives. Journal of Petroleum Science and Engineering, 208, 109633.

Baldridge AM, Hook SJ, Grove CI, Rivera G (2009) The ASTER Spectral Library Version 2.0. Remote Sens of Environ 113: 711-715. https://doi.org/10.1016/j.rse.2008.11.007

Berry, W., Rubinstein, N., Melzian, B., & Hill, B. (2003). The biological effects of suspended and bedded sediment (SABS) in aquatic systems: a review. United States Environmental Protection Agency, Duluth, 32(1), 54-55.

Breinl, A. (2016). UAVs in Pipeline Design and Rehabilitation of Construction Corridors (Doctoral dissertation, University of Southern Queensland).

Campbell JB, Wynne RH (2011) Introduction to remote sensing. 5th ed. Guilford Press, New York

Carabassa V, Montero P, Crespo M, Padró JC, Pons X, Balagué J, Brotons L, Alcañiz JM (2020) Unmanned aerial system protocol for quarry restoration and mineral extraction monitoring. J of Environ Manag 270: 110717. https://doi.org/10.1016/j.jenvman.2020.110717

Cederholm CJ, Lestelle LC (1974) Observations on the effects of landslide siltation on salmon and trout resources of the Clearwater River, Jefferson County, WA, 1972-73, Final Report, University of Washington

Certificated remote pilots including commercial operators. (n.d.). United States Department of Transportation, Federal Aviation Administration. (2022), from https://www.faa.gov/uas/commercial_operators

Chen, A. Y., Huang, Y. N., Han, J. Y., & Kang, S. C. J. (2014). A review of rotorcraft unmanned aerial vehicle (UAV) developments and applications in civil engineering. Smart Struct. Syst, 13(6), 1065-1094.

Chisholm, R. A., Cui, J., Lum, S. K., & Chen, B. M. (2013). UAV LiDAR for below-canopy forest surveys. Journal of Unmanned Vehicle Systems, 1(01), 61-68.

Cho, J., Lim, G., Biobaku, T., Kim, S., & Parsaei, H. (2015). Safety and security management with unmanned aerial vehicle (UAV) in oil and gas industry. Procedia manufacturing, 3, 1343-

1349.

Conrad, O., Bechtel, B., Bock, M., Dietrich, H., Fischer, E., Gerlitz, L., Wehberg, J., Wichmann, V., and Böhner, J. (2022). System for Automated Geoscientific Analyses (SAGA) v. 8.3.0, Geosci. Model Dev., 8, 1991-2007, doi:10.5194/gmd-8-1991-2015

DJI Matrice 600 Pro. (2022). DJI Official. Retrieved October 7, 2022, from https://www.dji.com/matrice600-pro

DJI Phantom 4 Pro V2.0. (2022). DJI Official. Retrieved October 13, 2022, from https://www.dji.com/phantom-4-pro-v2/specs

Doman L, Kahan A (2018) United States remains the world's top producer of petroleum and natural gas hydrocarbons. US Energy Information Administration, 21. https://www.eia.gov/todayinenergy/detail.php?id=36292. Accessed 12 April 2022

Enforcement Policy for Flame-Resistant Clothing in Oil and Gas Drilling, Well Servicing, and Production-Related Operations. (2010). Occupational Safety and Health Administration. United States Department of Labor. Retrieved September 13, 2022, from https://www.osha.gov/laws-regs/standardinterpretations/2010-03-19-0

Erosion and Sediment Control Best Management Practice Manual. (2016). West Virginia Department of Environmental Protection. Retrieved September 13, 2022, from https://dep.wv.gov/WWE/Programs/stormwater/csw/Documents/E%20and%20S_BMP_2006.pdf

Esri (2021) ArcGIS Pro 2.9.2. Redlands, California

General Water Pollution Control Permit. (2013). West Virginia Department of Environmental Protection. Retrieved September 13, 2022, from https://dep.wv.gov/WWE/Programs/stormwater/csw/Documents/OG%20stormwater%20GP%203_10_15.pdf

Goellner, J. F. (2012). Expanding the shale gas infrastructure. Gas, 2(C3), C4.

Gómez, C., & Green, D. R. (2017). Small unmanned airborne systems to support oil and gas pipeline monitoring and mapping. Arabian Journal of Geosciences, 10(9), 1-17.

Grushecky ST, Harris KJ, Strager MP, Wang J, Mesa AN (2022) Land Cover Change Associated with Unconventional Oil and Gas Development in the Appalachian Region. Environ Manage 70:869-880. https://doi.org/10.1007/s00267-022-01702-y

Grybas H, Congalton RG (2021) A Comparison of Multi-Temporal RGB and Multispectral UAS Imagery for Tree Species Classification in Heterogeneous New Hampshire Forests. Remote Sens 13: 2631. https://doi.org/10.3390/rs13132631

Guan, S., Fukami, K., Matsunaka, H., Okami, M., Tanaka, R., Nakano, H., ... & Takahashi, K.

(2019). Assessing correlation of high-resolution NDVI with fertilizer application level and yield of rice and wheat crops using small UAVs. Remote Sensing, 11(2), 112.

Hallermann N, Morgenthal G (2014) Visual inspection strategies for large bridges using Unmanned Aerial Vehicles (UAV). In Proceedings of the 7th International Conference on Bridge Maintenance, Safety and Management (IABMAS). 661-667

Hunt, E. R., Cavigelli, M., Daughtry, C. S. T., McMurtrey, J. E., & Walthall, C. L. (2005). Evaluation of digital photography from model aircraft for remote sensing of crop biomass and nitrogen status. Precision Agriculture, 6, 359–378.

iGage iG3s. (n.d.). iGage Static GPS-GNSS receivers. (2022), from https://ig3s.com/index.htm

Kargbo DM, Wilhelm RG, Campbell DJ (2010) Natural gas plays in the Marcellus shale: Challenges and potential opportunities. Environ Sci and Technol 44: 5679–5684. https://doi.org/10.1021/es903811p

Kemp P, Sear D, Collins A, Naden P, Jones I (2011) The impacts of fine sediment on riverine fish. Hydrol Process 25: 1800-1821. https://doi.org/10.1002/hyp.7940

Kim J, Kim S, Ju C, Son HI (2019) Unmanned aerial vehicles in agriculture: A review of perspective of platform, control, and applications. IEEE Access 7: 105100-105115. doi: 10.1109/ACCESS.2019.2932119

Klein Hentz, Â. M., Kinder, P. J., Hubbart, J. A., & Kellner, E. (2018). Accuracy and optimal altitude for physical habitat assessment (PHA) of stream environments using unmanned aerial vehicles (UAV). Drones, 2(2), 20.

Kokaly RF, Clark RN, Swayze GA, Livo KE, Hoefen TM, Pearson NC, Wise RA, Benzel WM, Lowers HA, Driscoll RL, Klein AJ (2017) USGS Spectral Library Version 7. U.S. Geol Surv Data Ser 1035: 61. https://dx.doi.org/10.5066/F7RR1WDJ

Kumar, P. S., S. I, Dutt. (2020). The global positioning system: Popular accuracy measures. Matrials Today: Proceedings.Vol. 33(7), pp4797-4801. https://doi.org/10.1016/j.matpr.2020.08.380

Langlois LA, Drohan PJ, Brittingham MC (2017) Linear infrastructure drives habitat conversion and forest fragmentation associated with Marcellus shale gas development in a forested landscape. J of Environ Manag 197: 167-176. https://doi.org/10.1016/j.jenvman.2017.03.045

LiDAR360 (Version 5.3). (2022). GreenValley International. Retrieved October 21, 2022, from https://greenvalleyintl.com/LiDAR360/

Lingua, A., & Rinaudo, F. (2000). Aerial triangulation data acquisition using a low cost digital photogrammetric system. International Archives of Photogrammetry and Remote Sensing, 33, B2.

Liu P, Choo KKR, Wang L, Huang F (2017) SVM or deep learning? A comparative study on remote sensing image classification. Soft Computing 21: 7053–7065. https://doi.org/10.1007/s00500-016-2247-2

Maizland, L., & Siripurapu, A. (2022, August 11). How the U.S. Oil and gas industry works. Backgrounder. Retrieved September 13, 2022, from https://www.cfr.org/backgrounder/how-us-oil-and-gas-industry-works

Marcellus Drilling News (2021) SWPA Olympus Well Becomes Longest Marcellus Onshore Lateral. Marcellus Drilling News. https://marcellusdrilling.com/2020/12/swpa-olympus-well-becomes-longest-marcellus-onshore-lateral/.

Matrice 200 series V2. (2022). DJI Official. Retrieved October 19, 2022, from https://www.dji.com/matrice-200-series-v2/info#specs

Maxwell, A. E., Sharma, M., Kite, J. S., Donaldson, K. A., Maynard, S. M., & Malay, C. M. (2021). Assessing the Generalization of Machine Learning-Based Slope Failure Prediction to New Geographic Extents. ISPRS International Journal of Geo-Information, 10(5), 293.

Meerdink SK, Hook SJ, Roberts DA, Abbott EA (2019) The ECOSTRESS spectral library version 1.0. Remote Sens of Environ 230: 1–8. https://doi.org/10.1016/j.rse.2019.05.015
Messersmith D, Brockett D, Loveland C (2015) Understanding natural gas compressor stations. Penn State Extension. https://extension.psu.edu/understanding-natural-gas-compressor-stations.

Murtagh, E. M., J. L. Mair, E. Aguiar, C. Tudor-Locke, and M. H. Murphy. (2021). Outdoor Walking Speeds of Apparently Healthy Adults: A Systematic Review and Meta-analysis. Sports Medicine. 51:125-141. doi: 10.1007/s40279-020-01351-3

Natural Resources Conservation Service (2019) Web Soil Survey. http://websoilsurvey.sc.egov.usda.gov/.

Nex, F., & Remondino, F. (2014). UAV for 3D mapping applications: a review. Applied geomatics, 6(1), 1-15.

Nikolic J, Burri M, Rehder J, Leutenegger S, Huerzeler C, Siegwart R (2013) A UAV system for inspection of industrial facilities. In 2013 IEEE Conference on Aerospace Conference: Big Sky, MT. 1-8

NOAA CORS Network - National Geodetic Survey. (2022). NOAA. Retrieved October 13, 2022, from https://geodesy.noaa.gov/CORS/

Noor, N. M., Abdullah, A., & Hashim, M. (2018). Remote sensing UAV/drones and its applications for urban areas: A review. In IOP conference series: Earth and environmental science (Vol. 169, No. 1, p. 012003). IOP Publishing.

OCI™-F Hyperspectral Imager (vis-nir, SWIR). (2020). BaySpec. Retrieved October 19, 2022, from https://www.bayspec.com/spectroscopy/oci-f-hyperspectral-imager/

Olmstead SM, Muehlenbachs LA, Shih JS, Chu Z, Krupnick AJ (2013) Shale gas development impacts on surface water quality in Pennsylvania. PNAS. 110: 4962–4967. https://doi.org/10.1073/pnas.1213871110

Operations Over People General Overview. (2021). United States Department of Transportation, Federal Aviation Administration. Retrieved November 18, 2022, from https://www.faa.gov/uas/commercial_operators/operations_over_people#:~:text=Night%20Operations&text=The%20small%20unmanned%20aircraft%20must%20have%20lighted%20anti%2Dcollision%20lighting,sufficient%20to%20avoid%20a%20collision.

OPUS: The online positioning user service, process your GNSS data in the National Spatial Reference System. (2022). NOAA. Retrieved October 13, 2022, from https://geodesy.noaa.gov/OPUS/

Padoan, R., Steemers, T. A., Klein, M., Aalderink, B., & De Bruin, G. (2008). Quantitative hyperspectral imaging of historical documents: technique and applications. Art Proceedings, 25-30.

PIX4Dmapper: Professional photogrammetry software for drone mapping. (2022). Pix4D. Retrieved October 24, 2022, from https://www.pix4d.com/product/pix4dmapper-photogrammetry-software

Popova O (2017a) Marcellus Shale Play: Geology Review. U.S. Energy Information Administration. https://www.eia.gov/maps/pdf/MarcellusPlayUpdate_Jan2017.pdf.

Popova O (2017b) Utica Shale Play: Geology Review. U.S. Energy Information Administration. https://www.eia.gov/maps/pdf/UticaShalePlayReport_April2017.pdf. Accessed 03 January 2022
Richards C, Bacon KL (1994) Influence of fine sediment on macroinvertebrate colonization of surface and hyporheic stream substrates. The Gt Basin Nat 54: 106-113. http://www.jstor.org/stable/41712819

POSPac MMS 8. (2022). Applanix. Retrieved October 20, 2022, from https://www.applanix.com/products/pospac-mms.htm

Redtail LiDAR Systems. (2022). Retrieved October 6, 2022, from https://www.redtaillidar.com/

Rieke, M., Foerster, T., Geipel, J., & Prinz, T. (2011). High-precision positioning and real-time data processing of UAV systems. International Archives of the Photogrammetry, Remote Sensing and Spatial Information Sciences, 38(1/C22).

Royo, S., M. Ballesta-Garcia. (2019). An Overview of Lidar Imaging Systems for Autonomous Vehicles. Applied Science, 9(19), 4093, https://doi.org/10.3390/app9194093

Sabat-Tomala A, Raczko E, Zagajewski B (2020) Comparison of Support Vector Machine and Random Forest Algorithms for Invasive and Expansive Species Classification Using Airborne Hyperspectral Data. Remote Sens 12: 516. https://doi.org/10.3390/rs12030516

Schroder, W., Murtha, T., Golden, C., Scherer, A. K., Broadbent, E. N., Almeyda Zambrano, A. M., ... & Griffin, R. (2021). UAV LiDAR Survey for Archaeological Documentation in Chiapas, Mexico. Remote Sensing, 13(23), 4731.

6X Sensor. (2022). Sentera. Retrieved October 17, 2022, from https://sentera.com/products/fieldcapture/sensors/6x/

Sheykhmousa M, Mahdianpari M, Ghanbari H, Mohammadimanesh F, Ghamisi P, Homayouni S (2020) Support Vector Machine Versus Random Forest for Remote Sensing Image Classification: A Meta-Analysis and Systematic Review. IEEE J of Sel Top in Appl Earth Obs and Remote Sens 13: 6308-6325. doi: 10.1109/JSTARS.2020.3026724

SP80 GNSS receiver. (2022). Spectra Geospatial. Retrieved October 24, 2022, from https://spectrageospatial.com/sp80-gnss-receiver/

SPH Engineering. (n.d.). Drone flight planning and control software by SPH Engineering. UgCS. (2022), from https://www.ugcs.com/

Strager, M. P., Hentz, A. M. K., Kinder, P., & Grushecky, S. (2020). Using Unmanned Aerial Vehicles to Model Surface Runoff During Well Pad Development. Journal American Society of Mining and Reclamation. 10.21000/JASMR200100051

Tao, C. V., & Hu, Y. (2002). Assessment of airborne lidar and imaging technology for pipeline mapping and safety applications. In Integrated remote sensing at the global, regional and local scale, ISPRS commission I mid-term symposium in conjunction with Pecora 15/land satellite information IV conference proceedings.

The National Map - Data Delivery. (n.d.). U.S. Geological Survey. Retrieved October 19, 2022, from https://www.usgs.gov/the-national-map-data-delivery

Tucker CJ (1979) Red and photographic infrared linear combinations for monitoring vegetation. Remote Sens of Environ. 8: 127-150

3D Elevation Program. (n.d.). Topographic Data Quality Levels (QLs). U.S. Geological Survey. (2022), from https://www.usgs.gov/3d-elevation-program/topographic-data-quality-levels-qls

Trimble APX-18 LAND. (2022). Applanix. Retrieved October 20, 2022, from https://www.applanix.com/downloads/products/specs/ap-plus-land/APX-18Land-Datasheet.pdf

Tsouros, D. C., Bibi, S., & Sarigiannidis, P. G. (2019). A review on UAV-based applications for precision agriculture. Information, 10(11), 349.

U.S. Department of Energy. (2020). The Appalachian Energy and Petrochemical Renaissance: An Examination of Economic Progress and Opportunities. https://www.energy.gov/sites/prod/files/2020/06/f76/Appalachian%20Energy%20and%20Petrochemical%20Report_063020_v3.pdf.

U.S. Energy Information Administration. (2021). Natural gas explained. https://www.eia.gov/energyexplained/natural-gas/.

User Engagement and Services Branch. (2022). Global Surface Summary of the Day Dataset. National Climatic Data Center, NESDIS, NOAA, U.S. Department of Commerce. Available at: https://www.ncei.noaa.gov/access/search/data-search/global-summary-of-the-day.

Wallace, L., Lucieer, A., Watson, C., & Turner, D. (2012). Development of a UAV-LiDAR system with application to forest inventory. Remote sensing, 4(6), 1519-1543.

Wanasinghe, T. R., Gosine, R. G., De Silva, O., Mann, G. K., James, L. A., & Warrian, P. (2020). Unmanned aerial systems for the oil and gas industry: Overview, applications, and challenges. IEEE access, 8, 166980-166997.

Warner N, Christie C, Jackson RB, Vengosh A (2013) Impacts of shale gas wastewater disposal on water quality in western Pennsylvania. Environ Scie Technol 47: 11849-11857. https://doi.org/10.1021/es402165b

Weltman, B. (2019). How Much Does an Employee Cost You? U. S. Small Business Administration. Available at: https://www.sba.gov/blog/how-much-does-employee-cost-you.

West Virginia Department of Environmental Protection. (2013). General Water Pollution Control Permit. https://dep.wv.gov/WWE/Programs/stormwater/csw/Documents/OG%20stormwater%20GP%203_10_15.pdf.

West Virginia Department of Environmental Protection. (2016). Erosion and Sediment Control Best Management Practice Manual. https://dep.wv.gov/WWE/Programs/stormwater/csw/Documents/E%20and%20S_BMP_2006.pdf.

Worstell, B. B., Poppenga, S., Evans, G. A., & Prince, S. (2014). Lidar point density analysis: implications for identifying water bodies. US Geological Survey: Reston, VA, USA.

Wu, X., Shen, X., Cao, L., Wang, G., & Cao, F. (2019). Assessment of individual tree detection and canopy cover estimation using unmanned aerial vehicle based light detection and ranging (UAV-LiDAR) data in planted forests. Remote Sensing, 11(8), 908.

Zeng Y, Feng Z, Xiang N (2004) Assessment of soil moisture using Landsat ETM+ temperature/vegetation index in semiarid environment. IGARSS 2004 IEEE Int Geosci and Remote Sens Symp 6: 4306-4309. doi: 10.1109/IGARSS.2004.1370089

Zenmuse XT2 - DJI. (2022). DJI Official. Retrieved October 19, 2022, from https://www.dji.com/zenmuse-xt2

Zheng H, Zhou X, He J, Yao X, Cheng T, Zhu Y, Cao W, Tian Y (2020) Early season detection of rice plants using RGB, NIR-G-B and multispectral images from unmanned aerial vehicle (UAV). Comput and Electron in Agric. 169: 105223 https://doi.org/10.1016/j.compag.2020.105223